Copyright Warning & Restrictions

The copyright law of the United States (Title 17, United States Code) governs the making of photocopies or other reproductions of copyrighted material.

Under certain conditions specified in the law, libraries and archives are authorized to furnish a photocopy or other reproduction. One of these specified conditions is that the photocopy or reproduction is not to be "used for any purpose other than private study, scholarship, or research." If a, user makes a request for, or later uses, a photocopy or reproduction for purposes in excess of "fair use" that user may be liable for copyright infringement,

This institution reserves the right to refuse to accept a copying order if, in its judgment, fulfillment of the order would involve violation of copyright law.

Please Note: The author retains the copyright while the New Jersey Institute of Technology reserves the right to distribute this thesis or dissertation

Printing note: If you do not wish to print this page, then select "Pages from: first page # to: last page #" on the print dialog screen

ABSTRACT

LIQUID–LIQUID MIXING IN STIRRED TANKS WITH VARYING LIQUID DEPTHS

by
Sunil Mehta

Considerable attention has been devoted in the past to the determination of the minimum agitation speed, N_{cd}, required for the complete dispersion of two immiscible liquids in mechanically stirred tanks. When this situation is achieved the dispersed phase is no longer present as a distinct layer, such as a light oil phase above an aqueous solution, but becomes completely dispersed, in the form of droplets, throughout the continuous phase. The achievement of the dispersed state is of significant importance in many industrial operations. Nevertheless, the effect on N_{cd} of a number of operating variables remains poorly understood. In particular, the effect on N_{cd} of the liquid depth, H, has not been established, especially at different values of the impeller off-bottom clearances, C. This situation is especially common, and potentially critical, in a number of processes in the pharmaceutical and food industries, when the completely dispersed state must be maintained at all times as the vessel is either charged with a liquid or emptied.

This investigation is focused on the experimental determination of the minimum agitation speed and power dissipation required to completely disperse two immiscible liquids at different liquid heights and impeller off–bottom clearances. Two types of impellers were used here: a six–blade disc turbine and a six–blade (45°) pitched–blade turbine. The minimum agitation speed was first experimentally determined using a visual approach. In order to validate visual observation method, a previously developed sampling method was also used (Armenante, P.M. and Huang, Y.T., *Ind. Eng. Chem.*

Res., 31: 1395–1406, 1992). This method is based on sampling the liquid–liquid mixture at different agitation speeds, determining the content of the dispersed phase in each sample, and analyzing the data so obtained using a mathematical model.

N_{cd} and the corresponding power, P, drawn by the impeller at N_{cd} were found to be strongly affected by the impeller type, as expected. However, they were also significantly affected by both the liquid height and the impeller off–bottom clearance. Typically, both N_{cd} and P decreased with decreasing H. The effect of C was more complex. Of even greater significance, it was observed that, for specific combinations of H and C, and especially when the liquid head above the impeller was below a critical value, the state of complete liquid-liquid dispersion was not achievable, irrespective of the agitation speed. This implies that operating in regions where N_{cd} cannot be achieved should be avoided if complete liquid-liquid dispersion is to be maintained. The results of this investigation are expected to be of significant importance in the industrial practice.

LIQUID–LIQUID MIXING IN STIRRED TANKS WITH VARYING LIQUID DEPTHS

by
Sunil Mehta

A Thesis
Submitted to the Faculty of
New Jersey Institute of Technology
In Partial Fulfillment of the Requirements for the Degree of
Master of Science in Chemical Engineering

Otto H. York Department of Chemical Engineering

January 2003

APPROVAL PAGE

LIQUID–LIQUID MIXING IN STIRRED TANKS WITH VARYING LIQUID DEPTHS

Sunil Mehta

Dr. Piero M. Armenante, Thesis Advisor — Date
Distinguished Professor of Chemical Engineering, NJIT

Dr. Basil Baltzis, Committee Member — Date
Chair and Professor of Chemical Engineering, NJIT

Dr. Robert B. Barat, Committee Member — Date
Associate Professor of Chemical Engineering, NJIT

BIOGRAPHICAL SKETCH

Author: Sunil Mehta

Degree: Master of Science

Date: January 2003

Undergraduate and Graduate Education:

- Master of Science in Chemical Engineering
  New Jersey Institute of Technology, Newark, NJ, 2003

- Bachelor of Science in Chemical Engineering
  Sardar Vallabhbhai Regional College of Engineering & Technology, India, 2000

Major: Chemical Engineering

This thesis is dedicated to my parents.

ACKNOWLEDGMENT

I would like to express my appreciation to all the people who contributed to the successful completion of this thesis. My thesis advisor, Dr. Piero Armenante, deserves a very special acknowledgement for his guidance during this research. Completion of this thesis would not have been possible without his encouragement and moral support. I am thankful to my thesis committee members, Dr. Basil Baltzis and Dr. Robert Barat for their patience in reviewing the thesis and for their recommendations.

I would also like to thank analytical laboratory supervisor, Mr. Yogesh Gandhi, for his help in providing necessary lab equipment. I also appreciate the support received from the stock room supervisor, Mr. Thomas Boland. I would also like to thank ALPharma U.S. Pharmaceutical Division, Baltimore for giving me an opportunity to work on the thesis very well while working.

Finally, I would like to express my deepest gratitude towards my parents, whose love made it possible for me to complete this thesis.

TABLE OF CONTENTS

TABLE OF CONTENTS
(Continued)

LIST OF TABLES

LIST OF TABLES
(Continued)

LIST OF FIGURES

LIST OF FIGURES
(Continued)

Figure **Page**

LIST OF FIGURES
(Continued)

NOMENCLATURE

A	impeller blade angle (radian)
B	baffle width (m)
b	impeller blade height, i.e., blade width projected on vertical axis (m)
C	impeller off-bottom clearance measured from the middle of the impeller to the bottom of the tank for disk turbines, or measured from the top of the blade to the bottom of the tank for pitched-blade turbines (m)
C_b	impeller off-bottom clearance measured from the bottom of the impeller to the bottom of the tank (m)
C_o	a constant determined for different impeller types
D	impeller diameter (m)
H	liquid height (m)
ΔH	liquid head above the impeller (m) = $H - C_b$
H_{smp}	sampling point location measured from the bottom of the vessel (m)
h	liquid head of a pump (m)
K	constant
L	impeller blade length (m)
m	constant
mV	signal corresponding to strain gage (mV)
N	agitation speed (rpm)
n_b	number of blades of impeller (dimensionless)
N_{Bo}	Bond number, $D^2 g \Delta\rho/\sigma$ (dimensionless)
N_{cd}	minimum agitation speed for complete liquid-liquid dispersion (rpm)

$N_{cd\text{-}smp}$ N_{cd} determined experimentally with sampling method (rpm)

$N_{cd\text{-}vis}$ N_{cd} determined experimentally with the visual method (rpm)

N_{Fr} Froude number, $DN^2\rho_{mean}/g\Delta\rho$ (dimensionless)

N_{Ga} Galileo number, $D^3\rho_{mean}g\Delta\rho/\mu^2_{mean}$ (dimensionless)

N_p power number, $P/\rho_{mean}N^3D^5$ (dimensionless)

P power (watt)

Q flow rate (m^3/sec)

R volume of phase present in the sample (L)

Re impeller Reynolds number, $\rho_{mean}ND^2/\mu_{mean}$ (dimensionless)

S total sample volume (L)

T tank diameter (m)

V* volume fraction of dispersed phase

W blade thickness (m)

Greek Letters

α, α_o constants

μ_c, μ_d viscosities of continuous and dispersed phase (kg-m/sec)

ρ_c, ρ_d densities of continuous and dispersed phase (kg/m^3)

σ surface tension (joule/m^2)

$\Delta\rho$ $|\rho_c - \rho_d|$ (kg/m^3)

ρ_{mean} density of mixture (kg/m^3)

μ_{mean} viscosity of mixture (kg/(m·s))

τ torque (N·m)

CHAPTER 1

INTRODUCTION

Liquid-liquid mixing in a mechanically stirred vessel is a very common industrial operation encountered in many food, pharmaceutical, petrochemical, and biochemical industries. The main purpose of these processes is to promote good contact between the two immiscible phases and extend the interfacial area in order to increase the mass transfer rate. In these processes, it is important to operate at an agitation speed that ensures that the two phases are well mixed and the dispersed phase is completely incorporated into the continuous phase. In all above processes, involving mixing of two immiscible liquids, very small liquid droplets of one phase are created into the second phase. In these cases, the resulting mixture is often stable and will separate only after a long period of time. Therefore, mixing and the operating parameters that control it play a key role in the optimization of the overall process. As a result, multiphase mixing has become a very active area of research and investigation.

A number of studies have been published in the literature to determine the minimum agitation speed to completely disperse two immiscible liquids in mechanically stirred vessels, and the corresponding power dissipation as a function of several process variables such as tank geometry, impeller geometry, and physical properties of the fluids. However, no information is available on how the minimum agitation speed varies with changes in liquid heights. This situation is typically encountered during batching of ingredients and filling or emptying operations, where the vessel content is changed. In such situations, especially if the liquid height is dropped significantly and the liquid head

above the impeller is very small, it is of the utmost importance that the liquid-liquid dispersed product remains uniform throughout the operations.

Therefore, this study focused on the experimental determination of the agitation requirement in a mixing vessel to achieve complete liquid-liquid dispersion as a function of liquid level (liquid height). At or near this point, both phases are in contact with each other, thus promoting mass transfer and interphase reactions, while minimizing power consumption. The specific objective of this work was to experimentally investigate the effect of liquid depth (H), impeller off–bottom clearance (C), and impeller type on the minimum agitation speed (N_{cd}) and power (P) dissipation to achieve complete dispersion of two liquids. To achieve this objective a visual method for the experimental determination of N_{cd} was used ($N_{cd\text{-}vis}$). The validity of this approach was tested using another method based on sampling the mixture at different agitation speed and analyzing the data to obtain N_{cd} ($N_{cd\text{-}smp}$).

CHAPTER 2

LITERATURE SURVEY

2.1 Liquid–Liquid Dispersion

Liquid–liquid mixing in stirred tanks finds a wide range of application in mixer and mixing vessel design in extraction operations. By increasing the agitation intensity, the contact surface area is increased and the solute required for chemical reaction is transferred. The typical objectives of liquid–liquid mixing are as follows:

1. Increase the interfacial area by dispersing one liquid into another immiscible liquid;
2. Reduce the external mass transfer resistance outside the dispersed drops;
3. Promote internal mass–transfer by inducing convection within the dispersed drops;
4. Coalesce and redisperse the drops.

Of these four objectives, the first one is by far the most important since very high values of the interfacial area can be achieved even at moderate agitation intensities. The overall mass transfer rate is directly proportional to the interfacial area. The mass transfer coefficients are weak functions (through the power dispersed per unit volume) of the impeller agitation speed. By rotating an impeller, the liquid phase with the largest fraction typically becomes continuous, and the other liquid phase becomes dispersed. In a normal dispersion, especially in a system of small interfacial tension, it takes a long time to completely separate two liquid phases by settling after stopping agitator rotation, because fine droplets are difficult to separate from the bulk liquid.

Many types of impellers are used for agitation and mixing of liquids in vessels. The power consumption is not only dependent upon the type of impeller used and the

rotational speed, but also on the physical properties of the fluid and the geometric characteristics of the system, including the location of the impeller within the mixing vessel. A number of factors such as the shape, size of the impeller and the vessel, extent of baffling, impeller off–bottom clearance, and spacing between impellers typically produce changes in the flow pattern of the fluid being mixed and influence the power drawn. The most common configuration of mixing equipment used in industry consists of a vessel of a height nearly equal to the tank diameter where only one impeller is provided. However, agitated vessels having a value of the height–to–diameter ratio greater than unity and equipped with multiple impellers are commonly used in processes where shear–sensitive or high viscosity materials are treated, or where a high vessel surface–to–volume ratio is required.

When the agitation speed is increased (starting with a system at rest), one liquid phase begins to disperse into the other liquid. The progress of dispersion continues to increase the interfacial area available for mass transfer. The agitation speed at which an initially stratified immiscible layer disappears is called the minimum agitation speed for complete dispersion, and is denoted by N_{cd}. This speed is used as the main criterion of agitation intensity necessary for liquid–liquid systems. N_{cd} should be known to enable efficient design of mixer. Nagata (1960) obtained the following correlation for N_{cd} using a paddle (D=T/3, b=0.06T, θ=90 ^{o} and C=T/2) in a flat–bottom cylindrical vessel with liquid depth (H) equal to vessel diameter (T):

$$N_{cd} = K\, D^{-2/3} \left(\frac{\mu_c}{\rho_c}\right)^{1/9} \left(\frac{\rho_c - \rho_d}{\rho_c}\right)^{0.26} \qquad (2.1)$$

In this equation, K is a proportionality constant, ρ_c and ρ_d are the densities of the continuous and dispersed phases respectively in kg/m^3, and μ_c is the viscosity of the continuous phase in kg/(m·s). The value of K is taken 750 for a centrally located impeller and 610 for the off–center location. The effect of viscosity of the dispersed phase and the interfacial tension appeared to be negligible.

A related phenomenon was studied by Quinn and Sigloh (1963). They found that phase inversion, in most of the water–organic systems they studied, occurred at agitation speeds equal to two to three times $N_{cd,}$ for equal volume fractions of the two immiscible liquids.

Skelland and Seksaria (1978) studied the effects of liquid properties, impeller location, impeller type, and multiple impellers on N_{cd}. They proposed the following equation:

$$N_{cd} = C_o \, D^{\alpha_o} \, \mu_c^{1/9} \, \mu_d^{-1/9} \, \sigma^{0.3} \, \Delta\rho^{0.25} \qquad (2.2)$$

where C_o and α_o are functions of impeller type, location, and the ratio (H/T).

Skelland and Jai Moon Lee (1978) correlated the minimum agitation speed needed for nearly uniform liquid–liquid dispersion in baffled vessels, and described the effects of impeller type, size and location, and the effect of liquid properties on the degree of mixing. They expressed the degree of mixing in terms of the mixing–index concept developed by Hixon and Tinney (1935) in their work on solid-liquid systems. They calculated the composition of each sample as "percentage mixed" by the formula:

$$\text{Percentage mixed} = \frac{R}{S/2} \times 100 \qquad (2.3)$$

where R is the volume of the phase present in the smaller amount in the sample and S is the total sample volume. They defined the minimum impeller speed for nearly uniform mixing (N_{cd}) as the speed corresponding to the mixing index (defined as [R/(S/2)] x 100) of 98 % at all sampled parts of the vessel.

Skelland and Ramsey (1987) obtained an empirical correlation for the minimum agitation needed for complete liquid–liquid dispersion in baffled vessels. They correlated their observations from 251 runs, the observations of 35 runs by van Heuven and Beek (1971) and the observations from 195 runs by Skelland and Sakesaria (1978) with the expression:

$$(N_{Fr})_{min} = C^2 \left(\frac{T}{D}\right)^{2\alpha} \phi^{0.106} (N_{Ga} N_{Bo})^{-0.084} \qquad (2.4)$$

where C and α are functions of impeller type, location, and the ratio (H/T).

In these and the most of the other studies in the area of liquid–liquid dispersion, N_{cd} was determined visually. However, Armenante and Huang (1992) developed a new method to experimentally determine N_{cd} by taking samples from the liquid mixture at different agitation speeds and plotting the fraction of the dispersed phase in each sample against the corresponding agitation speed. They found that when connecting the resulting points by straight lines, a sharp change in the slope occurred in correspondence of the visually determined minimum agitation speed. They also found that their method was independent of sampling point location and type of agitation. By analyzing their data with the method they developed to determine $N_{cd\text{-}smp}$, they found a good agreement between the values so obtained and those obtained visually.

The flow pattern generated by the impeller plays a very important role in liquid – liquid dispersion. The experimental technique to determine the flow pattern include the use of colored tracer liquid, neutrally buoyant particles, hydrogen bubble generation and mean velocity measurement using Pitot probes, hot–film devices and laser-doppler velocimeters. A qualitative picture of the flow field created by an impeller in a single–phase liquid is useful to establish whether there are 'dead zones' in the vessel, or whether particles are likely to be suspended in the liquid. The typical flow patterns generated by a disc turbine and a propeller, respectively, operating with Newtonian liquids in the turbulent region is illustrated in Figures 2.1 and 2.2.

The flat–bladed turbine produces a strong radial flow outwards from the impeller (Figure 2.1) creating circulation zones in the top and bottom of the tank. The type of flow can be altered by changes in the impeller geometry. For example, if the turbine blades are angled, a stronger axial flow component is produced and this could be advantageous for solids suspension and the liquid-liquid dispersion. The flat paddle produces a flow field with large tangential components of the velocity.

The propeller creates a mainly axial flow through the impeller and this central axial flow may be upwards or downwards depending upon the direction of rotation. The predominant circulation pattern for a downward pumping propeller is shown in Figure 2.2. Of course, the velocities at any point will be three-dimensional, but circulation patterns, such as those in Figure 2.2, are useful in the selection of appropriate impellers for a given duty.

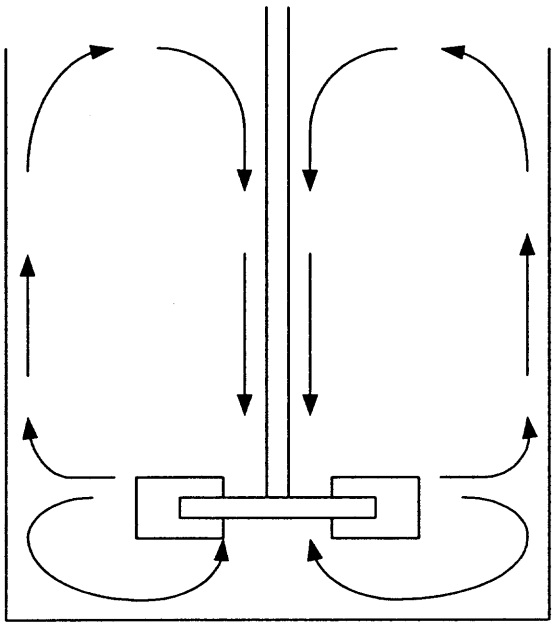

Figure 2.1 Radial Flow Pattern.

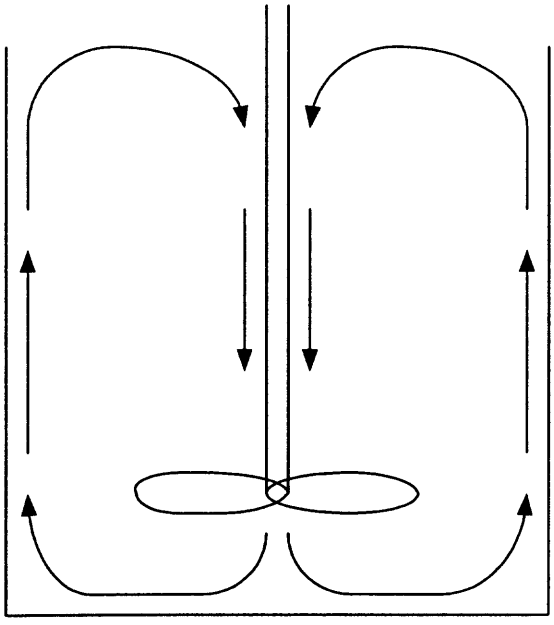

Figure 2.2 Axial Flow Pattern.

2.2 Power Number Theory

A number of investigators have reported impeller power characteristic in terms of two dimensionless groups, the Power Number, N_p, and the impeller Reynolds Number, Re. White and his coworkers (1934) were the first to point out the possibility and advantage of correlating impeller power using dimensional analysis. A general power relationship as a function of physical and geometrical parameters was reported as the following (Rushton, 1950; Bates et al., 1963):

$$\frac{P}{\rho N^3 D^5} = k \left(\frac{\rho N D^2}{\mu}\right)^a \left(\frac{N^2 D}{g}\right)^b \left(\frac{T}{D}\right)^c \left(\frac{H}{D}\right)^d \left(\frac{C}{D}\right)^e \left(\frac{p}{D}\right)^f \left(\frac{W}{D}\right)^g \left(\frac{L}{D}\right)^h \left(\frac{n_2}{n_1}\right)^i \qquad (2.5)$$

where the group on the left hand side is called the impeller power number, N_p. The first group on the right hand side is known as the impeller Reynolds Number, Re, and the second group is known as the Froude Number, N_{Fr}. The remaining terms account for the effects of the tank geometry and impeller configuration. The Reynolds Number describes the hydrodynamic effect in the system. The Froude Number accounts for the effect of vortex in swirling systems. Bates et al. (1963), also pointed out that Equation 2.5 should be expanded to include baffle number and width, spacing between impellers, and off–center impeller location. All of these additional geometrical parameters may be included in a form similar to that in Equation 2.5.

Chudacek (1985) proposed that the effect of vessel bottom shapes should be included in the above analysis, because the vessel bottom shape represents a significant geometrical factor with respect to the recirculation pattern and is also likely to influence the impeller power consumption.

However, the full form in Equation 2.5 is seldom used in practical power calculation. If geometrical similarity is assumed and if no vortex is present, Equation 2.5 reduces to

$$N_p = k\,(Re)^a \tag{2.6}$$

Furthermore, if the mixing process is carried out in a baffled tank in the turbulent regime (McCabe & Smith) and for a given geometry of configuration, Equation 2.6 reduces to

$$N_p = \frac{P}{\rho N^3 D^5} = \text{constant} \tag{2.7}$$

Therefore, the dimensionless power number, N_p, represents an important parameter, since its knowledge enables the designer to predict the impeller power requirement for a given mixing condition.

2.3 Power Dissipation and Power Relationships

2.3.1 Power Dissipation in Liquid Dispersions

The power consumed in mixing processes is the energy per unit time, which is transferred from the impeller to the fluid. Power is one of the most important fundamental parameters associated with the intensity of mixing and completeness of dispersion. The power consumption in agitated vessels is a function of impeller type, agitation speed, the physical properties of the fluid being mixed, and the geometric characteristics of the impeller and the system. Several investigators studied the power required to attain certain mixing conditions.

The action of a turbine or propeller in a Newtonian liquid of low viscosity can be likened to that of the impeller in a radial or axial flow pump, respectively. The use of flow rate (or discharge), Q, from a pump and the fluid head, h, is well known. Thus for a pump of unit efficiency these variables can be related to the power input:

$$P = \rho Qgh \tag{2.8}$$

For a mixing vessel, a given input of power, P, to the impeller creates a 'flow rate' Q (and thus a circulation throughout the vessel) and a 'head h' which is dissipated on circulation through the vessel. For low–viscosity liquids the head can be thought of in terms of the turbulence, which is generated. This is most intense in the region of the impeller and decays in regions away from impeller.

These regions of high intensity of turbulence are suitable for 'dispersive' processes such as liquid–liquid, gas–liquid contacting and for promoting mass transfer. It is desirable to 'circulate' the liquid through the regions of high intensity of turbulence as frequently as possible. Thus mixing in low–viscosity systems is seen to be influenced by:

1. intensity of turbulence
2. rate of circulation

Good impeller selection will ensure that the power input to the agitator provides the correct balance between flow and head.

2.3.2 Power Dissipation in Single–Impeller Systems

Agitation systems consisting of a single impeller and a mixing vessel with various impeller–tank geometries have been studied extensively, especially disc turbines (DTs) in vessels of standard geometry and in low viscosity fluid (Hudcova et al., 1989). Many

investigators have experimentally determined the power characteristics and behavior of single impeller systems. All the results so obtained indicate that the impeller power number, N_p, reaches a constant value, for a given geometry (McCabe & Smith), if the agitation intensity is high enough to produce turbulent flow (associated with Re > 10,000).

White and Brenner (1934) were the first to determine the various power law exponents by dimensional analysis. They found the drag coefficient group ($Pg_c/\rho N^3D^5$), called the power number, N_p, and proposed that this dependent variable characterizes the flow pattern. Their final power correlation was given as:

$$\frac{P}{D\mu N^2 T^{1.1} W^{0.3} H^{0.6}} = 0.000129 \left(\frac{\rho N D^2}{\mu} \right)^{0.88} \tag{2.9}$$

This equation fitted the data for Reynolds numbers from 10^4 to 10^5 but diverged from the data for Reynolds numbers below 10. They showed that viscosity has a minor effect on the power consumed in turbulent regimes.

Rushton, Costich and Everett (1950) studied the power characteristic of mixing impellers using five impeller types of diameters from 0.06 m to 1.2 m. They used baffled and unbaffled configurations, vessels of diameters from 0.2 m to 2.5 m, and fluids of viscosity from 0.001 kg/m-sec to 40 kg/m-sec. They obtained a correlation, using dimensional analysis, for the power number, N_p, in terms of the impeller Reynolds number, Re. Their correlation is:

$$N_p = k\,(Re)^m \tag{2.10}$$

O'Connell and Mack (1950) investigated the power relationship for flat–blade turbines by varying the number of blades and impeller width–length ratios in both the

laminar and turbulent regions under fully baffled conditions. In the laminar region, they found that:

$$\frac{Pg_c}{\rho N^3 D^5} = k\left(\frac{\mu}{\rho N D^2}\right)\left(\frac{W}{D}\right)^b \tag{2.11}$$

and in the turbulent regime (Re > 10,000):

$$\frac{Pg_c}{\rho N^3 D^5} = k\left(\frac{W}{D}\right)^b \tag{2.12}$$

Nagata et al. (1957) [from Tatterson, 1991] obtained an equation for N_p in the turbulent region for fully baffled tanks:

$$N_p = \frac{A}{R} + B\left(\frac{H}{T}\right)^{(0.35 + W/T)} \tag{2.13}$$

where A, B, and R were determined from:

$$A = 14 + \left(\frac{W}{T}\right)\left[70\left(\frac{D}{T} - 0.6\right)^2 + 185\right] \tag{2.14}$$

$$\log_{10}(B) = 1.3 - 4\left(\frac{W}{T} - 0.5\right)^2 - 1.14\left(\frac{D}{T}\right) \tag{2.15}$$

$$R = \frac{25(D/T - 0.4)^2}{W/T} + \left(0.11 - \frac{0.0048T}{W}\right)^{-1} \tag{2.16}$$

Bates et al. (1963) reported a conventional log–log plot of the simplified power equation for some impeller types under the "standard conditions", D/T=1/3, C/T=1/3, H/T=1. The value of N_p that they reported for DTs was 4.8 for four T/12 baffles and 5.0 for four T/10 baffles. Flat–blade turbines (FBTs) and curved–blade turbines (CBTs) were shown, from the plot, to have similar power numbers in the turbulent region, while PBTs

consumed the least power. Their measurements showed that the impeller off–bottom clearance has a definite effect on power consumption.

O'Kane (1974) investigated the effect of blade width and number of blades on power consumption. He demonstrated that it was not possible to find a value of exponents in the generalized power relationship, which could be applied to all types of impellers. The power number obtained at standard conditions for a DT and a 45^{o} PBT with six blades was 5.05 and 1.52, respectively.

Gray et al. (1982), proposed a power correlation for DTs with six flat blades. The result was a constant power number of 5.17 representing the data for C/D > 1.1. For C/D <1.1, N_p varied with $(C/D)^{0.29}$. The baffling effect was found to be negligible over the range of standard size baffling, $1/12 \leq W/T \leq 1/10$. The effect of D/T was small under these conditions.

Chudacek (1985) conducted a power study in profiled bottom vessels. For the standard flat bottom vessel, the 45^{o} PBT exhibited a power number of 1.63.

Rao and Joshi (1988) studied the flow pattern and power consumption in liquid phase mixing with DTs, PBTs (down flow and up flow). For the case of DT, the measured power numbers were 5.18 and 4.40 for clearances equal to T/3 and T/6, respectively. At lower clearance, the impeller pumping action was greater, thereby increasing the power consumption. For the case of PBT (down flow), when the clearance was decreased from T/3 to T/4 and further to T/6, an increase in the value of N_p equal to 1.29, 1.35, and 1.61, respectively, was observed. Their reports also pointed out that the PBT (down flow) with D/T=1/3 was found to be most energy efficient out of all PBT impellers.

Rewatkar et al. (1990), conducted a series of measurements using PBT impellers and compared them to DT impellers. A number of geometrical factors, D, W, H, C, blade angle, and blade thickness, were studied in detail. The power number of the standard DTs (D/T=1/3, C=D) and PBTs was found to be 5.18 and 1.67, respectively. The power number was observed to have a strong dependence on the flow pattern generated by the impeller. In general, N_p decreased when the clearance was more than T/4 because of surface tension. Without the effect of surface tension, the liquid height was found to have little effect on power consumption. Rewatkar et al. (1990), obtained an overall correlation for the impeller power number for PBT:

$$N_p = 0.653 \left(\frac{T}{D}\right)^{0.11} \left(\frac{C}{T}\right)^{-0.23} \left(n_b\right)^{0.68} (A)^{1.82} \qquad (2.17)$$

for $3 \leq T/D < 6$, W/D=0.3, H/T=1, $0.125 \leq C/T \leq 0.33$, $0.5 \leq A$ (impeller blade angle, radian) ≤ 1.05, $4 \leq n_b \leq 8$.

CHAPTER 3

EXPERIMENTAL APPARATUS AND PROCEDURE

3.1 Apparatus and Material

A schematic of the basic experimental set–up is shown in Figure 3.1. The work was carried out in an open, flat–bottomed, cylindrical, Plexiglas vessel with different liquid height to tank diameter ratios (H/T) and impeller off–bottom clearances (C). Table 3.1 gives the vessel dimensions.

Table 3.1 Vessel Dimensions

Diameter, T (m)	0.286
Height, T_0 (m)	0.483
Number of Baffles, N_B	4 (90^O apart)
Baffle Thickness, $B_{thickness}$ (m)	0.006
Baffle Height, B_{height} (m)	0.483
Baffle Width, B (m)	0.028
Baffle Clearance from the tank wall, B_C (m)	0
Material of Construction	Plexiglas

All the experiments were performed at room temperature (23–25 ^oC). The fluids used in this work were mineral oil (Sigma-Aldrich, Inc.) and distilled water. The ratio of mineral oil to distilled water was always 10 % (v/v). The physical properties of the fluids at 25 ^oC are given in Table 3.2. The mean density and a mean viscosity used in correlating the power consumption were calculated from (Laity and Treybal, 1957):

$$\rho_{mean} = V^*\rho_d + (1-V^*)\rho_c \tag{3.1}$$

$$\mu_{mean} = \frac{\mu_c}{1-V^*}\left(1+\frac{1.5\mu_d V^*}{\mu_d+\mu_c}\right) \tag{3.2}$$

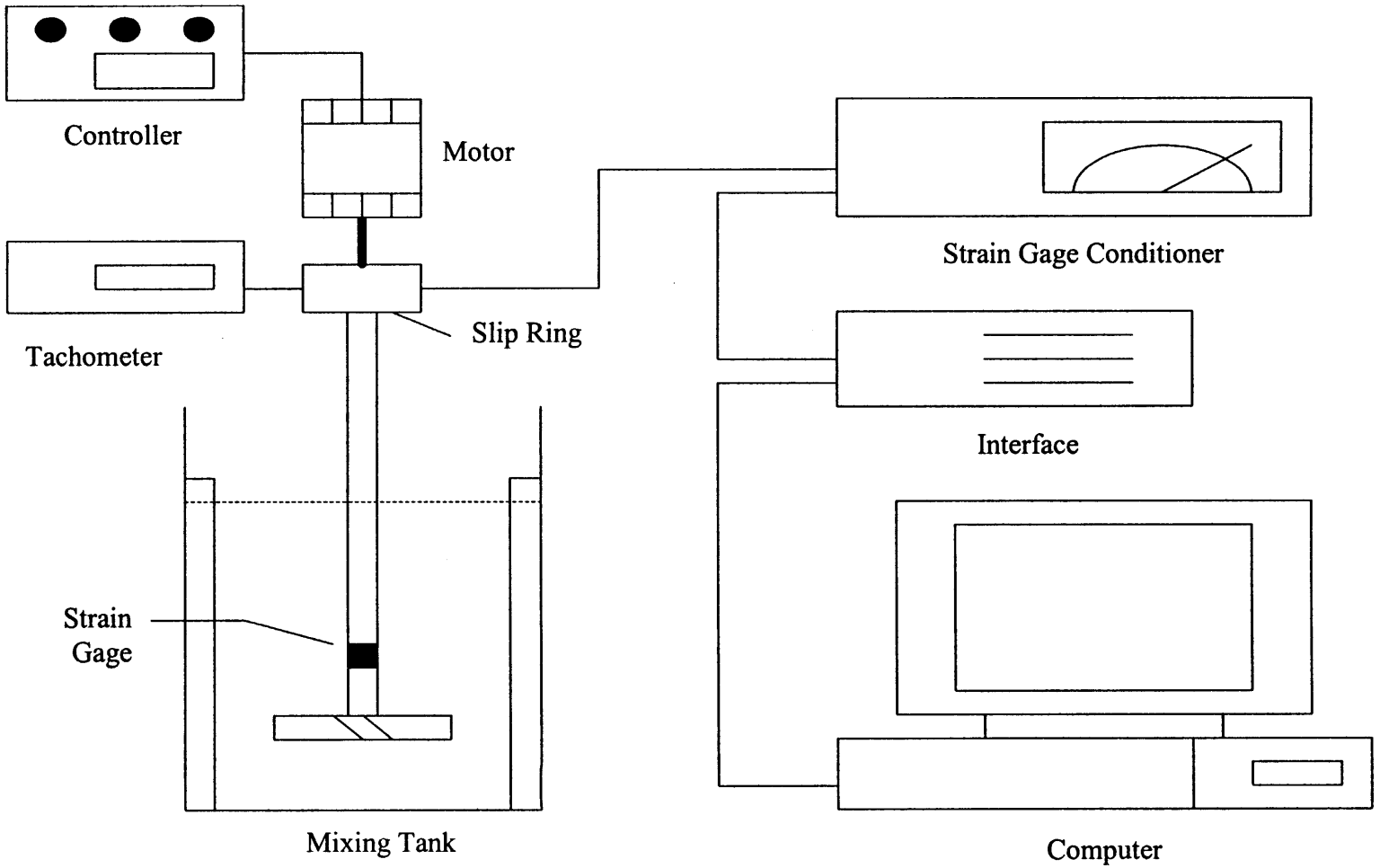

Figure 3.1 Experimental Set-up.

Table 3.2 Fluid Properties

Fluid	Volume Fraction, V* (%)	Density, ρ (Kg/m^3)	Viscosity, μ (Kg-m/sec)	Surface Tension or interfacial tension, σ ($Joule/m^2$)
Mineral oil, White, light	10	838	0.085	0.031
Distilled Water	90	1000	0.000862	0.069
Oil-water interfacial tension	-	-	-	0.034

The values of surface tension for oil and water, as well as the oil-water interfacial tension were obtained using a Cenco-DuNouy tensiometer (Table 3.2). Two types of impellers, i.e. disc turbine (DT) and 45° pitched–blade turbine (PBT, pumping downward) were used in the experiments. Their shapes and dimensions are listed in Table 3.3. A schematic of impellers used is shown in Figure 3.2.

Table 3.3 Impeller Dimensions

Impeller Properties	DT (m)	PBT (m)
Diameter (D)	0.102	0.102
Blade Length (L)	0.025	0.038
Blade Height (b)	0.019	0.015
Blade Thickness (W)	0.0012	0.0015
No. of Blades (N_{bl})	6	6
Disk Diameter (D_{disk})	0.076	-
Disk Thickness (t_{disk})	0.0015	-
Total Height of Impeller (H_{total})	0.035	0.0254
Height of Hub (H_{hub})	0.025	0.011
O.D. of Hub ($H_{O.D.}$)	0.025	0.025
I.D. of Hub ($H_{I.D.}$)	0.0123	0.013

All impellers had six blades and a bore diameter of 0.0127 m. The off–bottom clearance (C), liquid height (H) and type of impeller were varied with each experiment. The impeller off–bottom clearance (C) was measured from the vessel bottom to the middle of the impeller. A schematic of the stirred vessel (DT) is shown in Figure 3.3.

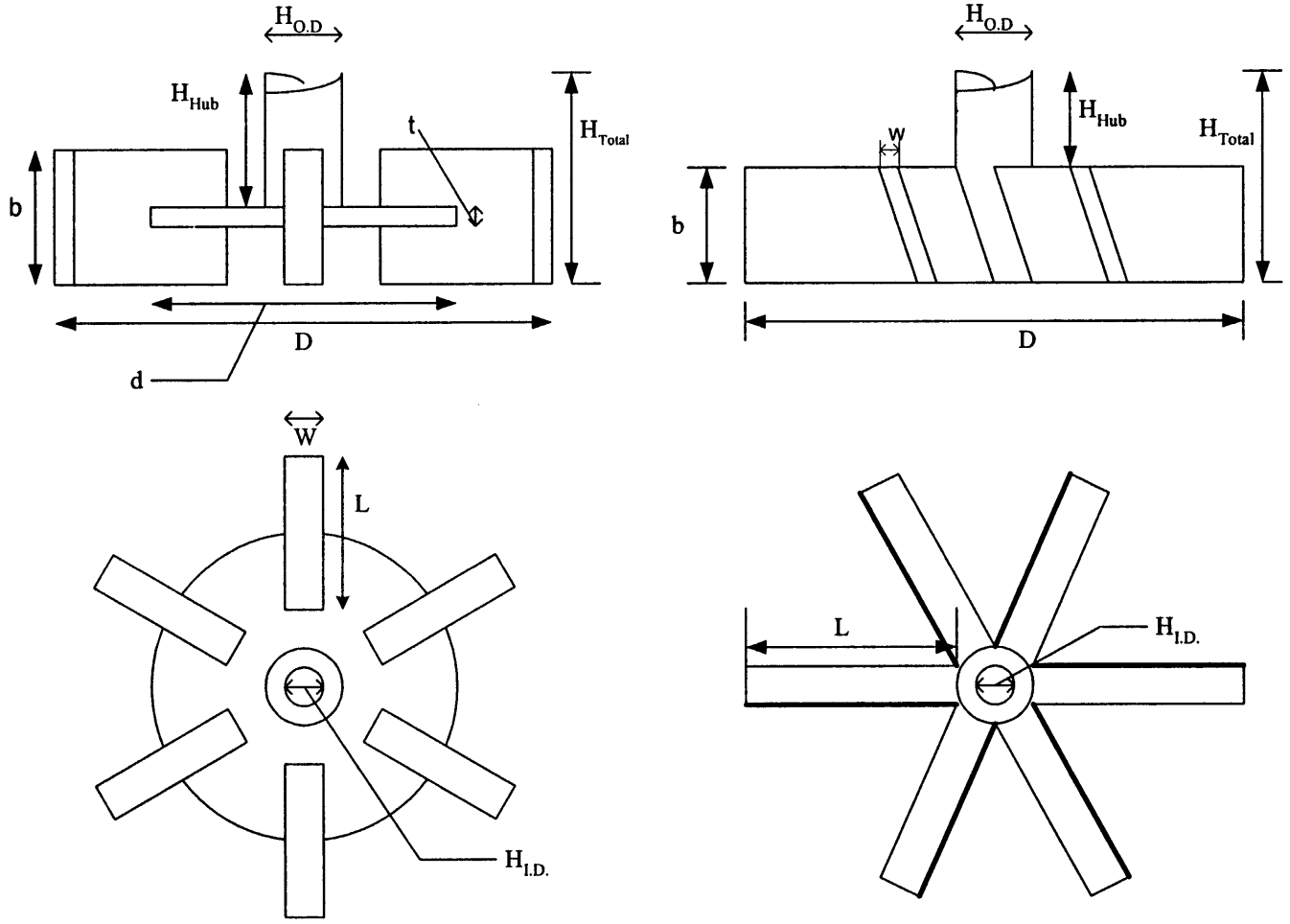

Disk Turbine

45^{O} - Pitched Blade Turbine

Figure 3.2 Impeller Properties.

The experimental system consisted of a variable speed reversible motor (G.K. Heller Corp., Floral Park, NY) with a maximum speed of 2,000 rpm. The rotational speed was measured independently using a digital tachometer with a photoelectric sensor (Cole-Parmer, Chicago, IL) and was accurate within ± 1 rpm. Three strain gages (Measurements Group Co., Raleigh, NC, Part No.CEA-06-18UV-350) were mounted on an aluminum hollow shaft having an O.D of 0.0095 m and a wall thickness of 0.00165 m. Before attaching the strain gages to the shaft, metal collars having an internal diameter equal to the O.D of the shaft and an external diameter equal to the bore diameter of the impellers were slid onto the shaft between the points where the strain gages were to be inserted. After attaching the strain gages, these collars, having a length of 0.0254 m, could be moved along the shaft between the two strain gages. This arrangement was designed so that the impellers could be mounted on the shaft without touching the protruding strain gages. In addition, this arrangement enabled the impeller–collar assemblies to be moved along the shaft thus permitting to vary the distance between impellers. The experiments were carried out using a 0.838 m long shaft. The locations of top, middle and bottom strain gage were 0.49 m, 0.34 m and 0.03 m from the open end of the shaft, respectively.

The strain gages were connected with insulated lead wires passing through the hollow core of the shaft to a signal conditioner and an amplifier system (2120A system, Measurement Group Co., Raleigh, NC). A data acquisition system (Labtech Notebook) connected to a computer was used to analyze the gage signal (mV) from the strain gage conditioner, receive the signal from the tachometer, and calculate the power drawn by each impeller. Each strain gage measured the cumulative torque produced by all

impellers below it. The power drawn by the impeller was determined using the following equation:

$$P = \omega \cdot \tau = 2\pi N \cdot \tau = N \cdot K \cdot mV \tag{3.3}$$

where:

P is the power drawn by the impeller in watt;

ω is the angular velocity rad/s;

τ is the actual torque produced by the impeller N–m;

N is the agitation speed in rps;

mV is the signal corresponding to Strain Gages #1 in millivolts;

K is the proportionality factor for Strain Gages #1;

The sampling frequency of the data acquisition system was 1 Hz, and the representative power drawn was determined by calculating average of 60 readings. The corresponding Power Number, N_p, was calculated with the following equation (Rushton et al., 1950):

$$N_p = \frac{P}{\rho_{mean} N^3 D^5} \tag{3.4}$$

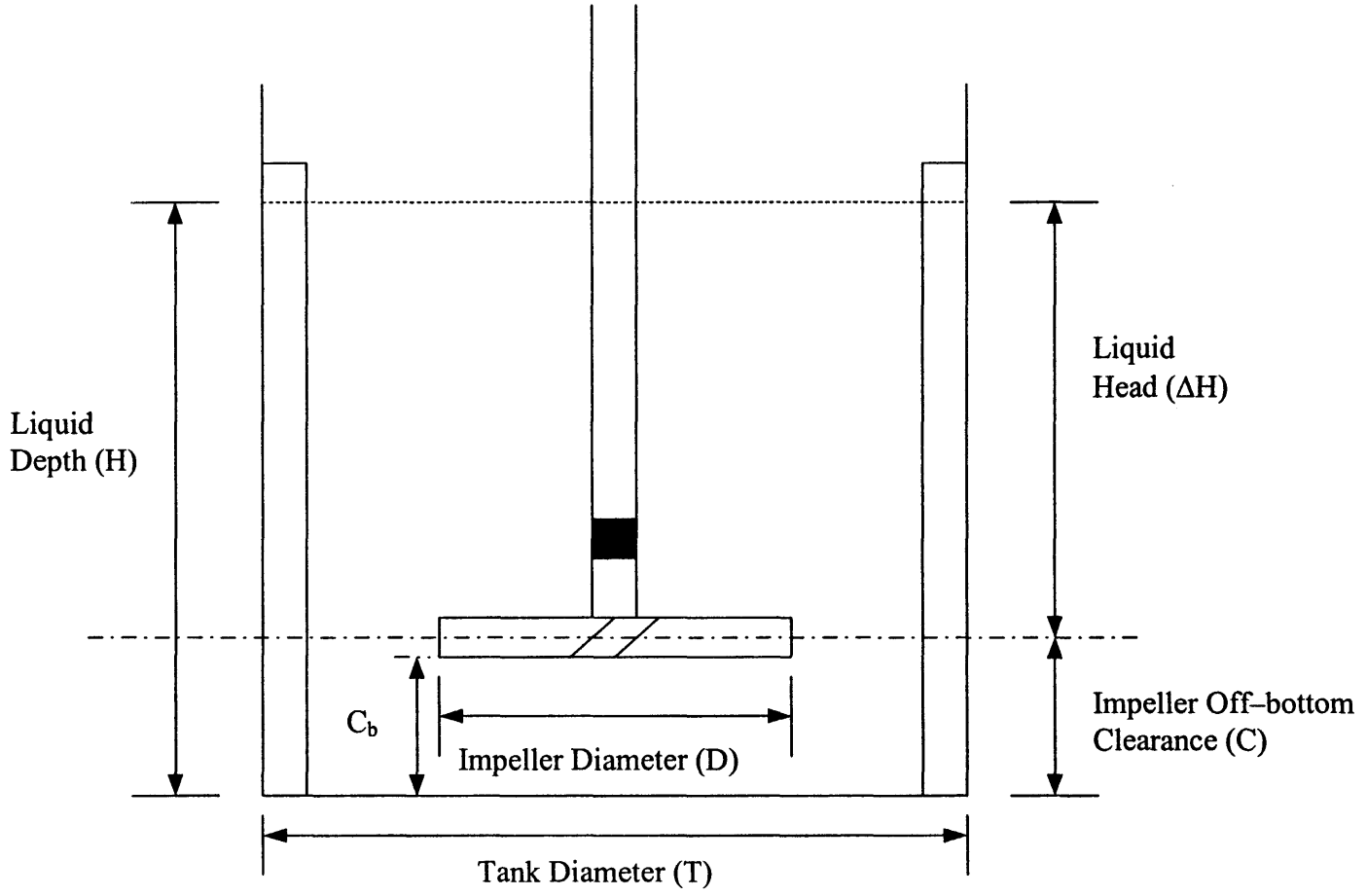

Figure 3.3 Tank Properties.

3.2 Experimental Procedure

The tank was filled with distilled water at the desired liquid height-to-tank diameter ratio (H/T) ranging from 0.088 to 1. The impeller off–bottom clearance was varied from C=0.0254 m to C=0.1016 m (corresponding to C_b/T=0.055 and C_b/T=0.322 for DT and C_b/T=0.037 and C_b/T=0.304 for PBT, respectively) for all H/T ratio from 0.088 to 1. The tank was located on a platform that could be translated vertically so that the distance between the (fixed) shaft with the impeller mounted on it and the tank bottom could be varied. Then, the tank was placed in its final position. The shaft was centrally located in the tank and was connected to the motor. The strain gages were connected with wires through the hollow core of the shaft to a slip ring. The slip ring, which was also mounted on the shaft, was connected to the external gage conditioner and amplifier. An optical sensor with a tachometer was used to measure the agitation speed. All experiments were carried out using a single impeller only.

The data acquisition system was used to collect data on line and to analyze all the signals from the strain gages and the optical sensor. The sampling frequency was 1 Hz for the duration of 60 seconds. The representative power drawn was determined by the average of 60 readings. The power consumed by impeller was determined using equation 3.3. The power consumption was measured at the minimum agitation speed, N_{cd}.

The sampling apparatus, shown in Figure 3.4, consisted of a glass tube, having an internal diameter of 0.004 m. The inlet point of the sampling tube was placed in the middle position between two baffles at a radial distance from the tank wall equal to 0.05 m and 0.08m from the tank bottom. The sampling point location was varied only in the cases where liquid depth was too low. The sampling tube was connected to series of

flasks and hooked to a vacuum system. Several valves were used to divert the flow from the vessel to either a reservoir or a graduated cylinder. In all experiments, the continuous phase was always water. The dispersed phase was always mineral oil.

3.3 Sampling Procedure and Visual Observation Method

The sampling procedure was as follows. The tank was charged with distilled water followed by mineral oil. The dispersed phase was always 10 % by the volume of the total liquid mixture. The combined height of the liquid phases was varied after each single run. After setting up the apparatus, the motor was started at a fairly low agitation speed. After an equilibrium period varying between 10 and 15 minutes, the vacuum system was activated by opening Valve C (Figure 3.4). Then, Valve A was opened so that the liquid would flow from the tank into the reservoir. This was done to ensure that the liquid initially contained in the sampling tube would not be included in the sample. When 30-50 ml of dispersion had accumulated in the reservoir, Valve A was closed and Valve B was opened, allowing the flow to be diverted to the graduated cylinder until some 100 ml were collected. The operation typically lasted only about ten seconds. The last bottle in the line was added only to protect the vacuum system from receiving any liquid. The sample so taken was allowed to separate into two phases, and the fraction of the dispersed phase was determined. Then, all liquid samples were returned to the tank. The same procedure was repeated until no dispersed phase was observed at the top of the continuous phase. In addition, the minimum agitation speed in correspondence of the complete dispersion state was determined in each experiment by visual inspection of the tank. The visually determined value for N_{cd}, $N_{cd\text{-}vis}$, was defined as the minimum agitation

visually determined value for N_{cd}, $N_{cd\text{-}vis}$, was defined as the minimum agitation speed at which no dispersed phase was observed at rest at the top of the continuous liquid phase.

In most of experiments, small pockets of fluid were observed near the baffle corners and around the impeller shaft. However, the presence of these pockets was neglected when $N_{cd\text{-}vis}$ was determined, since they were observed even at agitation speed much higher than $N_{cd\text{-}vis}$.

The same procedure was repeated at various liquid height-to-tank diameter ratios (H/T) and different impeller off–bottom clearances (C).

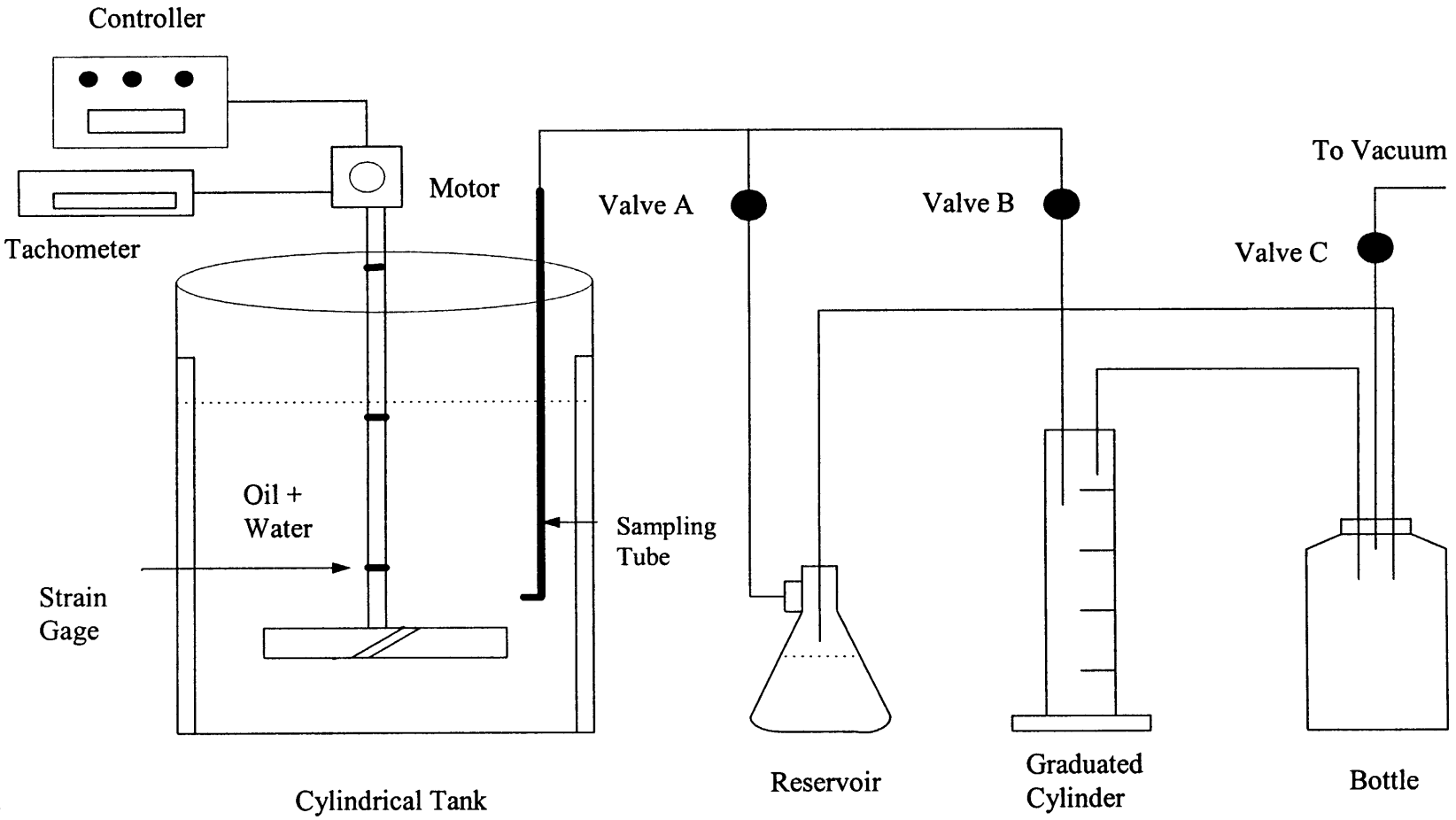

Figure 3.4 Sampling Procedure.

CHAPTER 4

SAMPLING METHOD FOR DETERMINATION OF N_{cd}

4.1 Determination of N_{cd-smp}

A survey of the literature shows that the visual method has been the most commonly used technique to determine the minimum agitation speed, N_{cd}, to completely disperse two immiscible liquids. According to the visual observation method, the minimum agitation speed is defined as the agitation speed at which no dispersed phase (the lighter phase) is observed at the top of the tank. At N_{cd}, the dispersed phase becomes completely incorporated into the continuous phase. However, an alternative method has been developed for the determination of the minimum agitation speed for complete liquid–liquid dispersion in mechanically agitated vessels (Armenante and Huang, 1992). The results that these authors obtained indicate that this method for determining N_{cd} has some significant advantages over the commonly used visual method, such as the reproducibility of the results obtained independently of the observer, and the applicability of the method to situations where visual inspection is impossible.

The method is based on the collection of samples from the bulk of the mixture at different agitation speeds. The volume fraction of the dispersed phase in the sample, V*, is then determined by allowing the sample to settle in a graduated cylinder. Then V* (expressed in %) can be calculated as the ratio of the volume of the dispersed phase to total liquid volume of the sample.

It was observed that when, in a given experiment, V* was plotted against the agitation speed, N, a sharp change in the slope of the resulting plot occurred just before

observing the visually determined minimum agitation speed, N_{cd-vis}. This can be seen in Figures 4.1 and 4.2. Figure 4.1 shows the case in which a sharp change in slope was observed, but in which V* never had a maximum value (No-Max Case). On the other hand, Figure 4.2 shows the case in which V* increases until a certain point and then starts to decrease. (Yes-Max Case). In order to distinguish the value of N_{cd} so obtained from that obtained using the visual method, the corresponding variables are labeled N_{cd-smp} (for sampling) and N_{cd-vis} (for visual).

N_{cd} Determination: No-Max Case

For the case of no maximum point, the following function was derived from V*=f (N):

$$\phi(N)=\frac{f''(N)}{f'(N)}$$

where f'(N) and f''(N) represent the first and second derivatives of f(N), respectively. The ratio Φ(N) is the rate of change of the slope (f'' (N)) with respect to the slope itself. The rate of change of slope will be maximum (in absolute value) when:

$$\Phi'(N)=0$$

The value of N in correspondence of which Φ'(N)=0 is taken to be the value of N_{cd}. Additional details of this rationale are given elsewhere (Armenante and Huang, 1992). Since V* increases with N at a declining rate in the neighborhood of N_{cd} the function Φ(N) must be negative in correspondence of this point. The numerical approach applied here is further illustrated in following example for Figure 4.1 and calculations are summarized in Table 4.1.

The variables were numerically calculated as follows:

$$f'(N)=\frac{V^*_2-V^*_1}{N_2-N_1}$$

$$f''(N) = \frac{f_2'(N) - f_1'(N)}{N_2 - N_1}$$

$$\phi(N) = f''(N) / f'(N)$$

$$\phi'(N) = \frac{\phi_2(N) - \phi_1(N)}{N_2 - N_1}$$

Table 4.1 N_{cd} Determination: No-Max Case

N (rpm)	V* (%)	f'(N)	f''(N)	Φ(N)	Φ'(N)
50.00	0.0	0.0	0.0	0.0	0.0
100.00	3.84	0.0768	0.0015	0.0200	0.0004
120.00	2.86	-0.0490	-0.0063	0.1284	0.0054
140.00	3.75	0.0445	0.0047	0.1051	-0.0012
165.00	6.93	0.1272	0.0033	0.0260	-0.0032
175.00	9.82	0.2890	0.0162	0.0560	0.0030

N_{cd} Determination: Yes-Max Case

In the case of V* having a maximum point, $N_{cd\text{-}smp}$ was determined by imposing that the derivative of the resulting interpolation function, f'(N) is equal to zero. Additional details of this rationale for this method are given elsewhere (Armenante and Huang, 1992). The method for the case of maximum is illustrated in Figure 4.2 and calculations are summarized in Table 4.2.

Table 4.2 N_{cd} Determination: Yes-Max Case

N (rpm)	V* (%)	f'(N)
150	0	0
200	1.92	0.0384
250	5.94	0.0804
300	9.8	0.0772
350	9.09	-0.0142

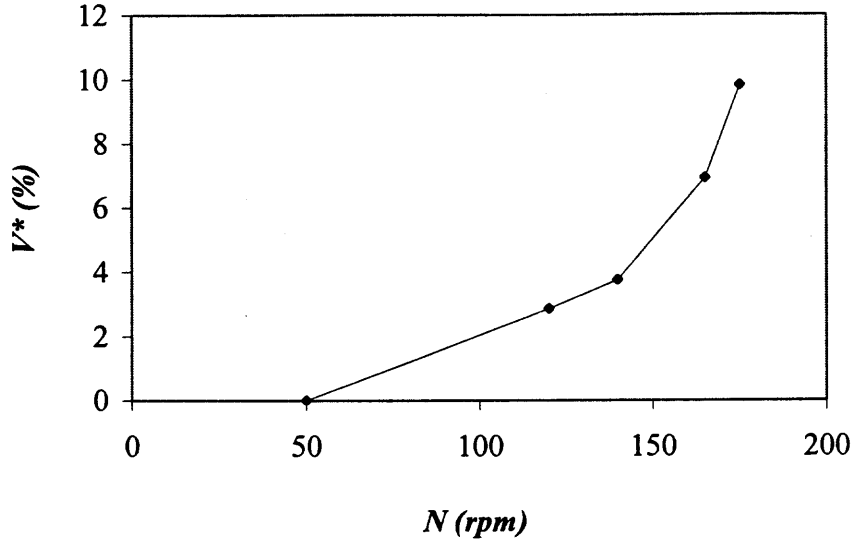

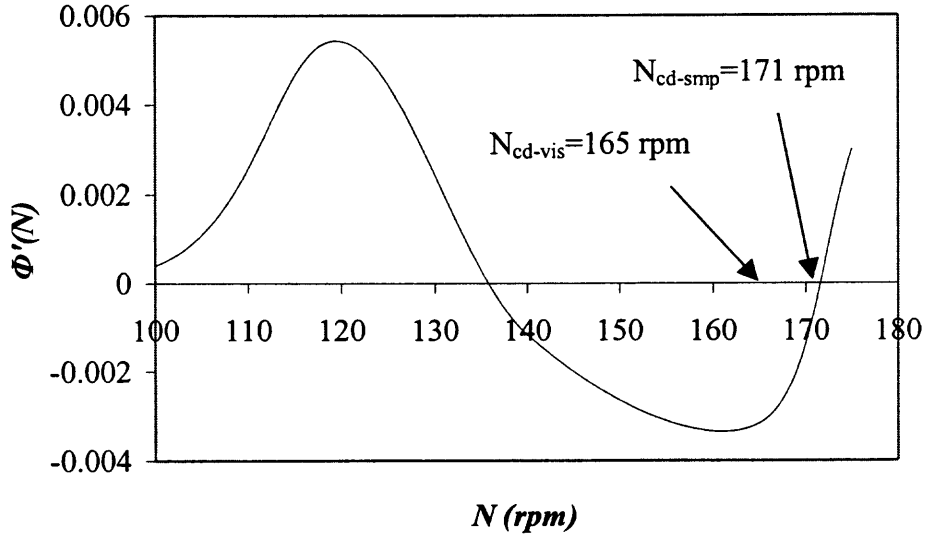

Figure 4.1 N_{cd} Determination: No – Max Case.

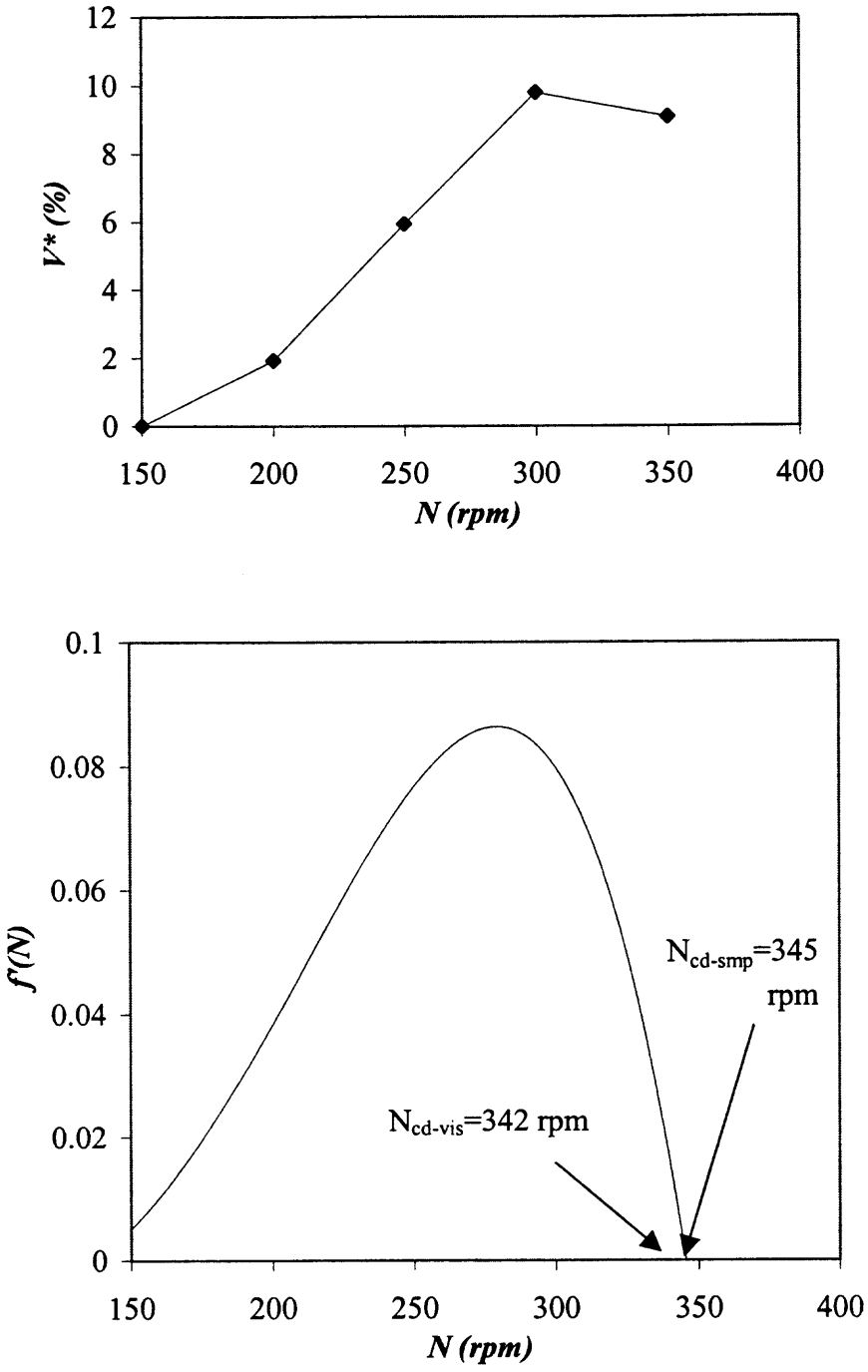

Figure 4.2 N_{cd} Determination: Yes – Max Case.

4.2 Validation of Visual Observation Method

In order to validate the method to obtain $N_{cd\text{-}vis,}$ the values of $N_{cd\text{-}smp}$ obtained in each experiment were plotted against the corresponding values of $N_{cd\text{-}vis}$. Each value of N_{cd-smp} was obtained by generating a plot, as described above, containing 5–6 experimental points. A parity plot of N_{cd-smp} (with or without maximum) against the corresponding N_{cd-vis} values is shown in Figure 4.3. From this figure, one can see that a good agreement between N_{cd-vis} and N_{cd-smp} exist. The results are given in Table B.17.

4.3 Reproducibility

A number of identical experiments were repeated at different times in order to determine the reproducibility of the results for $N_{cd\text{-}vis}$. The results are reported in Table B.18, and are expressed as the ratio of the standard deviation and the mean (for each set of data). The reproducibility was obtained for each type of impeller at various off-bottom clearances. The results are summarized in Table 4.3.

Table 4.3 Reproducibility of Experimental Results

Minimum Agitation Speed	DT	PBT
$N_{cd\text{-}vis}$	± 3.17 %	± 3.08 %

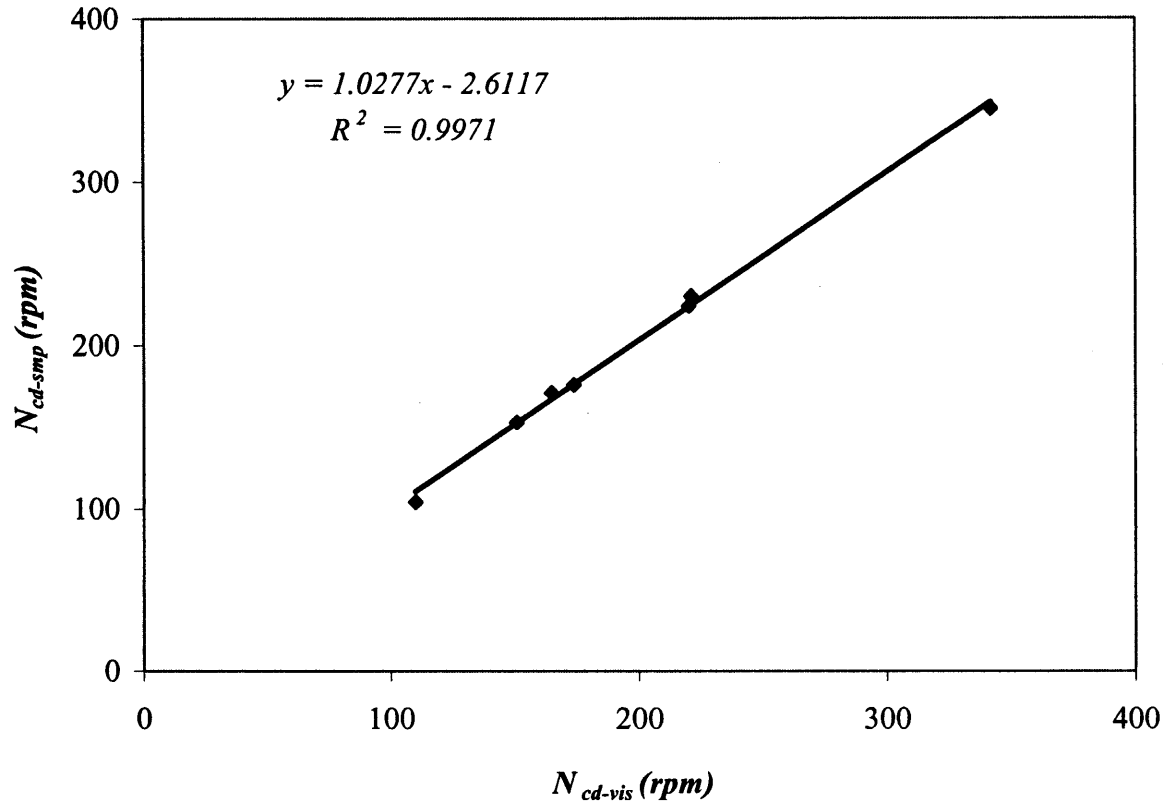

Figure 4.3 Comparison of $N_{cd\text{-}smp}$ vs. $N_{cd\text{-}vis}$.

CHAPTER 5

RESULTS AND DISCUSSION

A total of 76 experiments were conducted using the disc turbine (DT) and the 45° pitched–blade turbine (PBT). Both $N_{cd\text{-}vis}$ and $N_{cd\text{-}smp}$ were determined for each experiment. The power consumption was measured, as described in section 3.1. The D/T ratio was constant and equal to 0.352 in all experiments. The liquid depth (H) was varied from 0.0254 m to 0.286 m in 0.0254 m increments. The impeller off–bottom clearance (C_b) was varied from 0.0159 m to 0.092 m for DT and 0.011 m to 0.087 m for PBT in 0.0254 m increments. The results were interpreted by plotting the minimum agitation speed (N_{cd}), power (P), power/volume (P/V), and power number (N_p). Each of these variables was plotted against the liquid depth-to-tank diameter ratio (H/T), the impeller off–bottom clearance-to-tank diameter ratio (C_b/T) and the liquid head-to-tank diameter ratio (ΔH/T). The liquid head is defined as the height of the liquid above the impeller. ($\Delta H = H - C_b$).

5.1 Results for Disk Turbine (DT)

5.1.1 Effect of Liquid Depth (H) on Minimum Agitation Speed (N_{cd})

The results obtained in this study for DT are shown in Figures A.1 and A.2 in Appendix A. They are presented in detail in Table B.1 and Table B.2 in Appendix B. At constant impeller off–bottom clearance (C_b), the minimum agitation speed (N_{cd}) required to achieve uniform dispersion increased with increasing liquid height (H/T). For C_b/T=0.322, the minimum agitation speed (N_{cd}) decreased, when H/T went from 0.799 to

1.0. At constant liquid depths (H/T), the minimum agitation speed (N_{cd}) required to achieve uniform dispersion generally decreased with increasing impeller off–bottom clearance (C_b/T). Deviations were observed from the normal behavior at H/T=1, where C_b/T was increased from 0.055 to 0.144. At constant impeller off–bottom clearance (C_b/T), N_{cd} increased with increasing liquid head ($\Delta H/T$). The value of N_{cd} was fairly constant for different off–bottom clearance at low liquid head. At high liquid head, a significant difference was observed. When the liquid level reached the middle of the impeller (C/H=1), no mixing was observed even at very high agitation speeds.

5.1.2 Effect of Liquid Depth (H) on Power (P) at N_{cd}

The results obtained in this study for DT are shown in Figures A.3 and A.4 in Appendix A. They are presented in detail in Table B.3 and Table B.4 in Appendix B. At constant impeller off-bottom clearance (C_b/T), the power (P) required to achieve uniform dispersion at N_{cd} increased with increasing liquid depth (H/T). For C_b/T=0.055 and C_b/T=0.322, power dropped from H/T=0.88 to H/T=1.0. For C_b/T=0.144 and C_b/T= 0.233, power required was almost similar for small liquid depths. At constant liquid depths (H/T), the power (P) dissipated decreased with increasing impeller off–bottom clearances (C_b/T). Deviations in this behavior were observed at off–bottom clearance (C_b/T) of 0.233 for lower liquid depths. From H/T=0.88 to H/T=1, the power increased by almost 100% from that of observed at H/T=0.88. With increasing liquid head ($\Delta H/T$), the power required to achieve uniform dispersion increased. The behavior was similar to that of liquid depths. The power requirement approached infinity for $C_b \rightarrow 0$.

5.1.3 Effect of Liquid Depth (H) on Power/Volume (P/V) at N_{cd}

The results obtained in this study for DT are shown in Figures A.5 and A.6 in Appendix A. They are presented in detail in Table B.5 and Table B.6 in Appendix B. Power/volume curves were plotted to verify that the difference in power observed was not attributed to the change in volume. The power per volume increased with increasing liquid height at constant off-bottom clearance. For $C_b/T=0.055$ and $C_b/T=0.322$, power per volume dropped from H/T=0.88 to H/T=1.0. For $C_b/T=0.144$ and $C_b/T=0.233$, power per volume required was almost similar for small liquid depths. At constant liquid depths, power per volume decreased with increase in impeller off–bottom clearance. Deviations in this behavior were observed at off–bottom clearance of 0.0762m for H/T=0.53 and H/T=0.62. At low liquid head ($\Delta H/T$), power per volume for all off–bottom clearance was almost similar. Significant difference in the value of power per volume observed at high value of liquid head.

5.1.4 Effect of Liquid Depth (H) on Power Number (N_p) at N_{cd}

The results obtained in this study for DT are shown in Figures A.7 and A.8 in Appendix A. They are presented in detail in Table B.7 and Table B.8 in Appendix B. The power number varied from a minimum of 3.18 to a maximum of 5.91. For $C_b/T=0.233$ and $C_b/T=0.322$, the power number dropped with decreasing liquid heights from H/T=0.62 to H/C=1. For H/T=0.71 and above, power number did not vary significantly at $C_b/T=0.233$ m and $C_b/T=0.322$. The power number remained almost constant for $C_b/T=0.055$ and $C_b/T=0.144$. At all values of the off–bottom clearance examined here, the power number remained almost constant for H/T=0.88 to H/T=1. At constant liquid depth, the power

number increased with increasing off– bottom clearance. The increase in power number was not significant. With increasing liquid head, the power number increased up to a certain value. After that, it remained nearly constant for constant off–bottom clearance.

5.2 Results for 45° Pitched Blade Turbine (PBT)

5.2.1 Effect of Liquid Depth (H) on Minimum Agitation Speed (N_{cd})

The results obtained in this study for PBT are shown in Figures A.9 and A.10 in Appendix A. They are presented in detail in Table B.9 and Table B.10 in Appendix B. The minimum agitation speed (N_{cd}) required to achieve uniform dispersion increased with increasing liquid depth at constant impeller off–bottom clearances. At higher liquid depth, N_{cd} increased significantly compared to that of low liquid depth. From H/T=0.621 to H/T=1, N_{cd} increased with increasing impeller off–bottom clearances (C_b/T). Deviations from this behavior were observed for C_b/T=0.126 from H/T=0.79 to H/T=0.88. For H/T=0.177 to H/T=0.532, the minimum agitation speed decreased with increasing impeller off–bottom clearances. The minimum agitation speed increased with increasing liquid head (ΔH/T). For all the off–bottom clearances examined here, the values of minimum agitation speed at low liquid head were fairly close to one another. The differences increased at higher liquid head. At constant liquid head (ΔH/T), the minimum agitation speed increased with increasing off–bottom clearances for H/T=0.621 to H/T=1. Deviations were observed for the remaining values of liquid head. When the liquid level reached the middle of the impeller (C/H=1), no mixing was observed even at very high agitation speeds. Although the interface appeared to be disrupted by the agitation produced by the impeller, the oil droplets did not reach to the bottom of the

tank. When the agitation speed was increased beyond this point, the shaft started vibrating around its axis and the liquid was splashed in the tank. However, no air entrainment was observed under this condition.

5.2.2 Effect of Liquid Depth (H) on Power (P) at N_{cd}

The results obtained in this study for PBT are shown in Figures A.11 and A.12 in Appendix A. They are presented in detail in Table B.11 and Table B.12 in Appendix B. The power dissipated increased with increasing liquid height for H=C to H/T=0.88 for all off–bottom clearance examined. The differences in the value of power for all off–bottom clearances was similar for H=C to H/T=0.88. From H/T=0.88 to H/T=1, the power increased by almost 100% from that of observed at H/T=0.88. From H/T=0.177 to H=0.62, the power decreased with increase in impeller off–bottom clearance. From H/T=0.62 to H/T=1, the power decreased with increasing off–bottom clearances. The power increased with increasing liquid head (ΔH/T) for all values of the off–bottom clearance (C_b/T) examined. The differences in the value of power for low liquid head were smaller compared to high liquid head for impeller off–bottom clearance from C_b/T=0.037 to C_b/T=0.215. The difference in the value of power became significant for C_b/T=0.304, when compared to the values obtained at C_b/T=0.037, C_b/T=0.126, and C_b/T=0.215. The power requirement was infinitely large at H=C. No mixing was observed, even when agitating at very high speeds.

5.2.3 Effect of Liquid Depth (H) on Power/Volume (P/V) at N_{cd}

The results obtained in this study for PBT are shown in Figures A.13 and A.14 in Appendix A. They are presented in detail in Table B.13 and Table B.14 in Appendix B. Power/volume increased with increase in liquid height for all impeller off–bottom clearance. It increased significantly from H/T=0.088 to H/T=1. At H/T=0.88 and H/T=1, the value of power/volume obtained for C_b/T=0.037, C_b/T=0.126, and C_b/T=0.215, did not vary significantly from one another. From H/T=0.177 to H/T=0.71, the power/volume decreased with increasing impeller off–bottom clearances. From H/T=0.71 to H/T=1, the power/volume increased with increasing impeller off–bottom clearances. Deviations in this behavior were observed at particular combination of the impeller off–bottom clearance and liquid depth. The power/volume increased with increasing liquid head for all off–bottom clearances. For H/T=0.53, the power/volume decreased with increasing off–bottom clearances. From H/T=0.62 to H/T=1, the power/volume decreased with increasing impeller off–bottom clearances at C_b/T=0.037, C_b/T=0.126 and C_b/T=0.215. From C_b/T=0.215 to C_b/T=0.304, the power/volume increased at all liquid heights examined.

5.2.4 Effect of Liquid Depth (H) on Power Number (N_p) at N_{cd}

The results obtained in this study for PBT are shown in Figures A.15 and A.16 in Appendix A. They are presented in detail in Table B.15 and Table B.16 in Appendix B. The power number obtained at different combinations of liquid depth and impeller off–bottom clearance varied from 0.97 to 2.02. Fluctuations were observed at small liquid height (H/T) up to 0.355 for C_b/T=0.037. The power number did not vary significantly

with increasing liquid height at constant impeller off–bottom clearance. For all the cases examined, the power number decreased with increasing impeller off–bottom clearances. Deviation from this behavior was observed at $C_b/T=0.304$ and $H/T=0.71$, which yielded higher power number than at $C_b/T=0.215$ and $H/T=0.88$. The power number remained almost constant with increasing liquid head ($\Delta H/T$) at constant impeller off–bottom clearances. At constant liquid head, the power number decreased with increasing impeller off–bottom clearances. At higher liquid heads, the power number followed the same behavior at all impeller off–bottom clearance examined here.

5.3 Comparison of Results for DT vs. PBT

5.3.1 Minimum Agitation Speed (N_{cd})

A comparison between the results for N_{cd} obtained for DT and PBT is shown in Figures A.17, A.18, A.19, A.20, A.21, A.22, A.23, and A.24 in Appendix A. At constant off–bottom clearance (C), N_{cd} was plotted versus liquid depth (H/T) for DT and PBT to compare the results. The N_{cd} value required to achieve uniform dispersion at C=0.0254 m is higher for PBT than DT from H/T=0.177 to H/T=0.621. From H/T=0.621 to H/T=0.88, DT requires more agitation than PBT. At H/T=1, PBT yields higher value of N_{cd} than that of DT. At C=0.0508 m, C=0.0762 m, and C=0.1016 m, the value of N_{cd} obtained is more for PBT than that for DT for all liquid heights examined. N_{cd} followed the same behavior with variable liquid head ($\Delta H/T$), when compared to liquid depth (H/T). For both impeller types, N_{cd} approached an infinite value when C=H.

5.3.2 Power (P)

A comparison between the results for P obtained for DT and PBT is shown in Figures A.25, A.26, A.27, A.28, A.29, A.30, A.31, and A.32 in Appendix A. The power requirement to achieve uniform mixing is greater for DT than PBT in all cases examined at C=0.0254 m. The difference in the value of power between DT and PBT was small up to H/T=0.532. At H/T more than 0.532, this difference became significant. From H/T=0.88 to H/T=1, the power required for DT dropped, while it increased by almost 100 % in case of PBT. At C=0.0508 m, C=0.0762 m, and C=0.1016 m, DT required more power than PBT in all cases examined. The power requirement increased by almost 100% for both impellers from H/T=0.88 to H/T=1. At C=0.1016 m, the power required for DT dropped from H/T=0.88 to H/T=1, while it increased by almost 50 % in the case of the PBT.

5.3.3 Power/Volume (P/V)

A comparison between the results for P/V obtained for DT and PBT is shown in Figures A.33, A.34, A.35, A.36, A.37, A.38, A.39, and A.40 in Appendix A. At C=0.0254 m, the power per unit volume for DT is more than that of PBT. It kept increasing for PBT with increasing liquid height (H/T), while it dropped for DT in the range H/T=0.88 to H/T=1. At C=0.0508 m and C=0.0762 m, the power per volume increased with increasing liquid depth (H/T) for both types of impeller. It increased by almost 100% from H/T=0.88 to H/T=1. At C=0.1016 m, P/V increased with increase in liquid depth (H/T) up to 0.799. From H/T=0.799 to H/T=1, P/V dropped by almost 100% for DT. For PBT, it kept increasing up to H=T. At C=0.1016 m and H/T=1, PBT attained a higher value of P/V

than that of DT. Power per volume requirement for both types of impellers followed the same behavior with liquid head (ΔH/T) when compared to the behavior with liquid depth (H/T).

5.3.4 Power Number (N_p)

A comparison between the results for N_p obtained for DT and PBT is shown in Figures A.41, A.42, A.43, A.44, A.45, A.46, A.47, and A.48 in Appendix A. Power Number remains in the range of 3 to 4 for DT, and 1 to 2 for PBT, at C=0.0254 m and C=0.0508 m. It remained unchanged with increase in liquid height (H/T). At C=0.0762 m, N_p kept increasing for DT up to H/T=0.71. From H/T=0.71 to H/T=1, N_p remained almost constant in the vicinity of 5. For PBT, N_p remained in the range 1.3-1.67, without significant deviation with H/T. At C=0.1016 m, N_p increased with increasing H/T up to 0.62 for DT. From H/T=0.62 to H/T=1, it remained almost constant for DT. For PBT, N_p remained constant with increasing liquid depth (H/T). The liquid head (ΔH/T) has the same effect as the liquid depth (H) on power number.

CHAPTER 6

CONCLUSIONS

1. Disk turbines required lower agitation speeds than 45° pitched-blade turbine to achieve the uniform liquid-liquid dispersion state under all conditions examined in this work. A radial flow pattern was found to achieve the uniform dispersion state at lower values of N_{cd} than an axial flow pattern.
2. In all agitation systems, the power drawn was found to drop with decreasing liquid height.
3. In general, the power required by the disk turbine increased as the impeller off-bottom clearance decreased.
4. Unlike the case of disk turbine, the power required by the pitched-blade turbine decreased as the impeller off-bottom clearance decreased.
5. The disk turbine required more power than the 45° pitched-blade turbine in all cases examined.
6. When the N_{cd} results for the disk turbine were plotted against the liquid head (ΔH), the data obtained at different impeller clearances collapsed together. This was not true for the pitched-blade turbine.
7. At low off–bottom clearance ($C_b/T=0.055$ corresponding to $C_b/D=0.16$), the power consumption of the disk turbine was also low. A small increase in C_b/T from 0.055 to 0.144 (corresponding to $C_b/D=0.432$) produced a small increase in power number. For $C_b/T=0.233$ and $C_b/T=0.322$ (corresponding to $C_b/D=0.699$ and $C_b/D=0.966$ respectively), a moderate increase in power number was observed, possibly caused by

the establishment of a transition flow pattern around the impeller, which stabilized with increasing liquid depths (H). This is in agreement with the conclusion drawn by Armenante and Huang (1992).

8. When the liquid height was dropped to eventually reach the same level as the middle of the impeller (i.e., as H→ C), the state of complete liquid-liquid dispersion was not achievable, irrespective of the agitation speed. Although the interface appeared to be disrupted by the agitation produced by the impeller, the droplets of the dispersed phase did not reach to the bottom of the tank. When the agitation speed was increased beyond this point, the shaft started vibrating around its axis and the liquid was splashed in the tank. However, no air entrainment took place.

APPENDIX A

FIGURES FOR CHAPTER 5

This appendix includes figures showing effect of liquid depth on minimum agitation speed (N_{cd}), Power (P), power/volume (P/V) and power number (N_p) for DT (Figures A.1-A.8) and PBT (Figures A.9-A.16). It also includes the comparison of all examined variables between DT and PBT (Figures A.17-A.48).

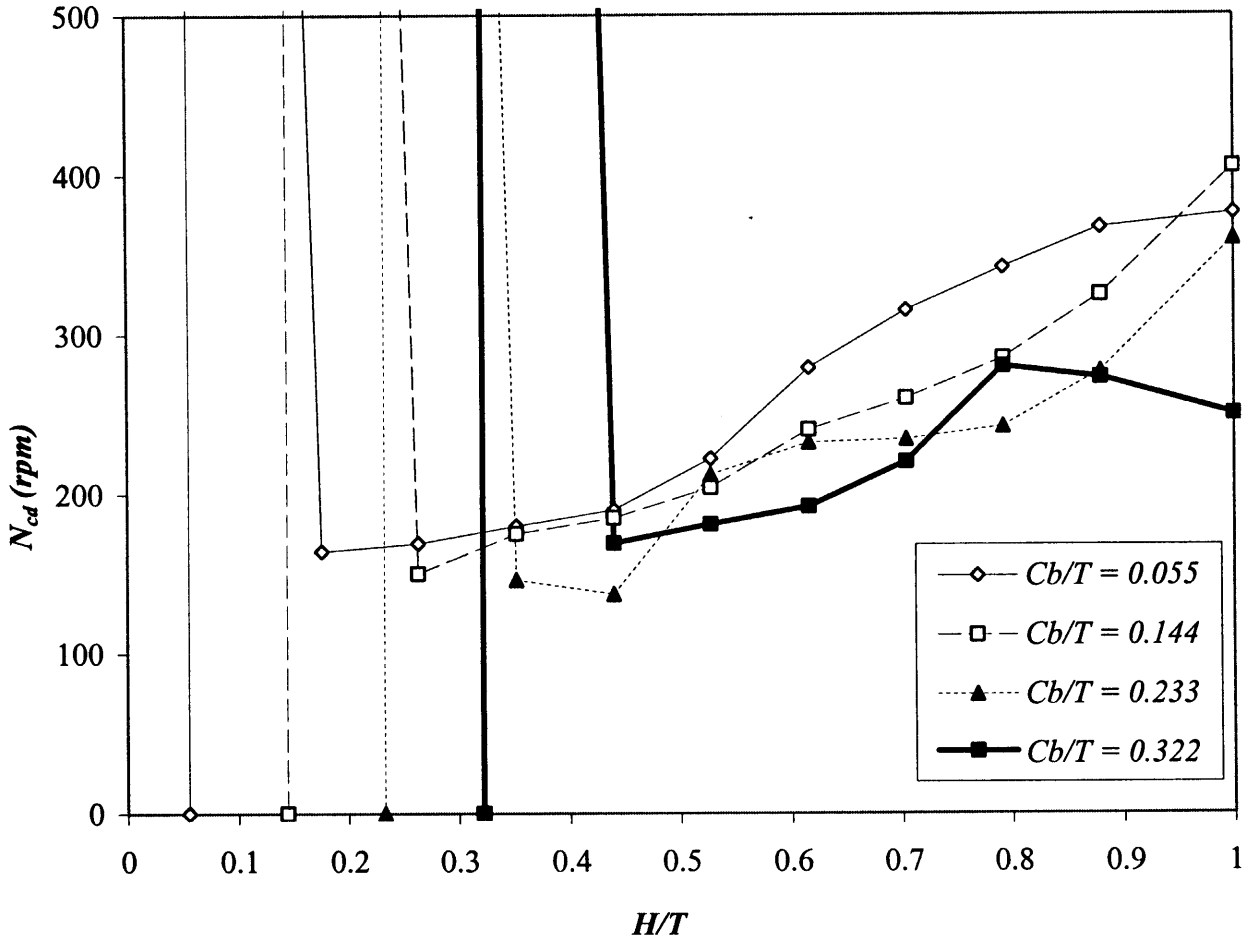

Figure A.1 Effect of H on N_{cd} (DT).
The vertical lines were drawn in correspondence of $H=C_b$ for each curve.

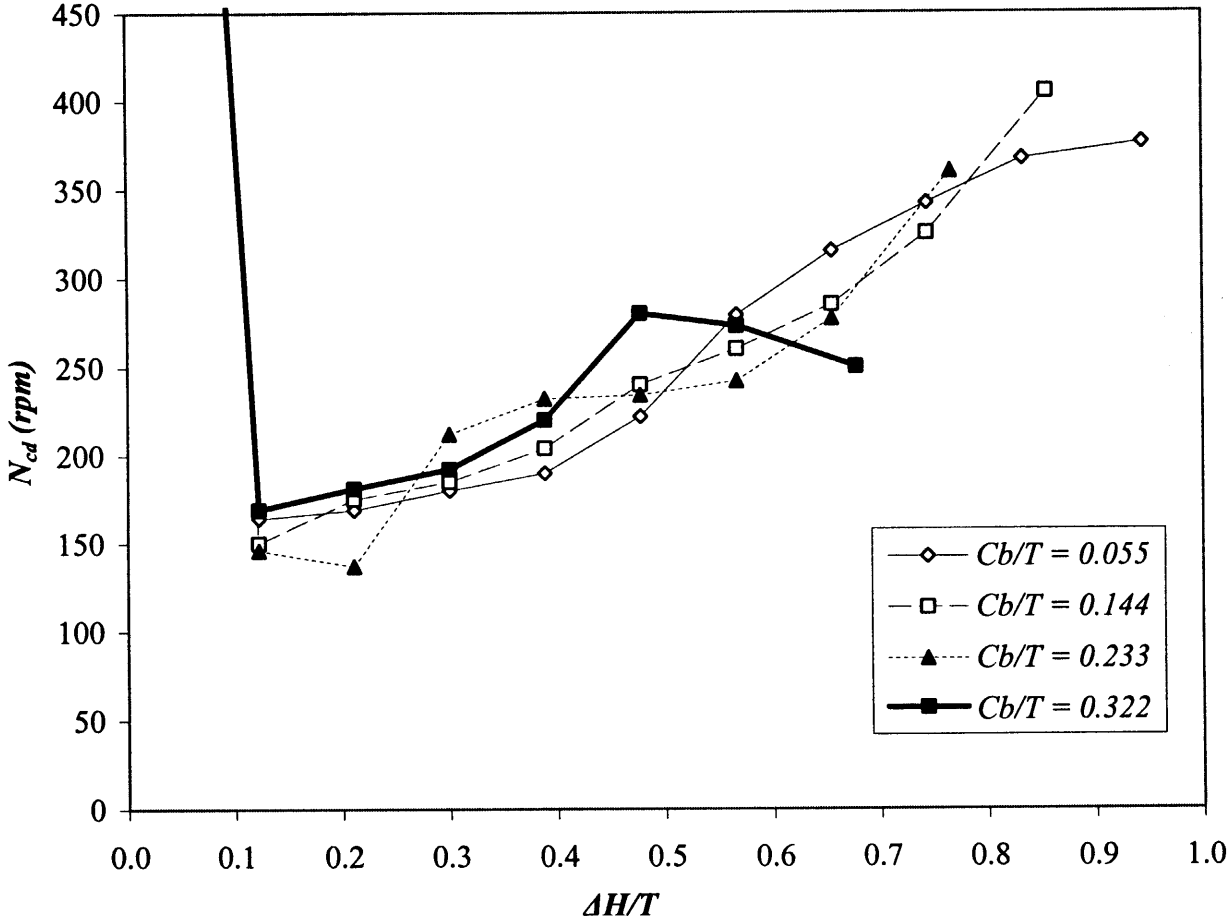

Figure A.2 Effect of ΔH on N_{cd} (DT).

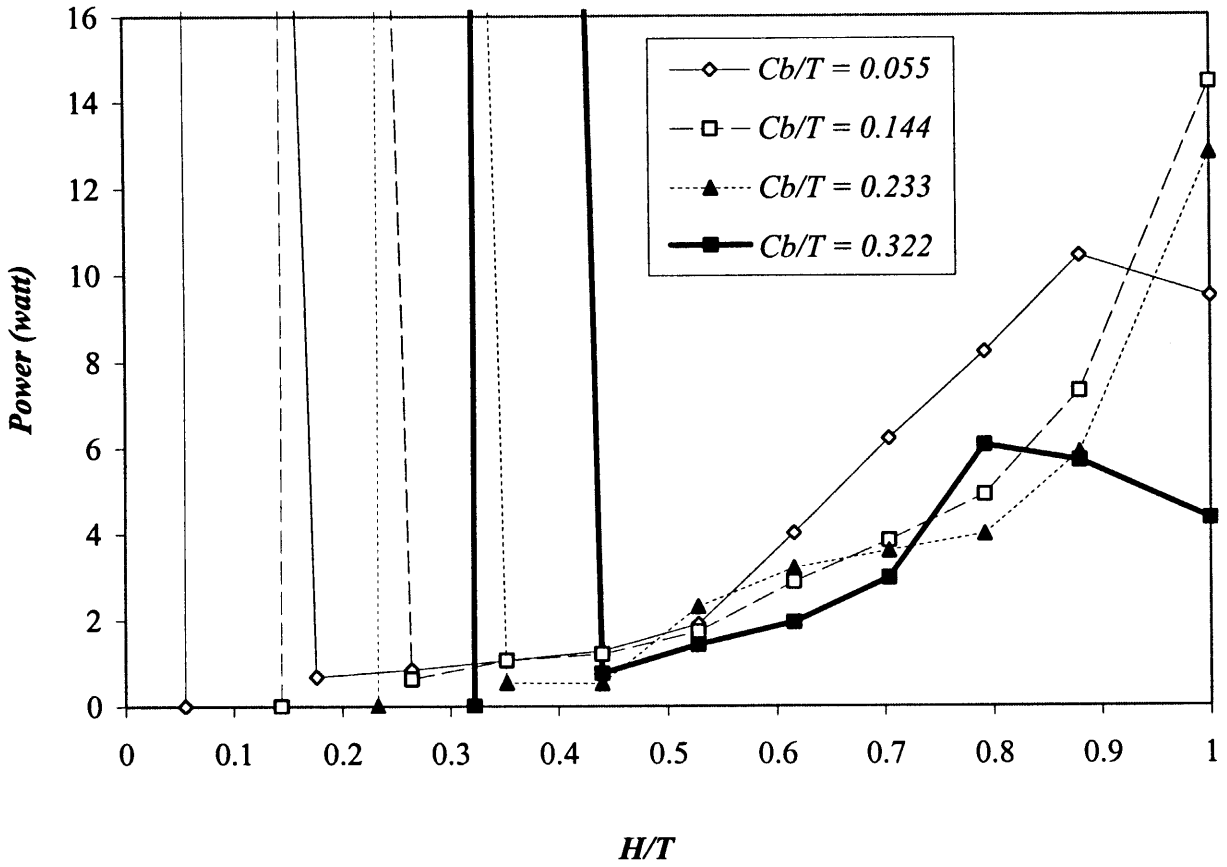

Figure A.3 Effect of H on P (DT).
The vertical lines were drawn in correspondence of $H=C_b$ for each curve.

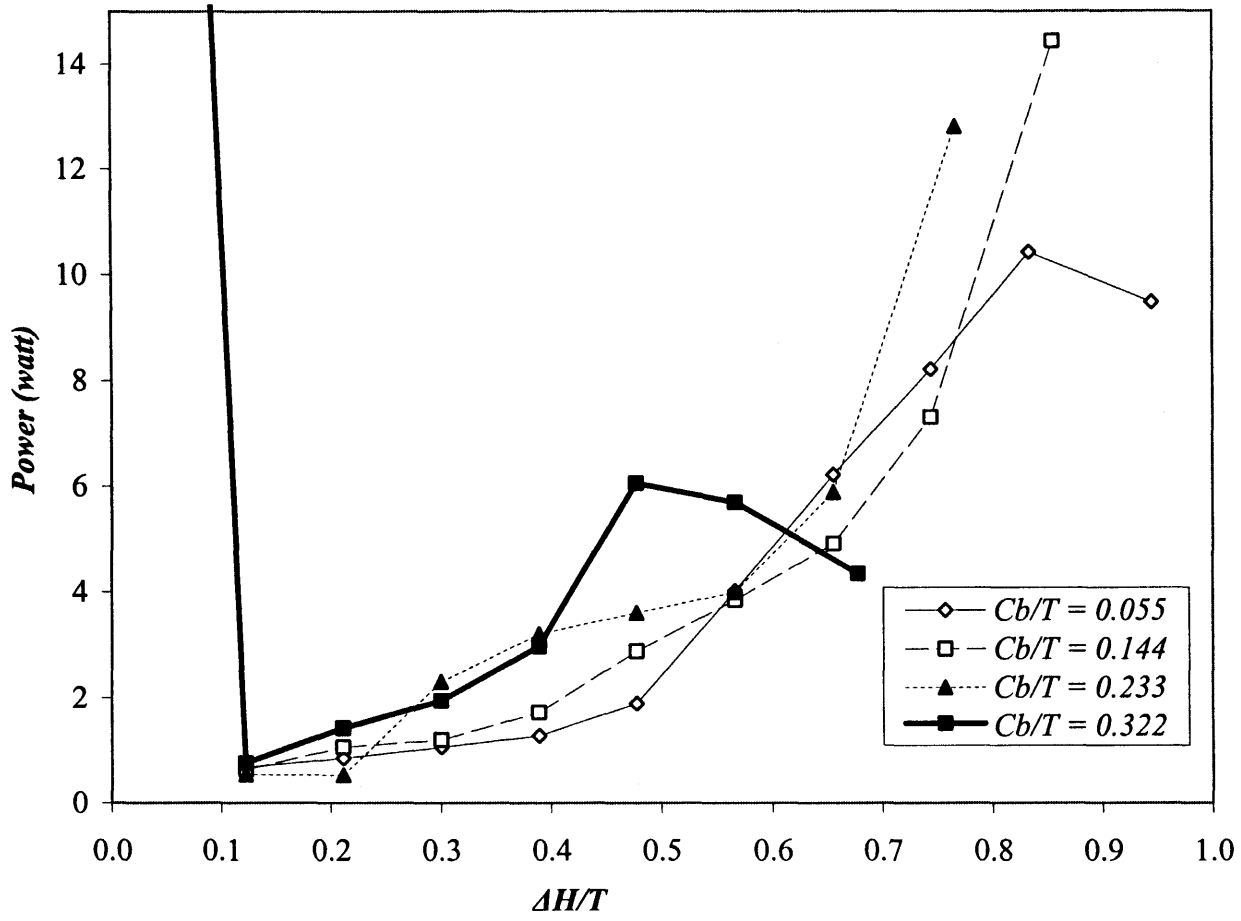

Figure A.4 Effect of ΔH on P (DT).

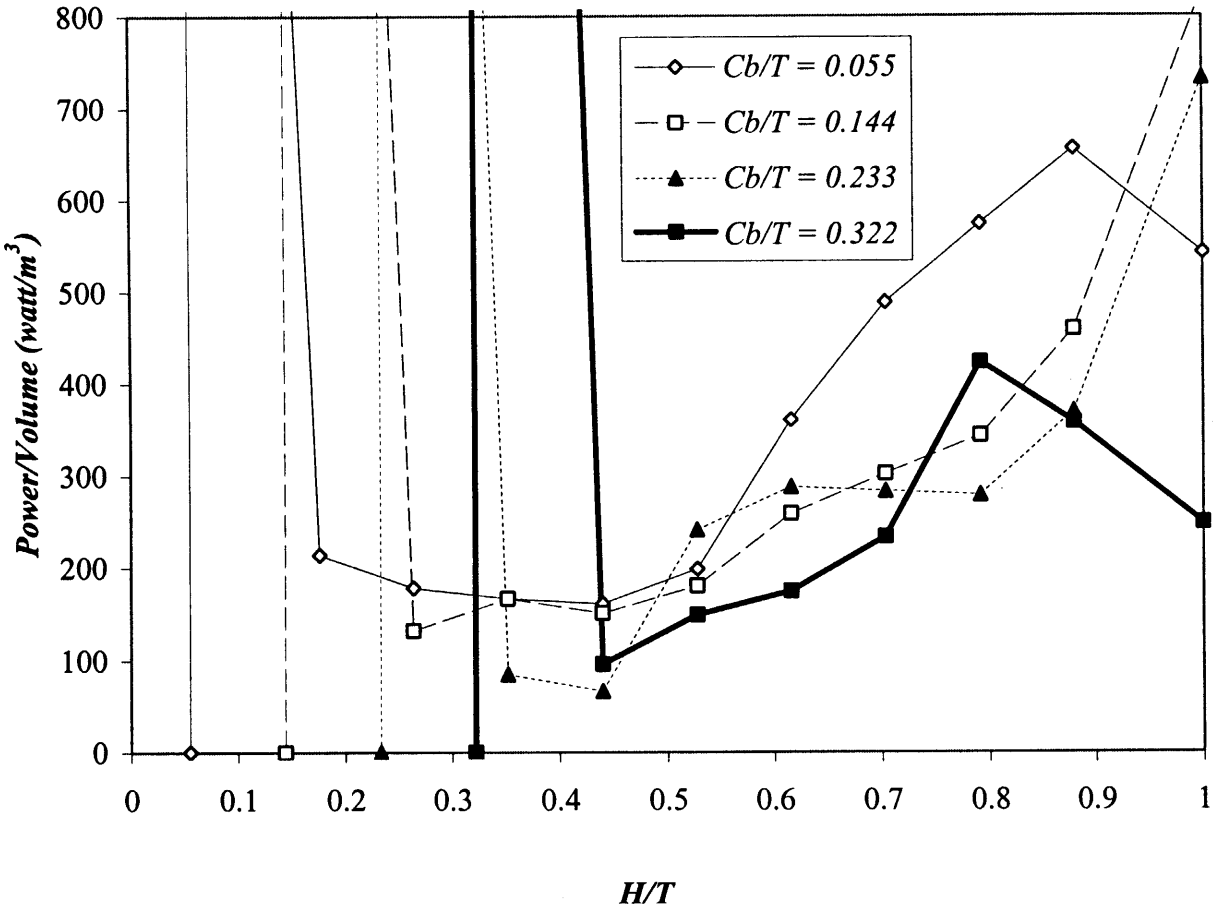

Figure A.5 Effect of H on P/V (DT).
The vertical lines were drawn in correspondence of $H=C_b$ for each curve.

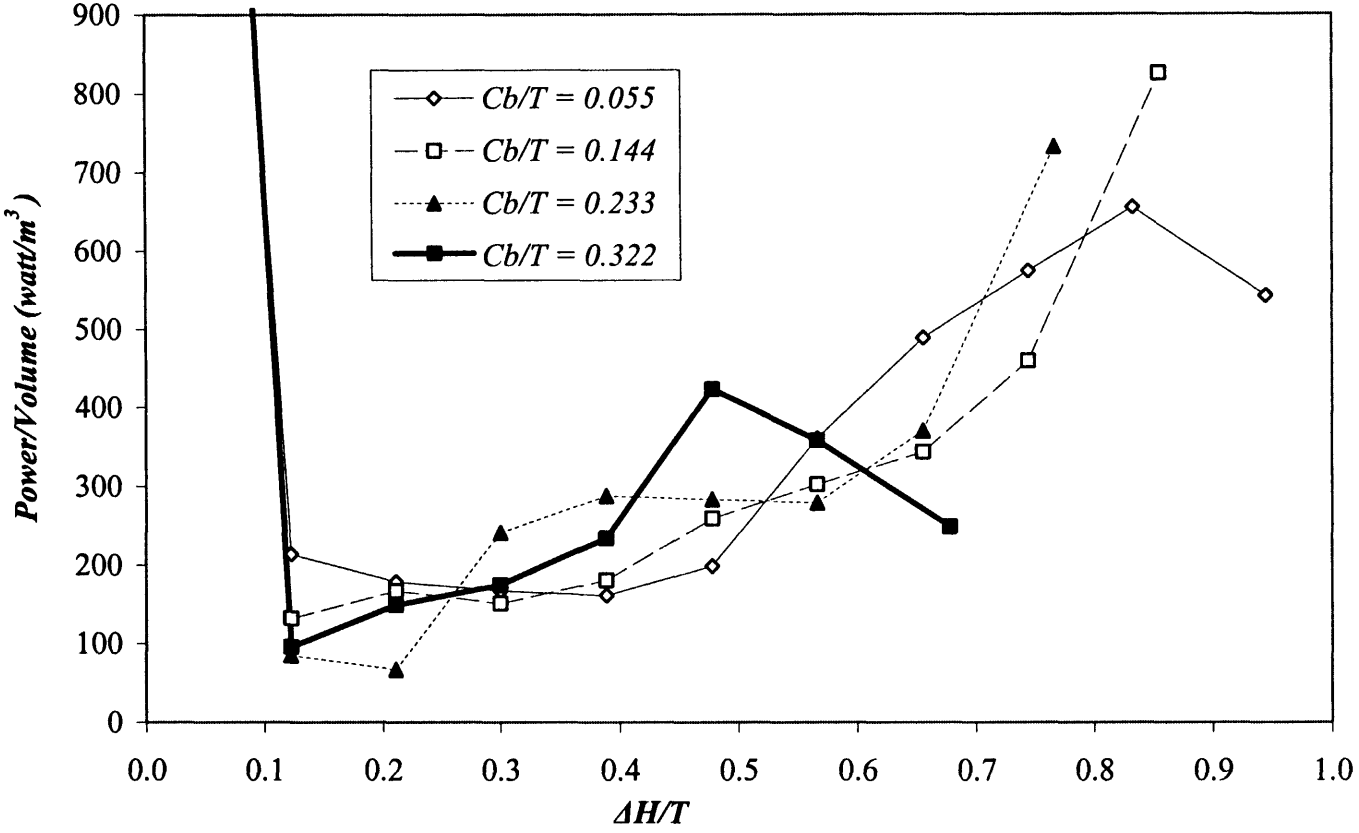

Figure A.6 Effect of ΔH on P/V (DT).

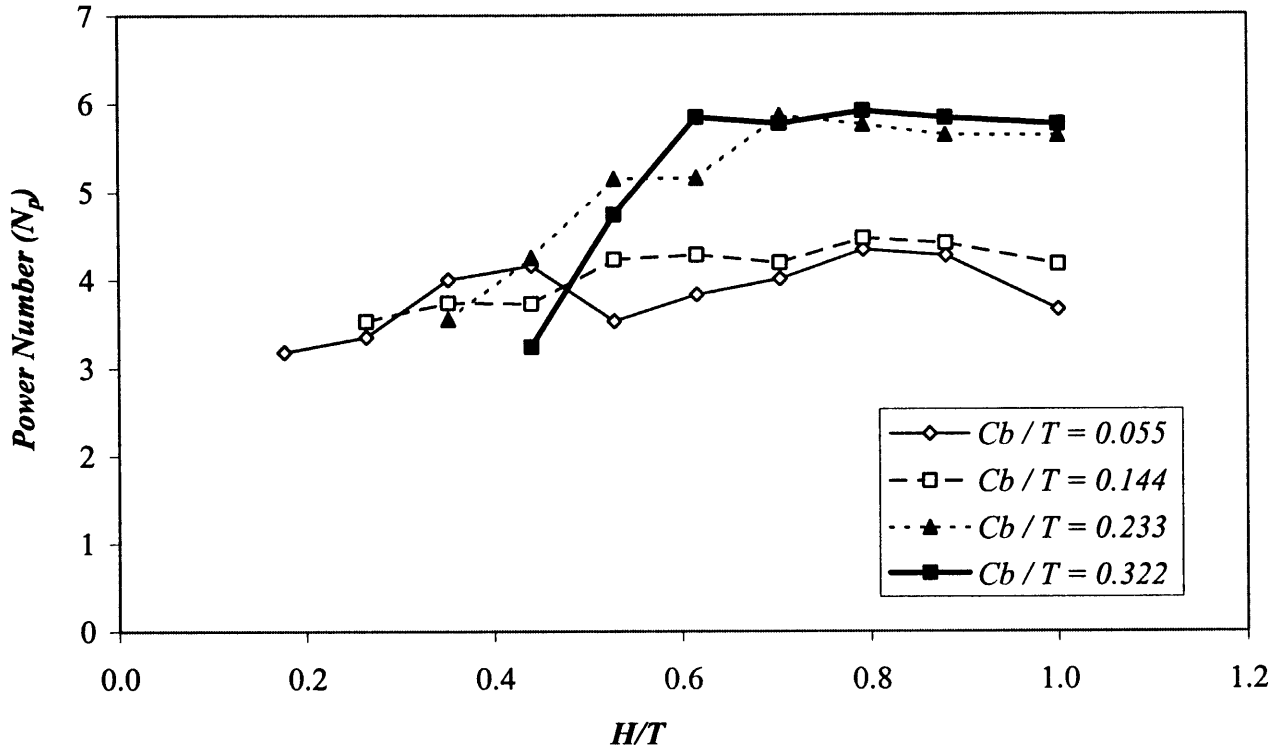

Figure A.7 Effect of H on N_p (DT)

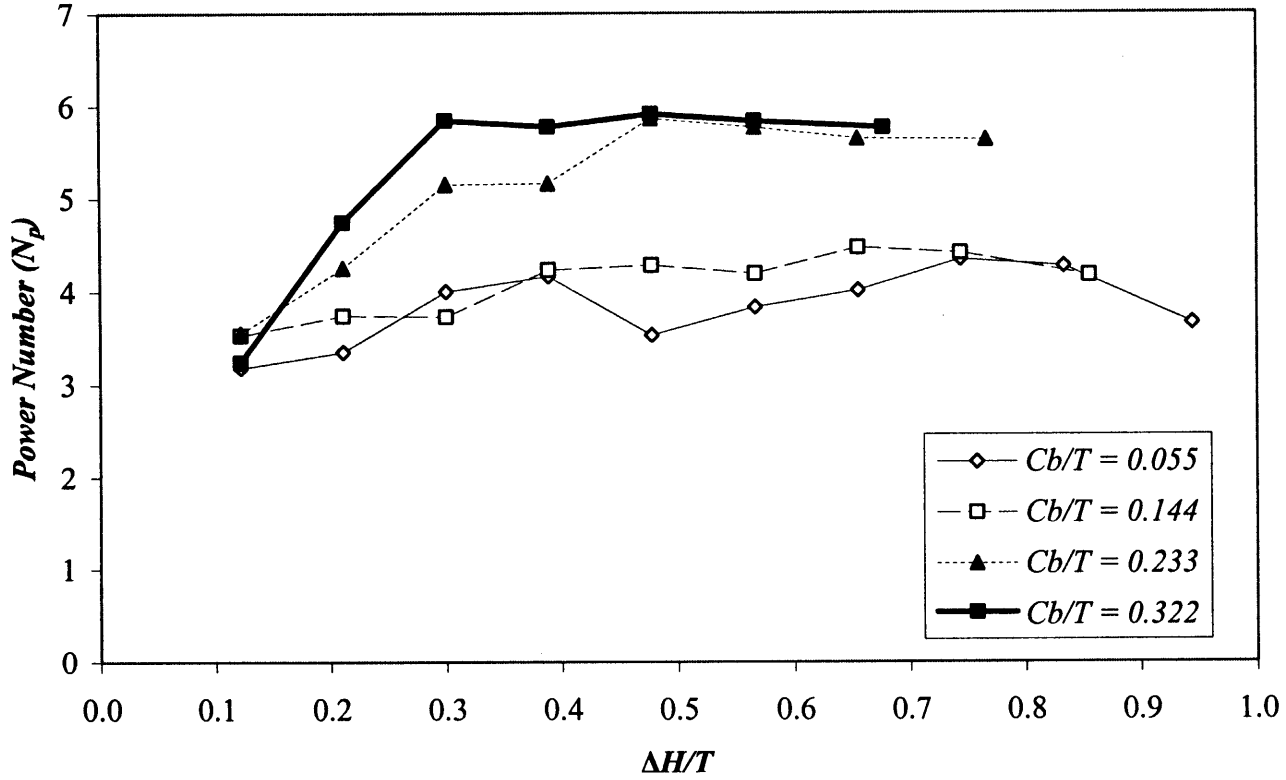

Figure A.8 Effect of ΔH on N_p (DT)

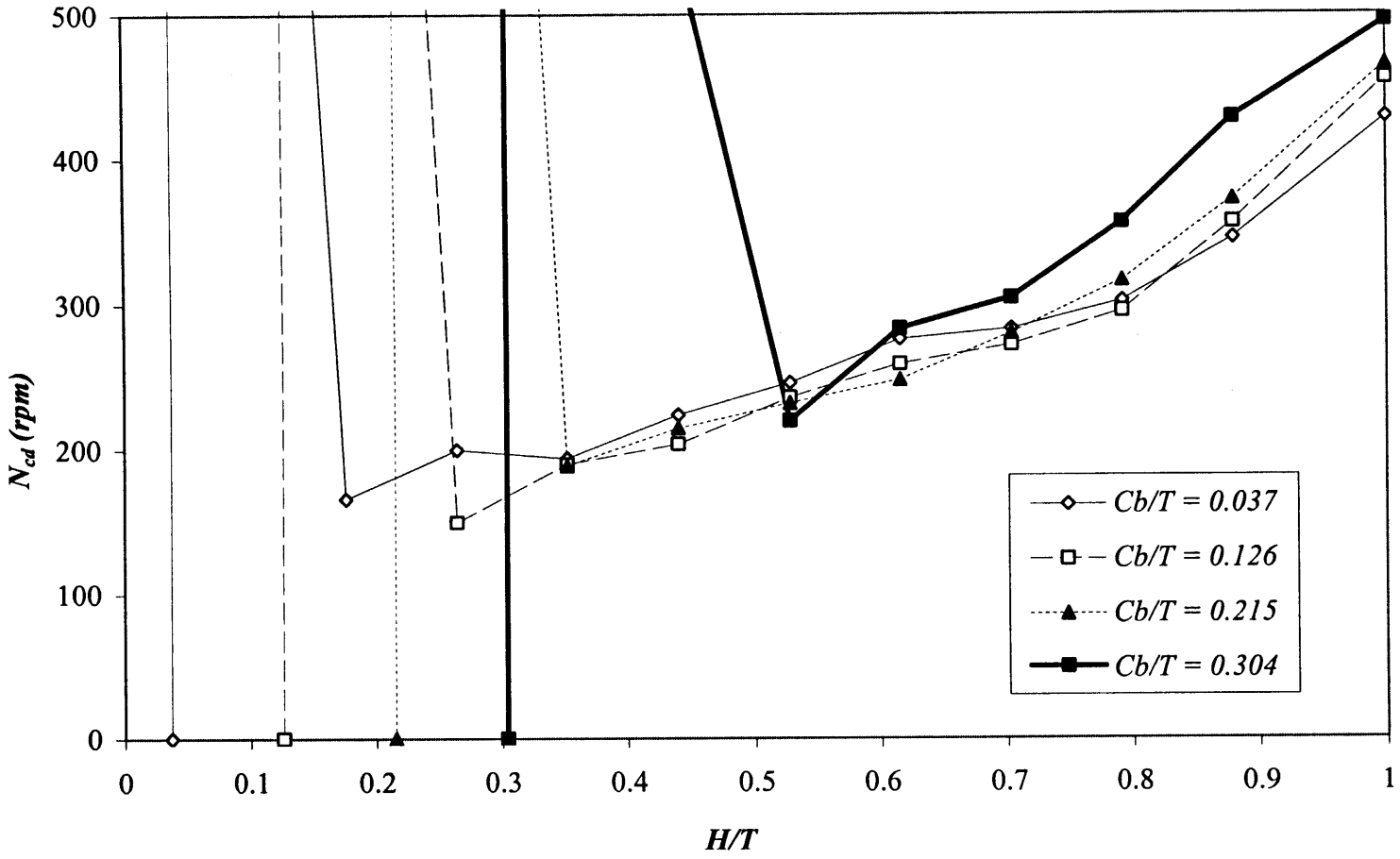

Figure A.9 Effect of H on N_{cd} (PBT).
The vertical lines were drawn in correspondence of $H=C_b$ for each curve.

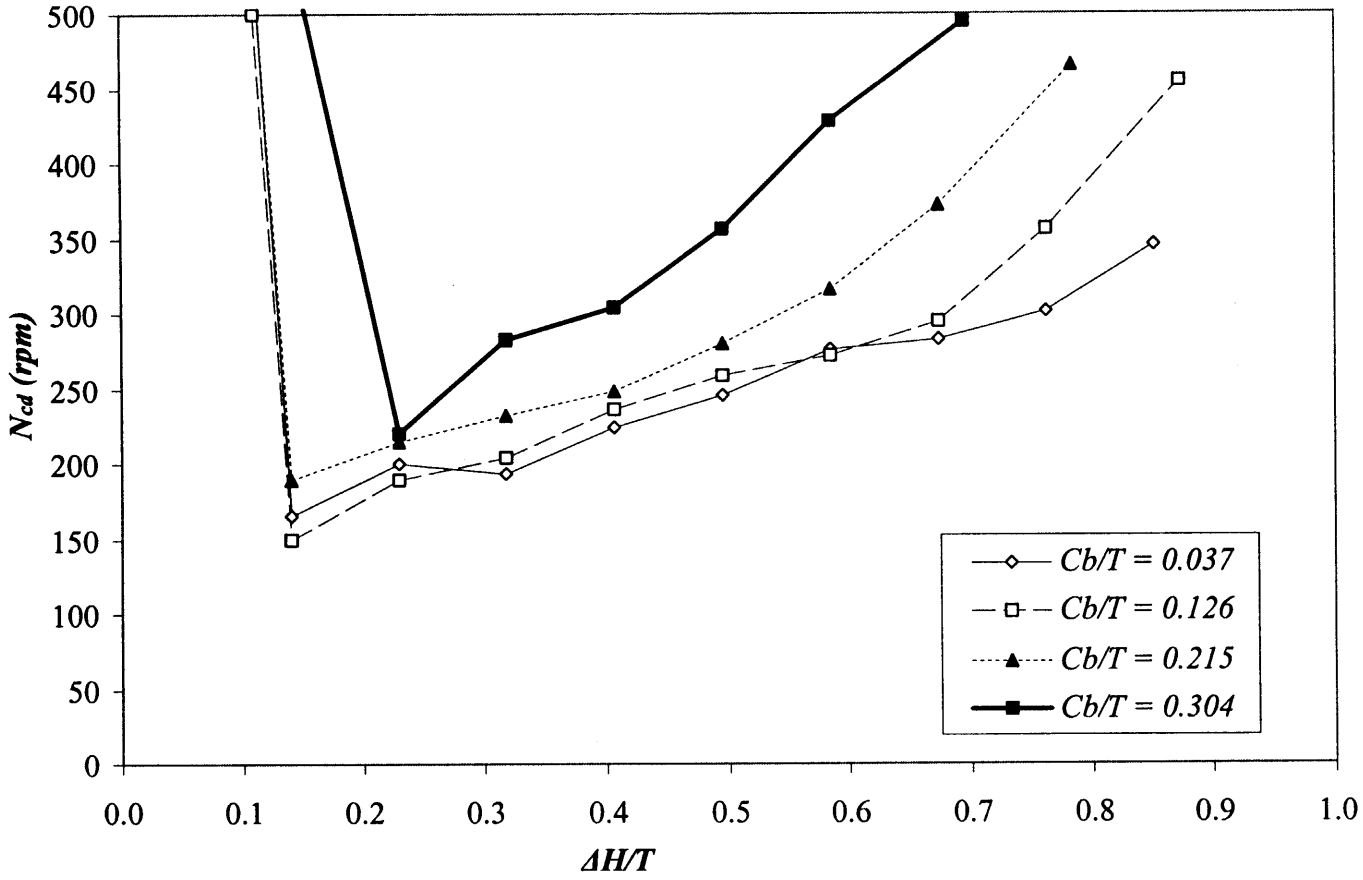

Figure A.10 Effect of ΔH on N_{cd} (PBT).

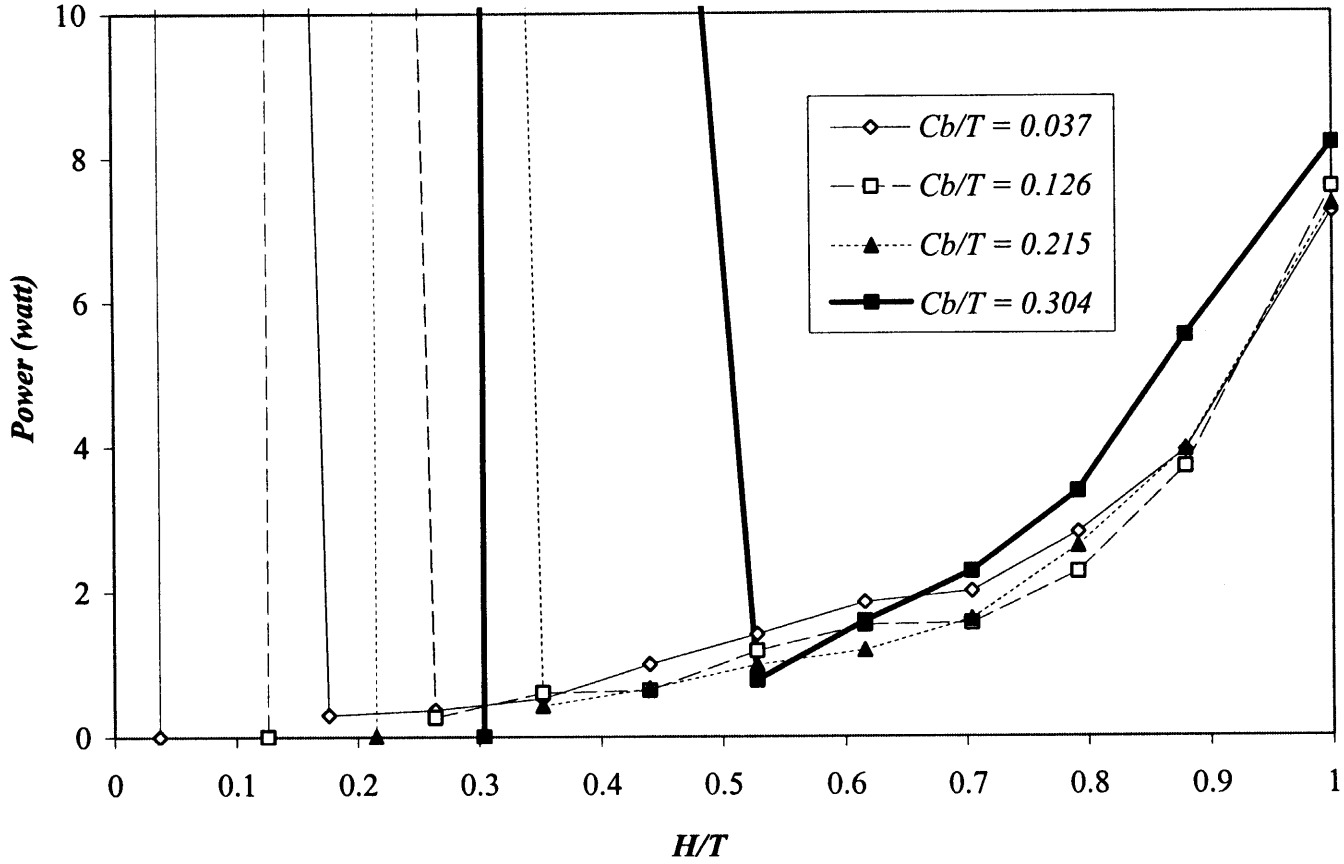

Figure A.11 Effect of H on P (PBT).
The vertical lines were drawn in correspondence of $H=C_b$ for each curve.

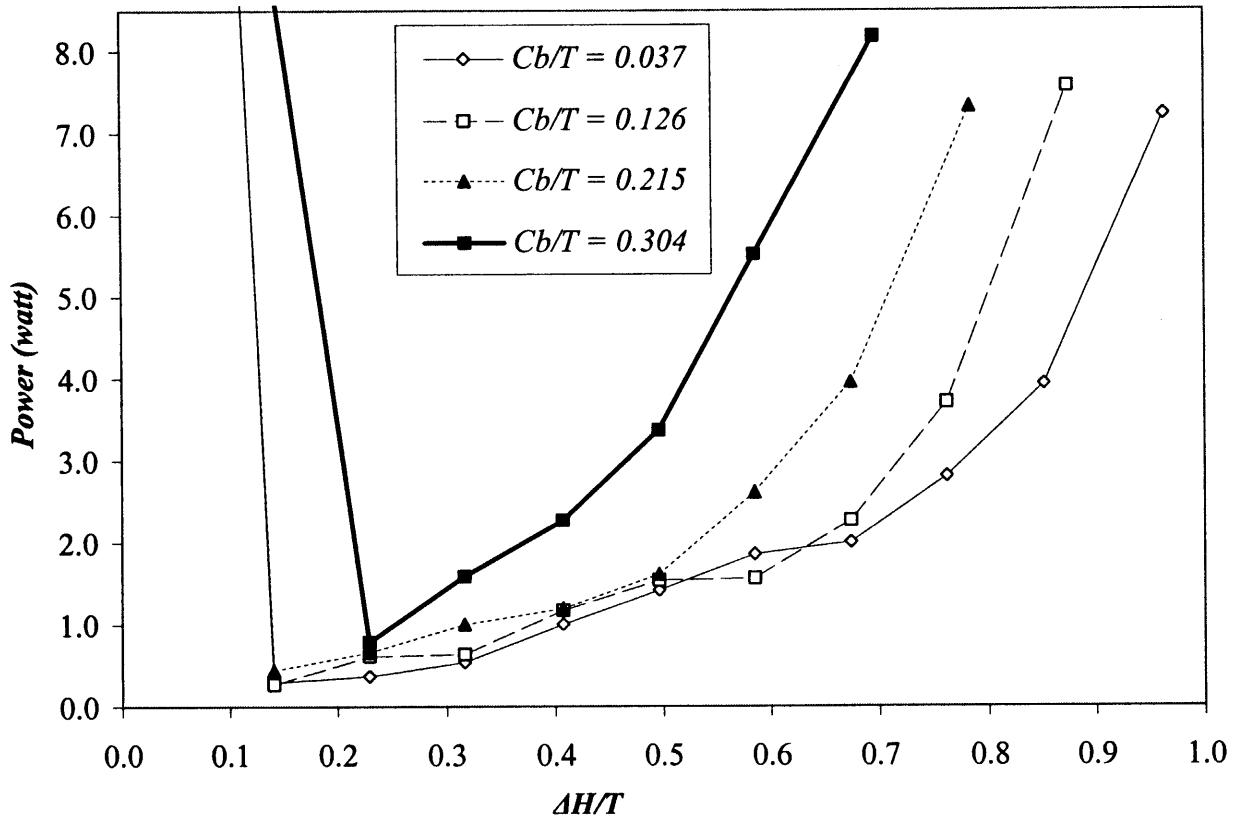

Figure A.12 Effect of ΔH on P (PBT).

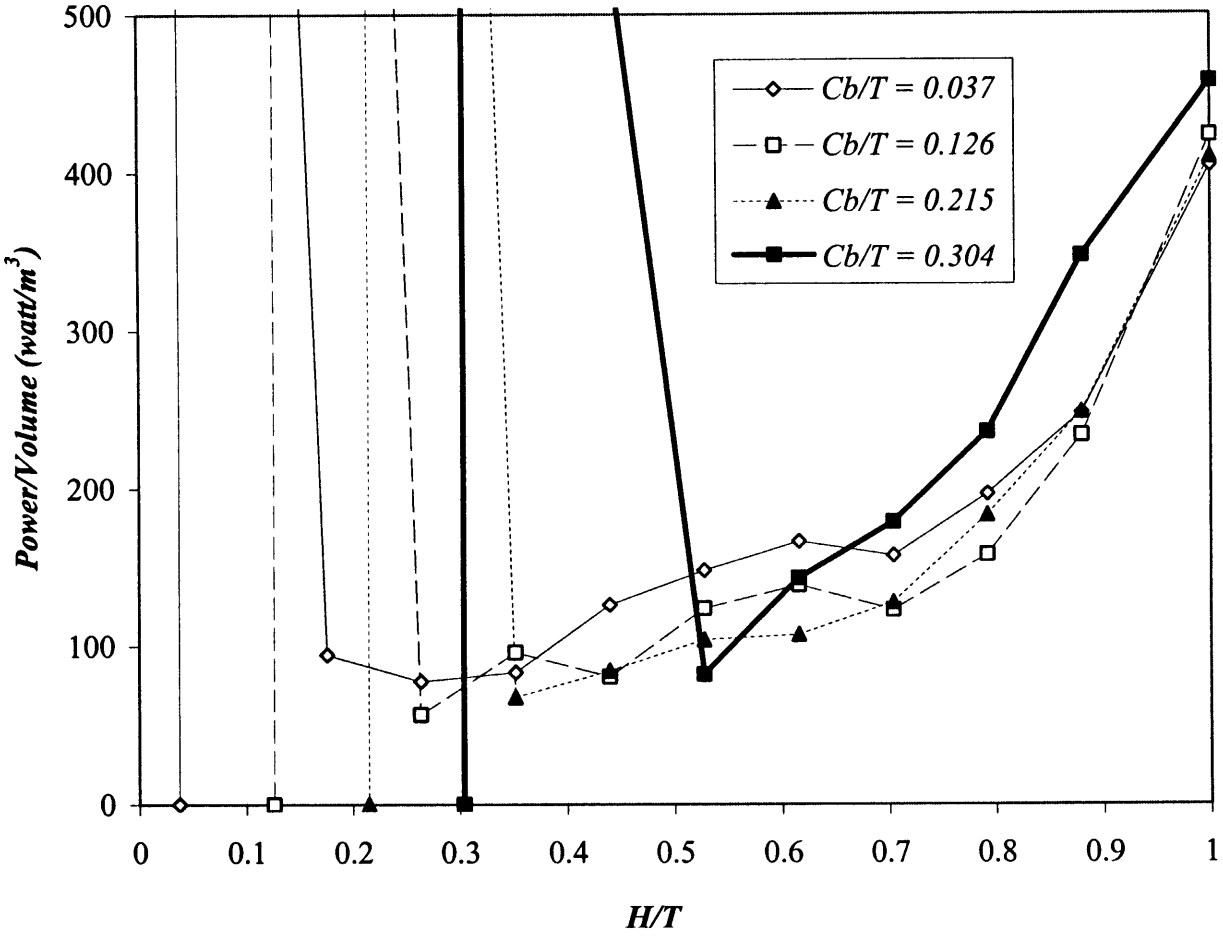

Figure A.13 Effect of H on P/V (PBT).
The vertical lines were drawn in correspondence of $H=C_b$ for each curve.

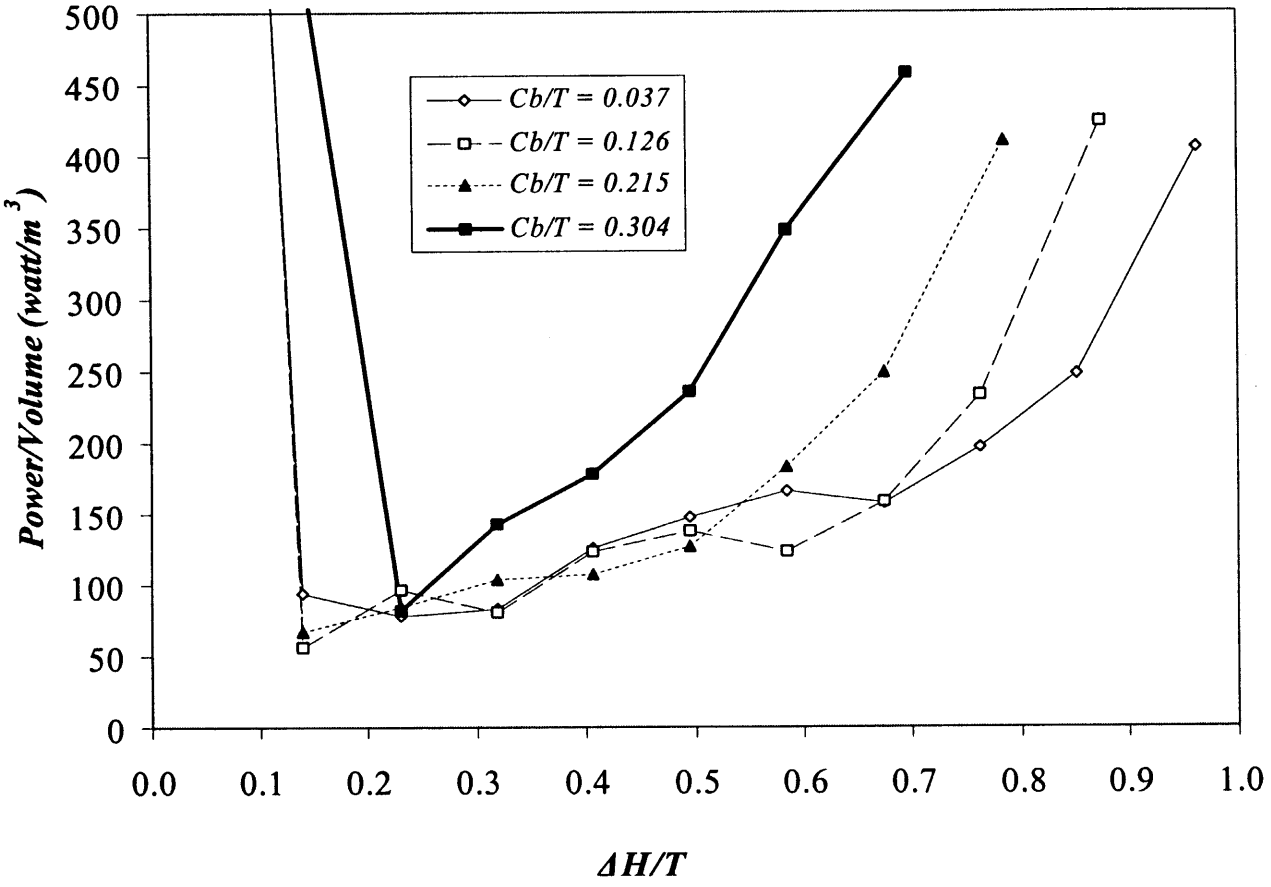

Figure A.14 Effect of ΔH on P/V (PBT).

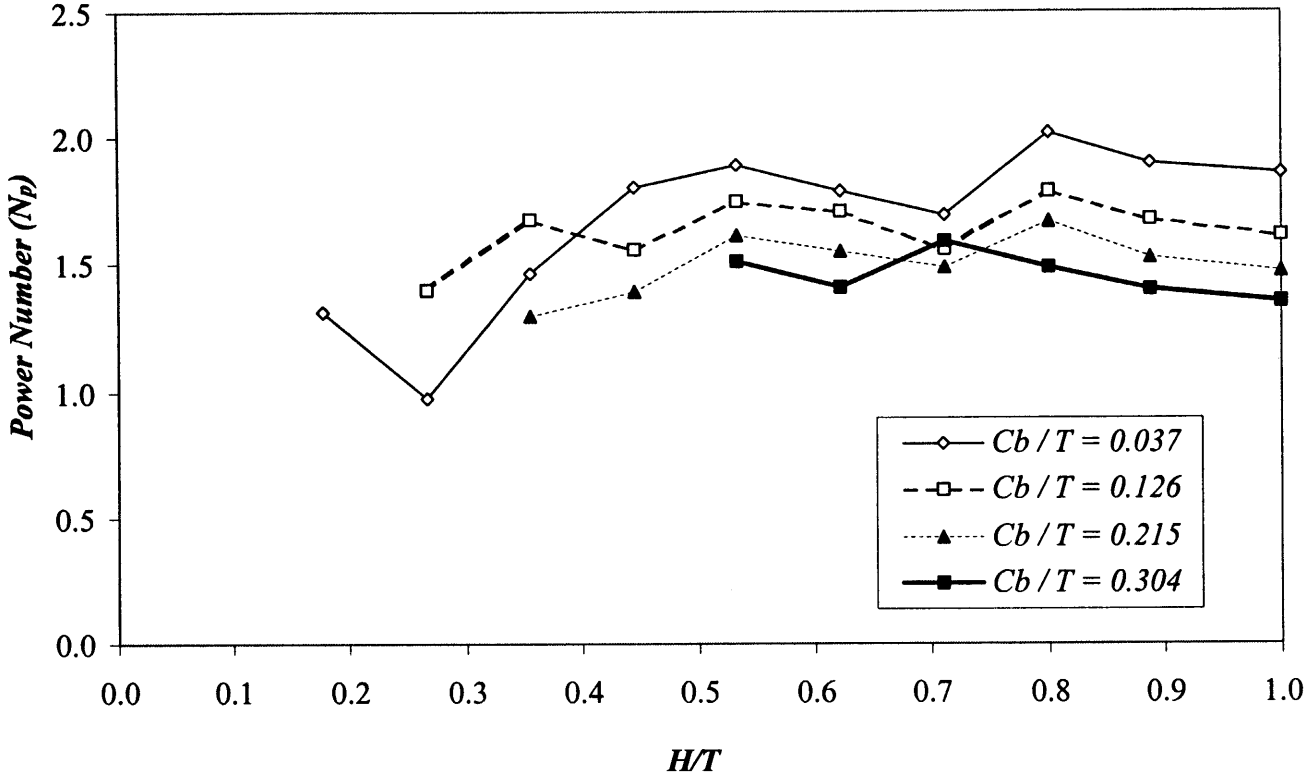

Figure A.15 Effect of H on N_p (PBT).

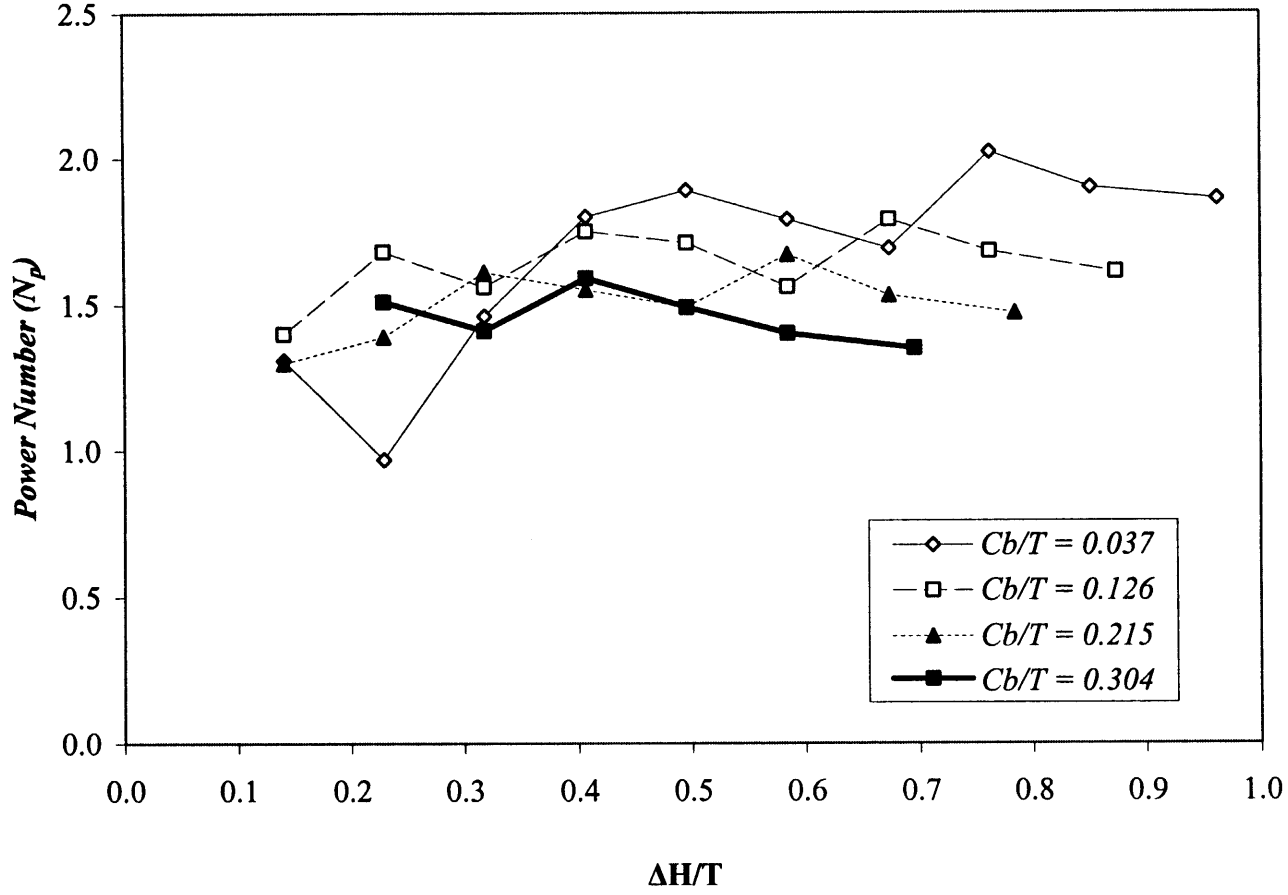

Figure A.16 Effect of ΔH on N_p (PBT).

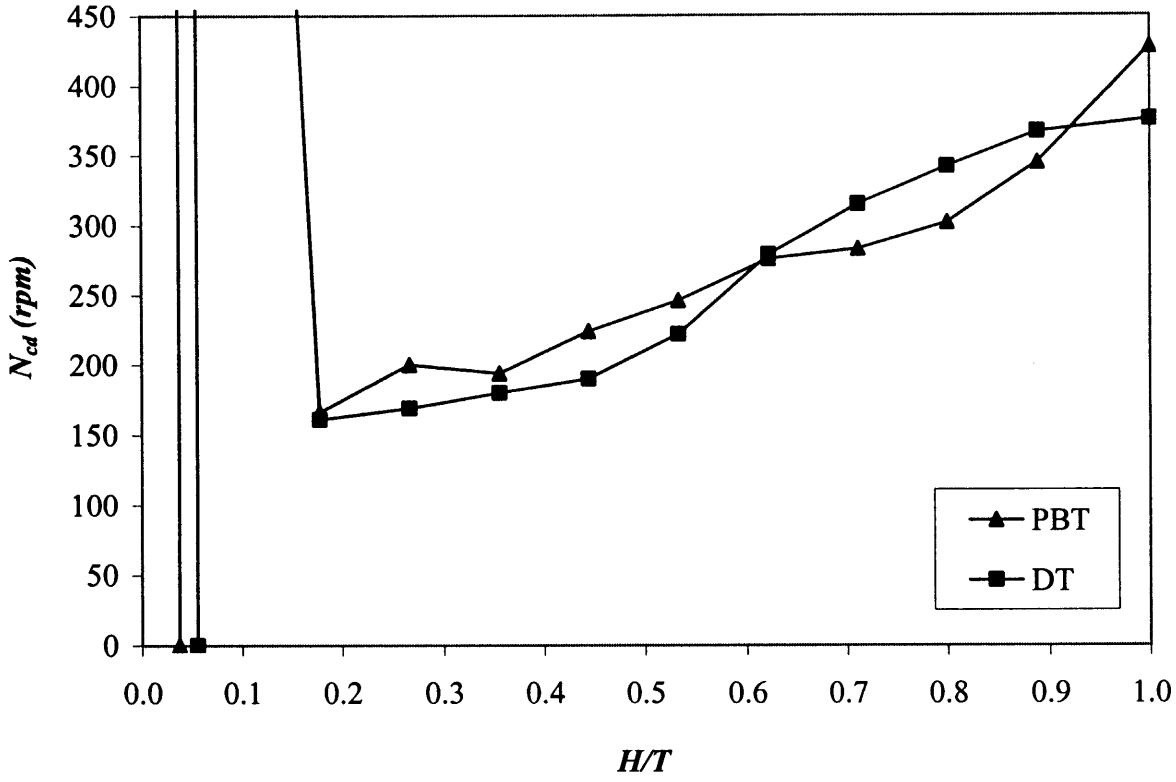

Figure A.17 Comparison of N_{cd} vs. H at C=0.0254m.
The vertical lines were drawn in correspondence of $H=C_b$ for each curve.

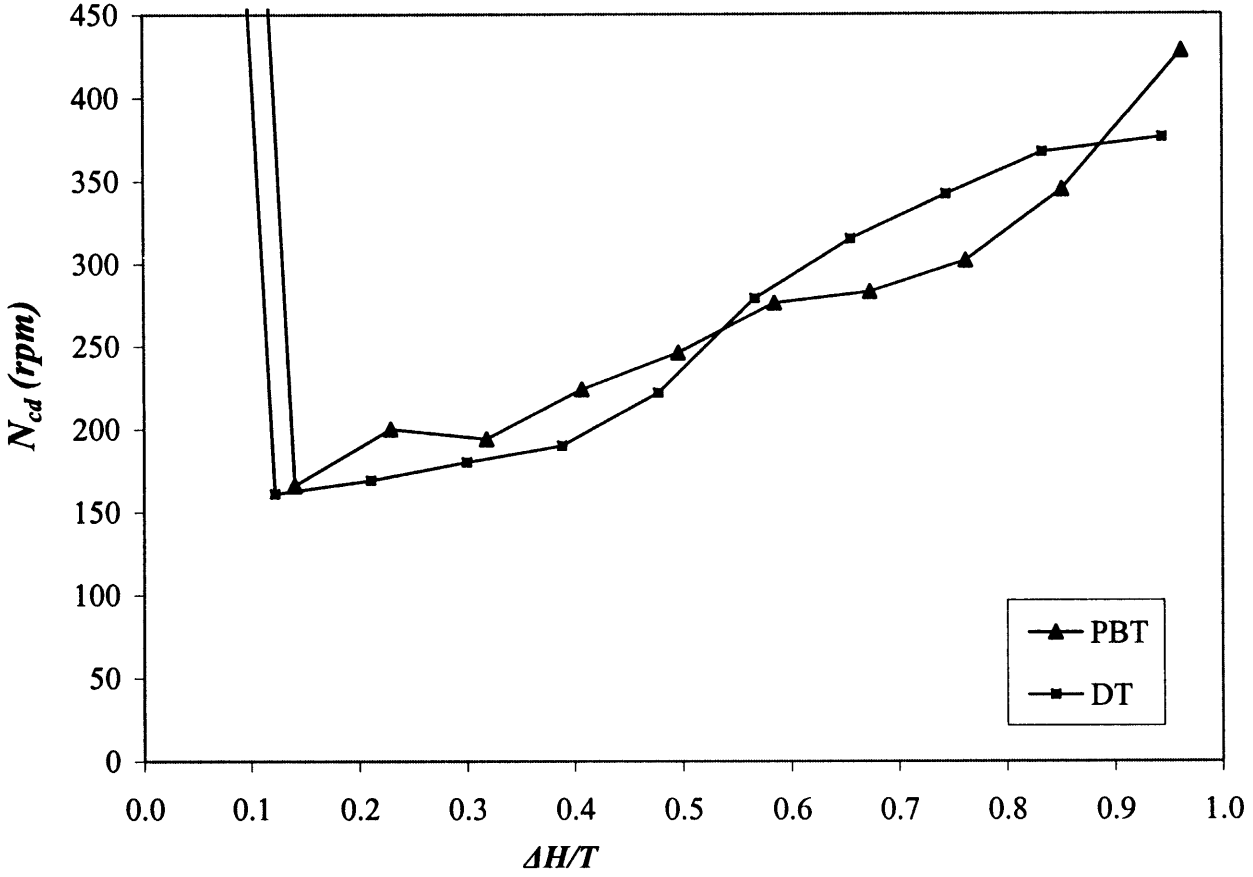

Figure A.18 Comparison of N_{cd} vs. ΔH at C=0.0254m.

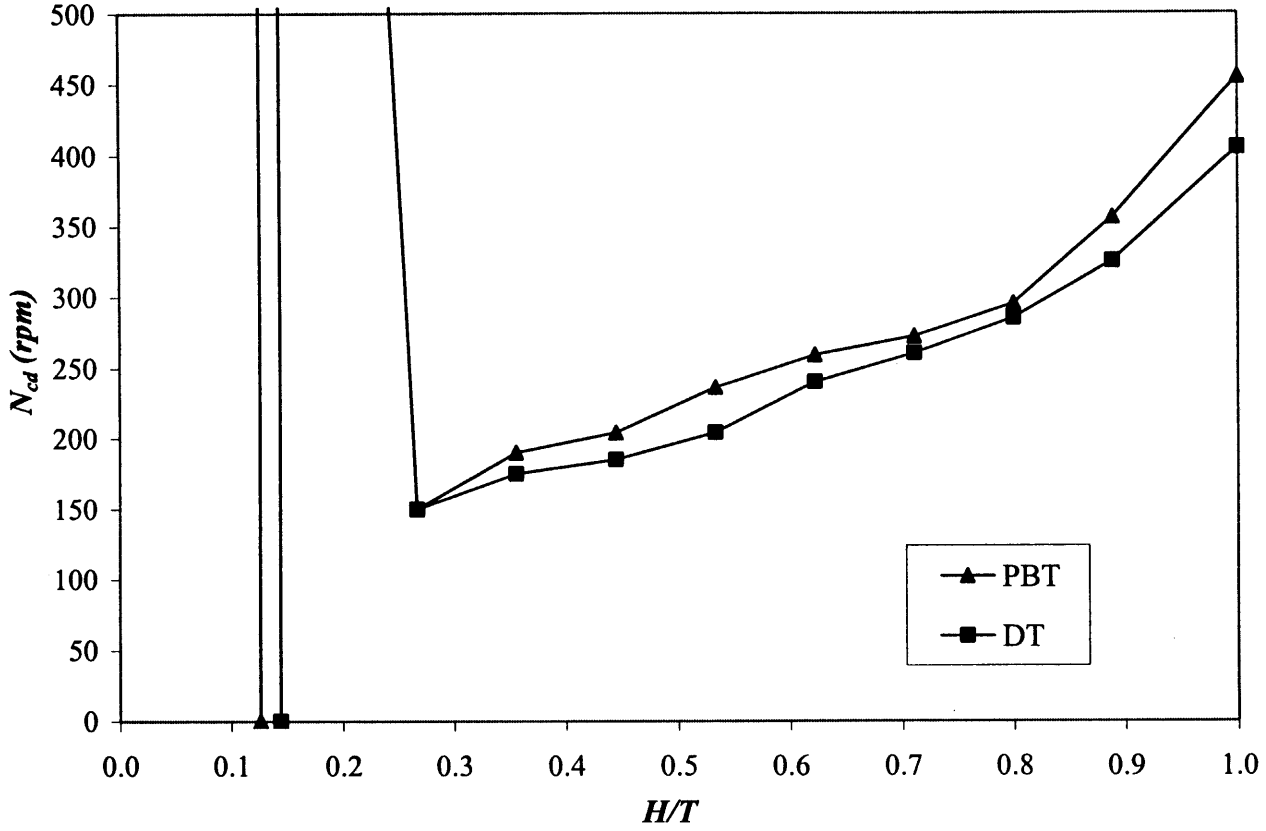

Figure A.19 Comparison of N_{cd} vs. H at C=0.0508m.
The vertical lines were drawn in correspondence of $H=C_b$ for each curve.

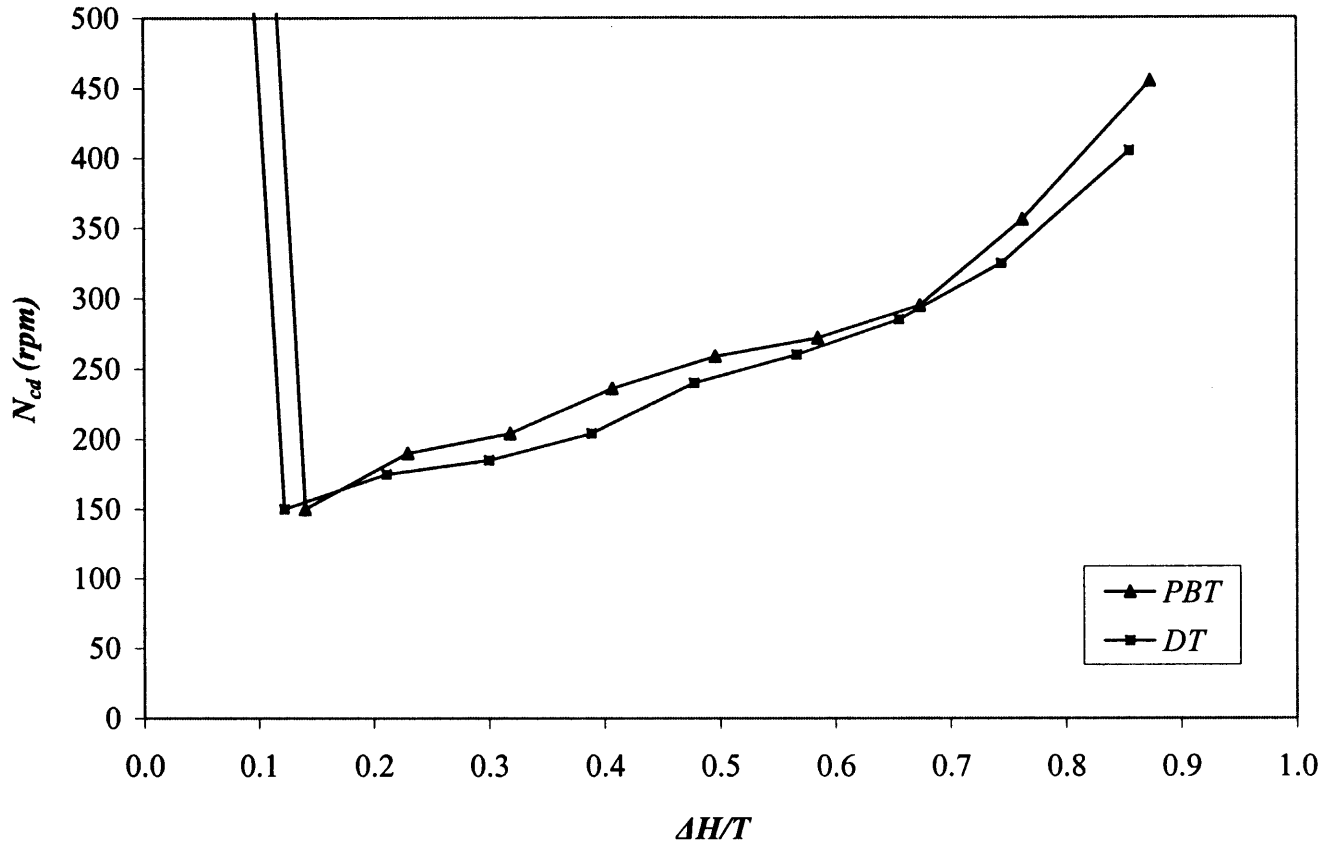

Figure A.20 Comparison of N_{cd} vs. ΔH at C=0.0508m.

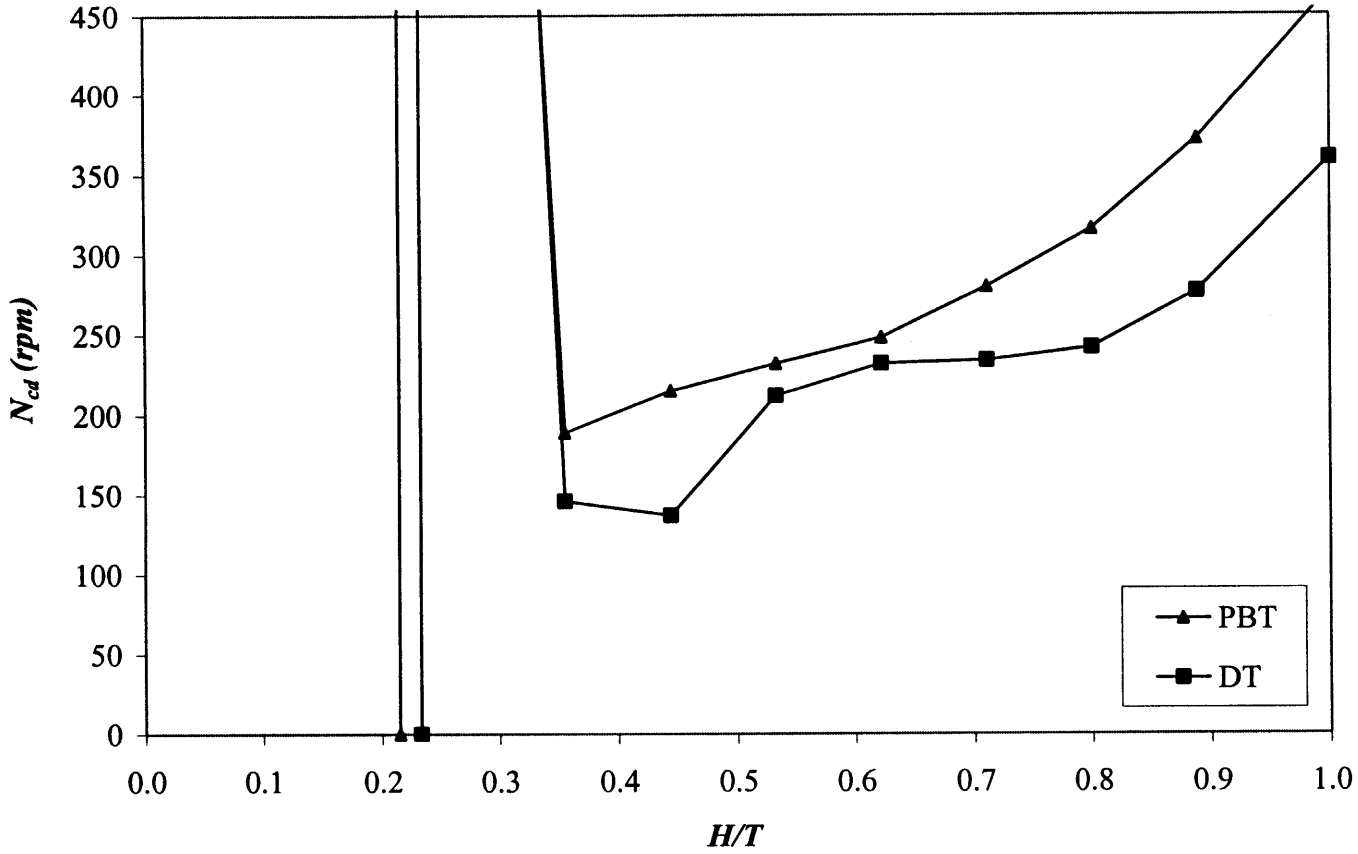

Figure A.21 Comparison of N_{cd} vs. H at C=0.0762m.
The vertical lines were drawn in correspondence of $H=C_b$ for each curve.

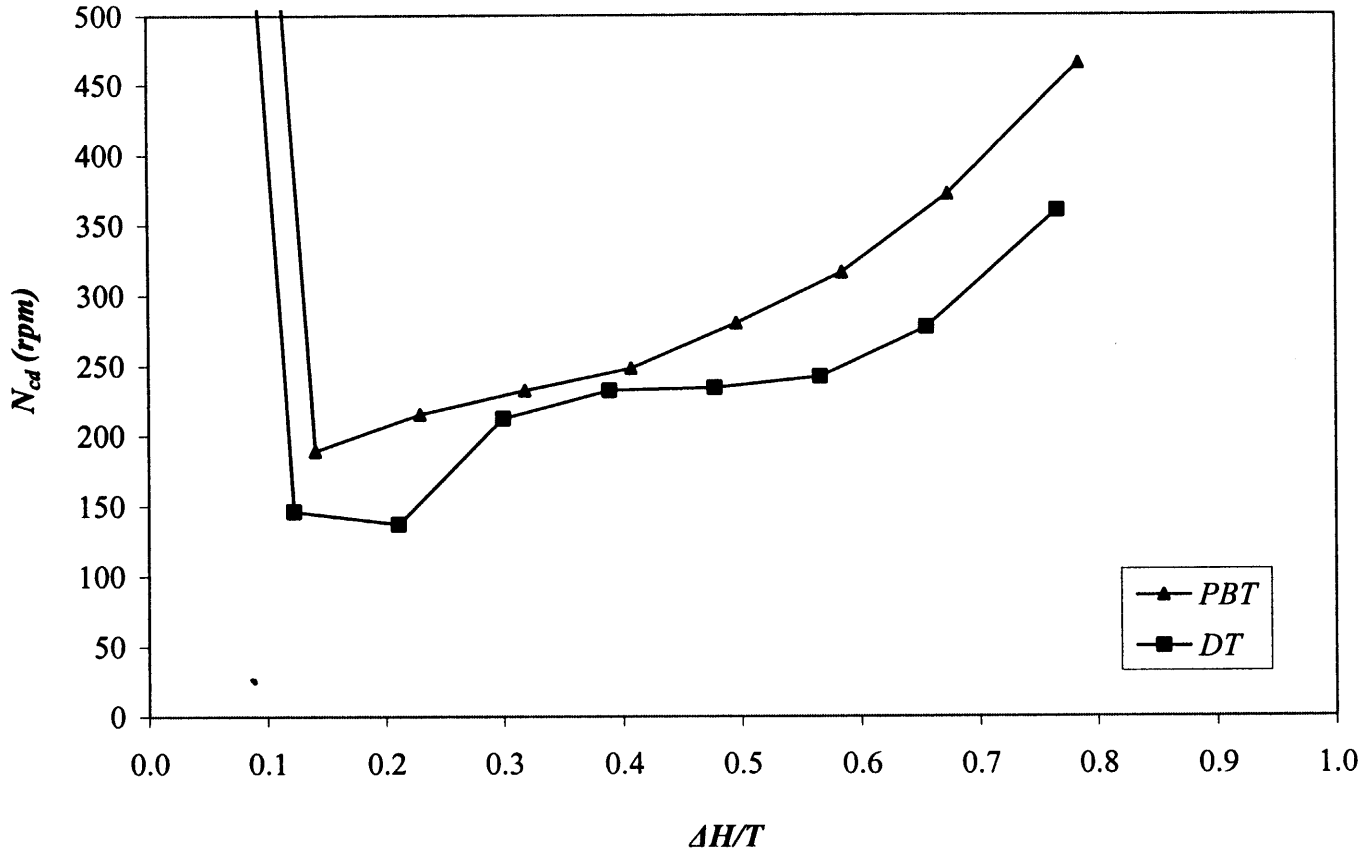

Figure A.22 Comparison of N_{cd} vs. ΔH at C=0.0762m.

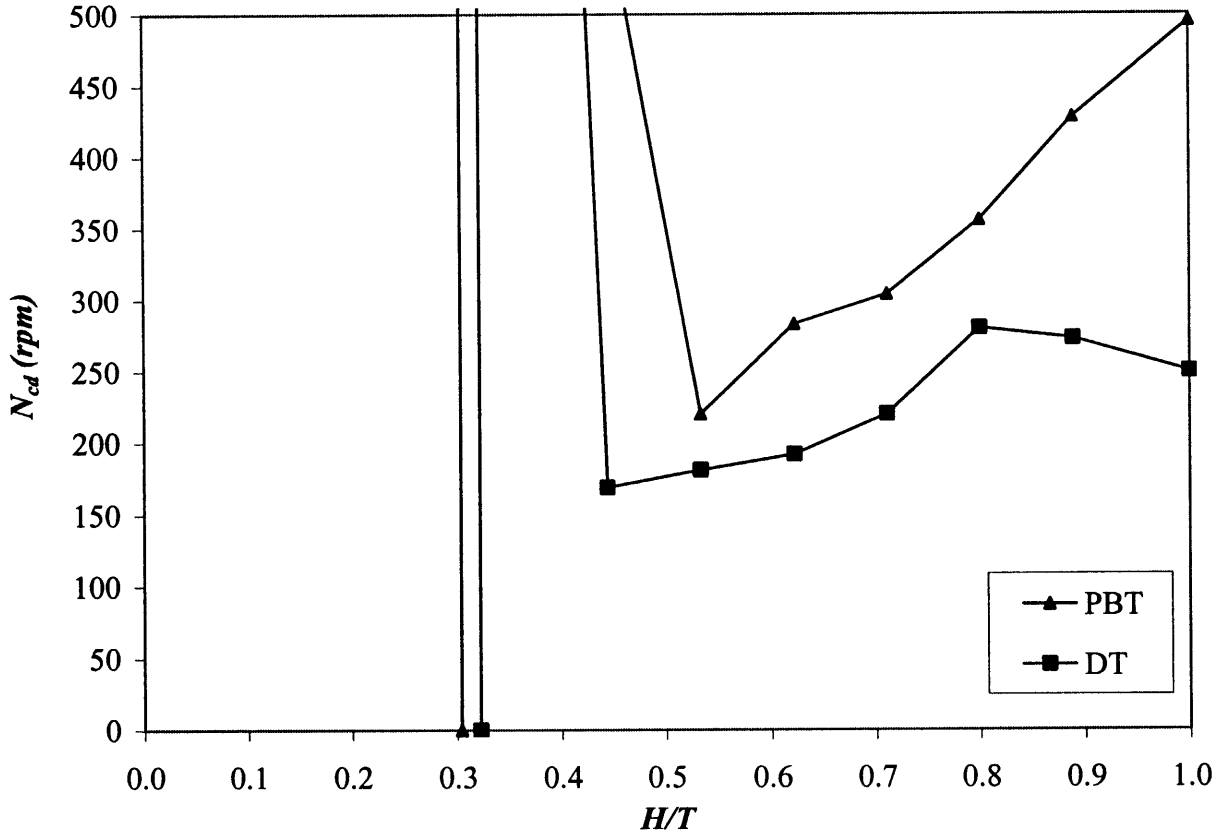

Figure A.23 Comparison of N_{cd} vs. H at C=0.1016m.
The vertical lines were drawn in correspondence of $H=C_b$ for each curve.

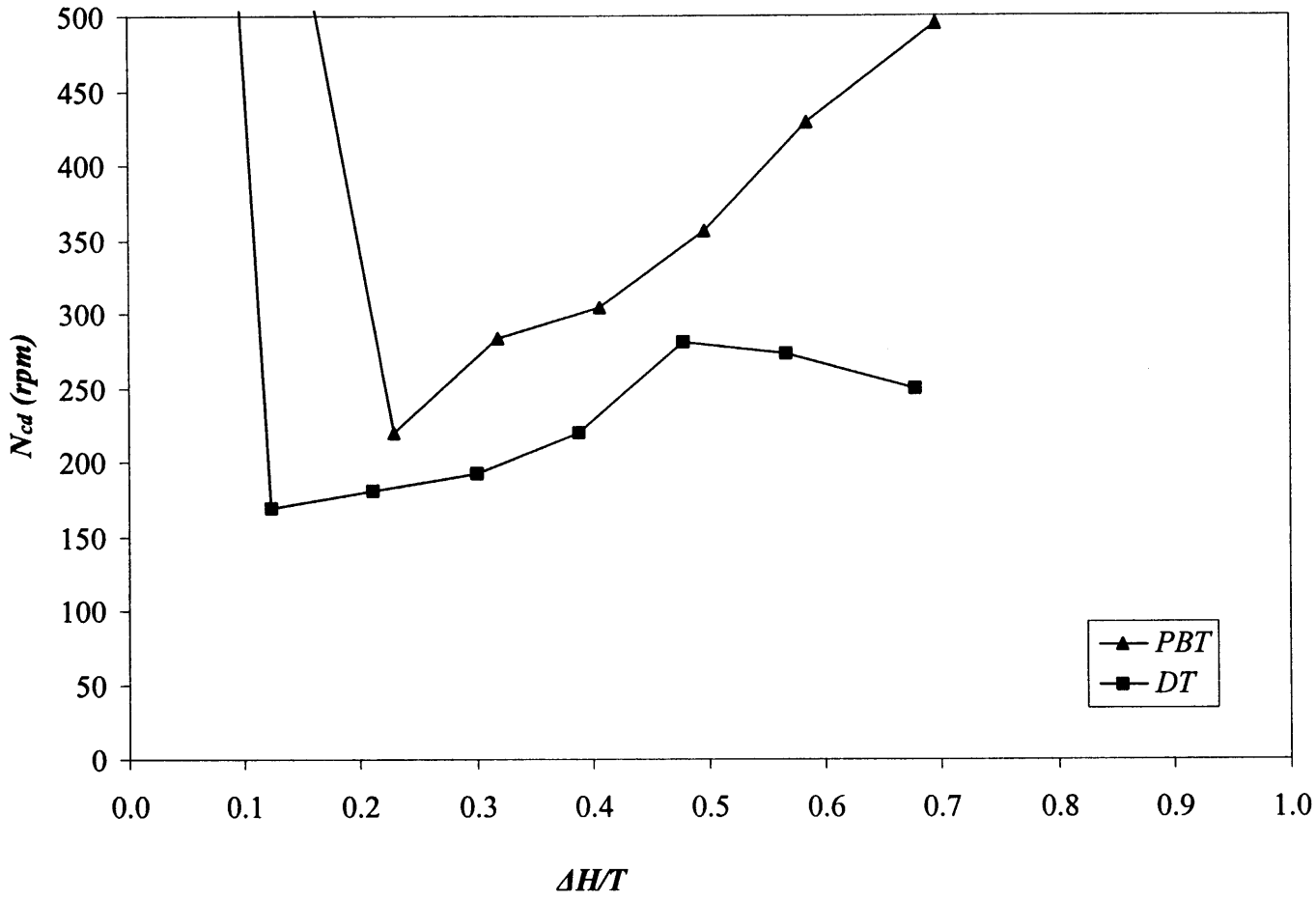

Figure A.24 Comparison of N_{cd} vs. ΔH at C=0.1016m.

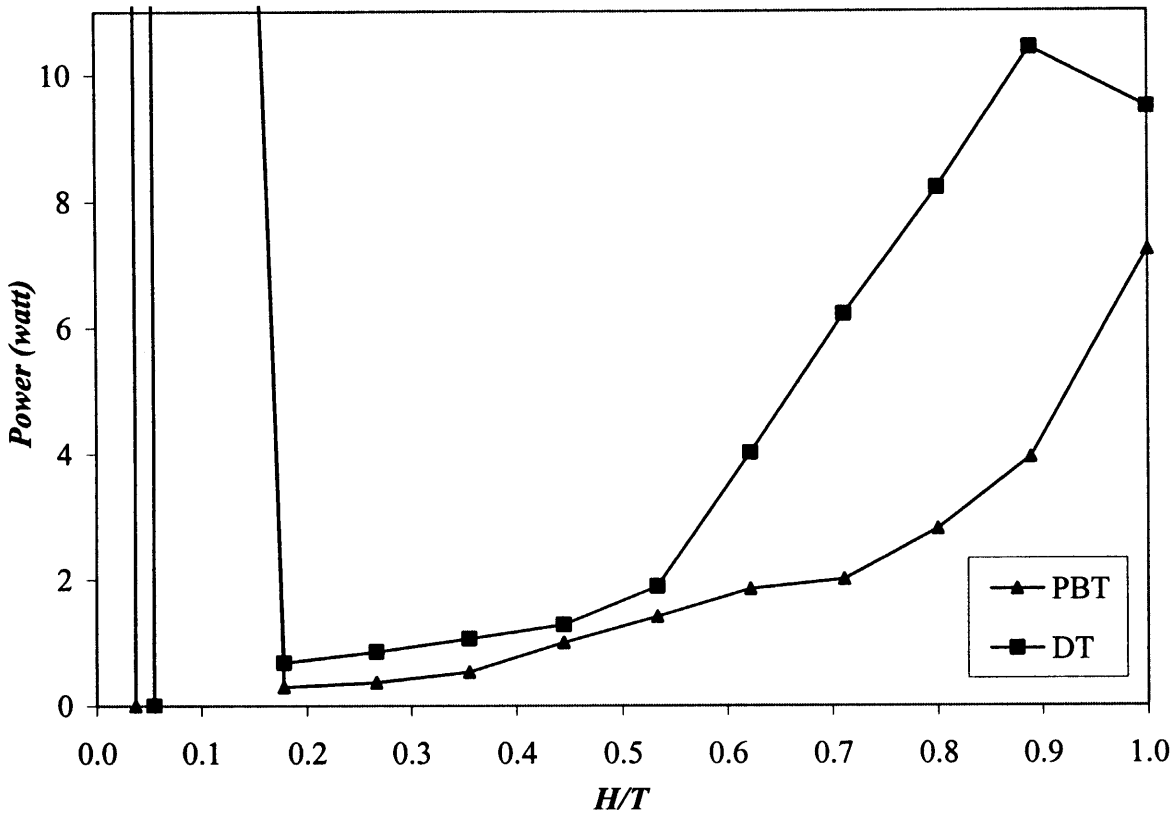

Figure A.25 Comparison of P vs. H at C=0.0254m.
The vertical lines were drawn in correspondence of $H=C_b$ for each curve.

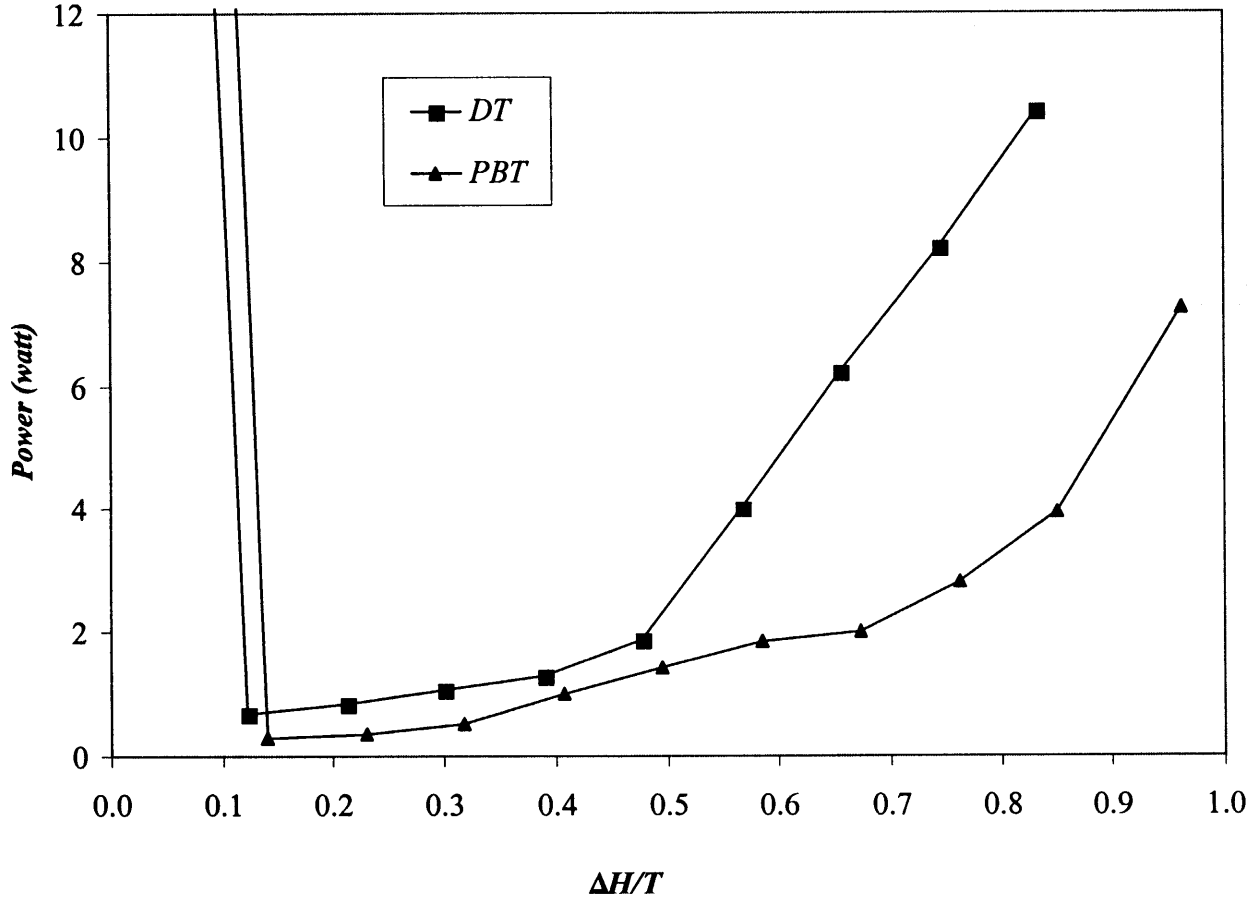

Figure A.26 Comparison of P vs. ΔH at C=0.0254m.

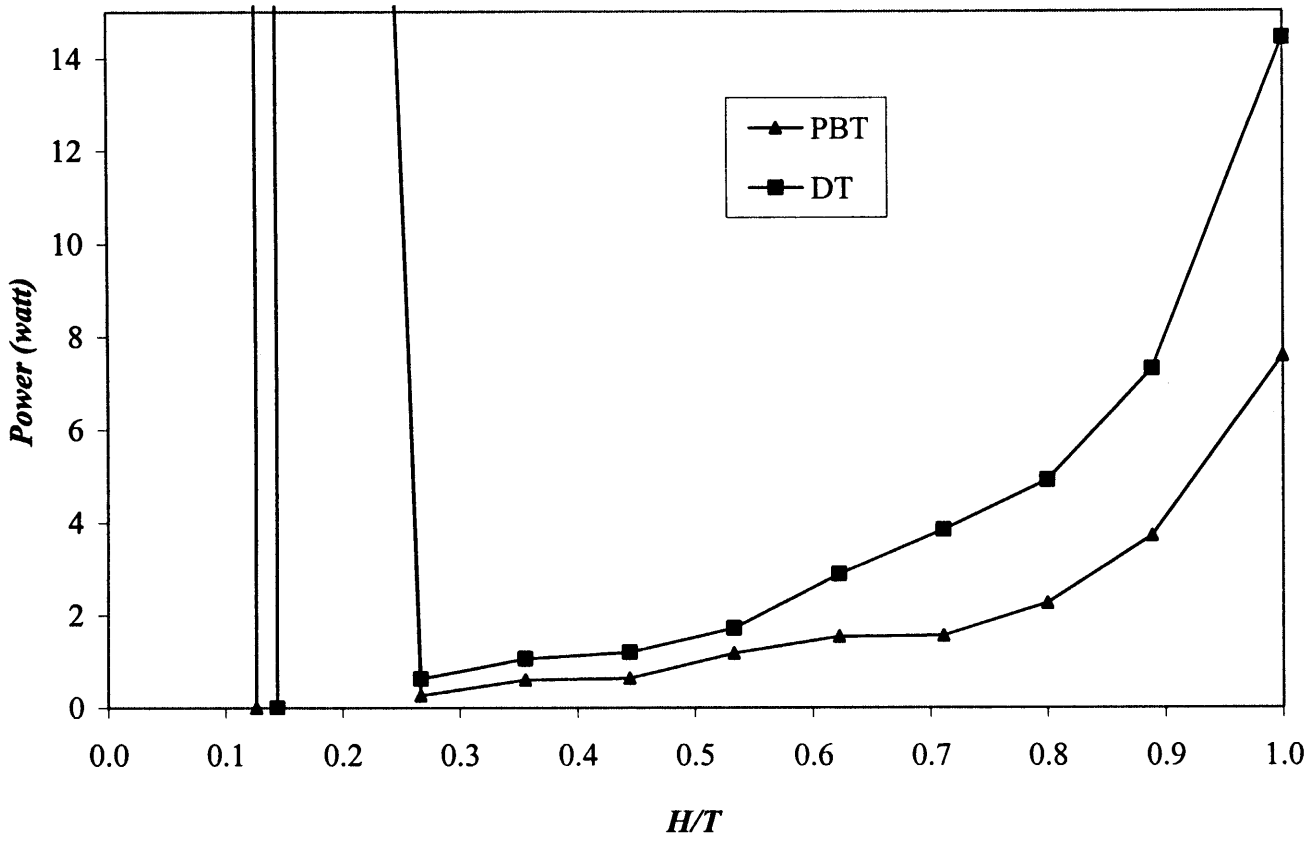

Figure A.27 Comparison of P vs. H at C=0.0508m.
The vertical lines were drawn in correspondence of $H=C_b$ for each curve.

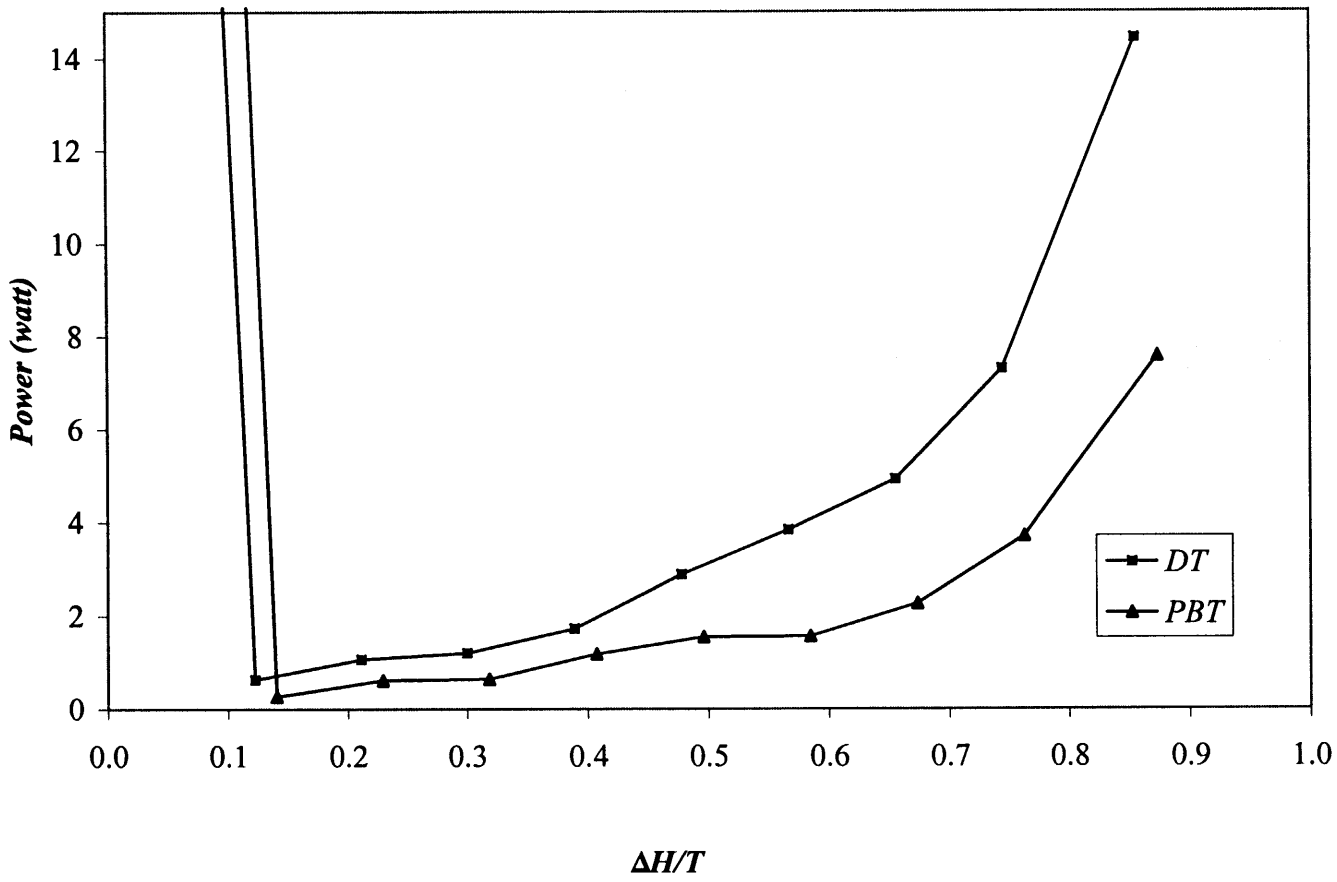

Figure A.28 Comparison of P vs. ΔH at C=0.0508m.

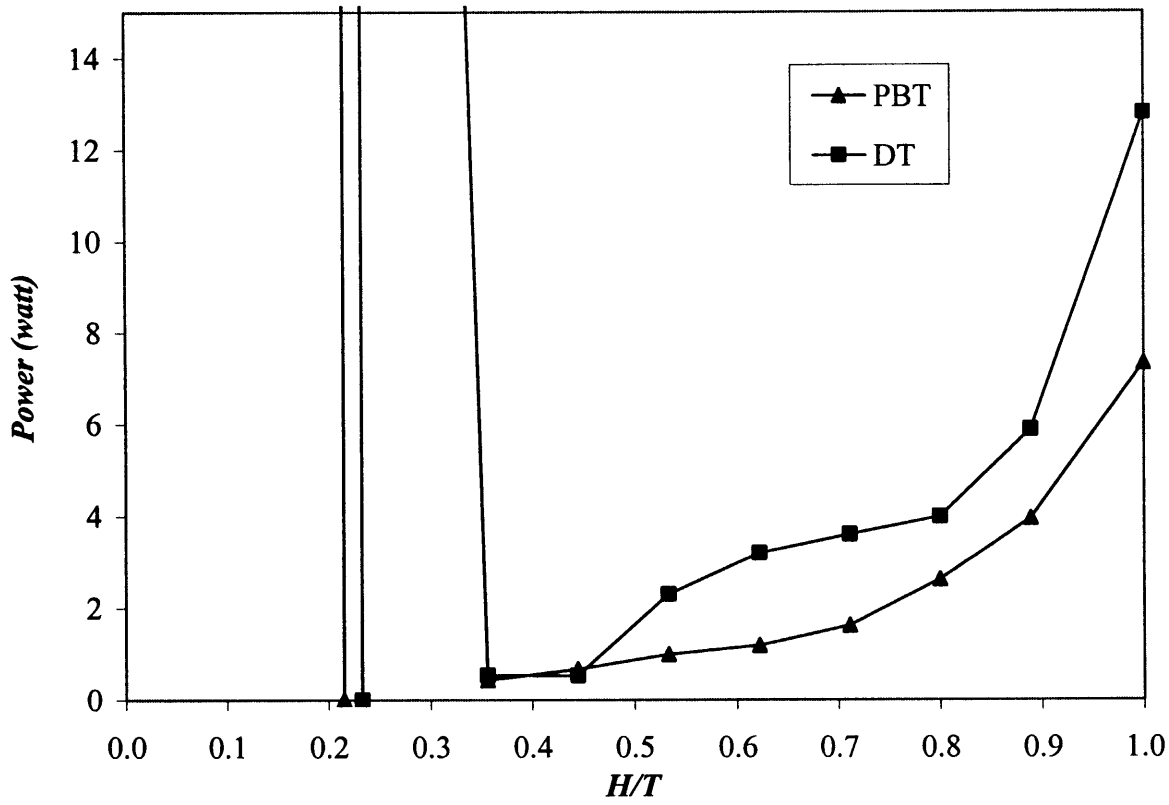

Figure A.29 Comparison of P vs. H at C=0.0762m.
The vertical lines were drawn in correspondence of $H=C_b$ for each curve.

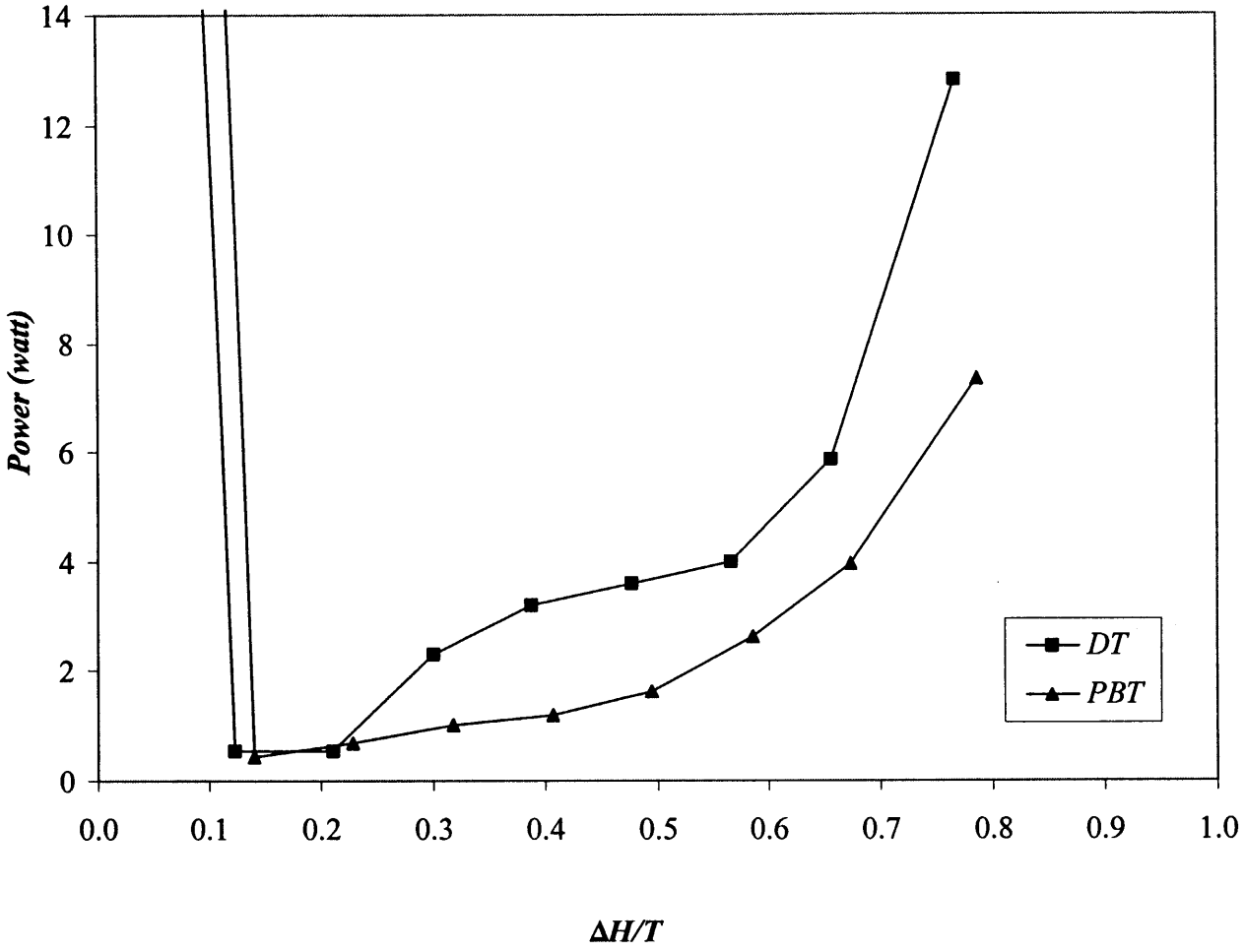

Figure A.30 Comparison of P vs. ΔH at C=0.0762m.

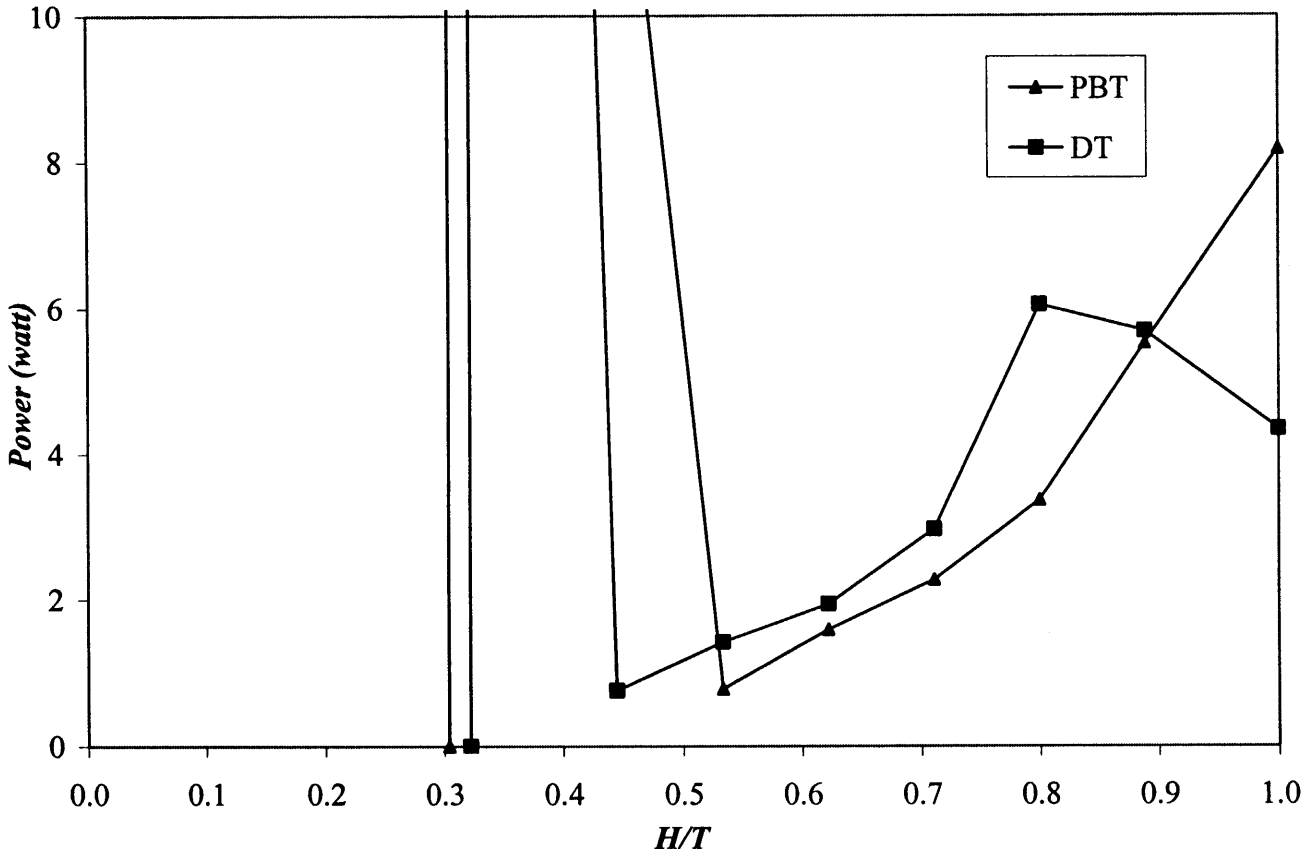

Figure A.31 Comparison of P vs. H at C=0.1016m.
The vertical lines were drawn in correspondence of $H=C_b$ for each curve.

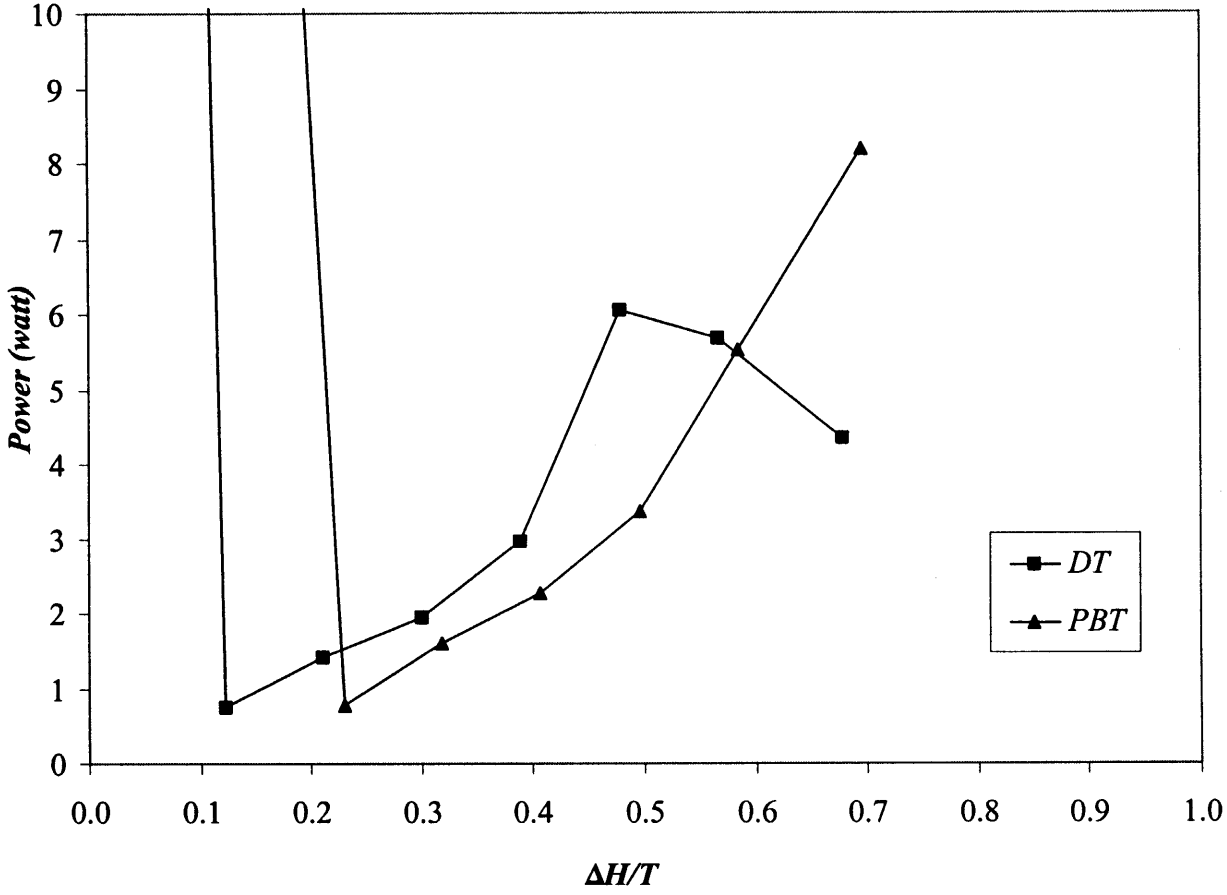

Figure A.32 Comparison of P vs. ΔH at C=0.1016m.

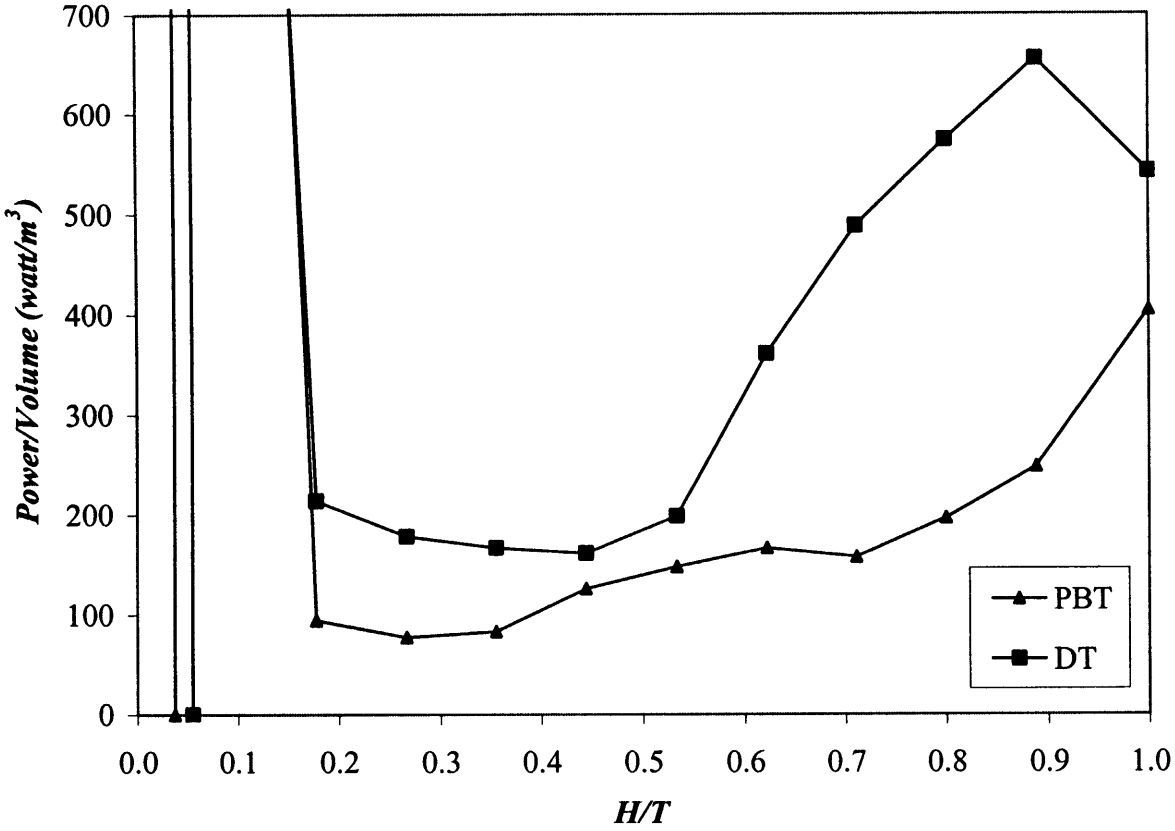

Figure A.33 Comparison of P/V vs. H at C=0.0254m.
The vertical lines were drawn in correspondence of $H=C_b$ for each curve.

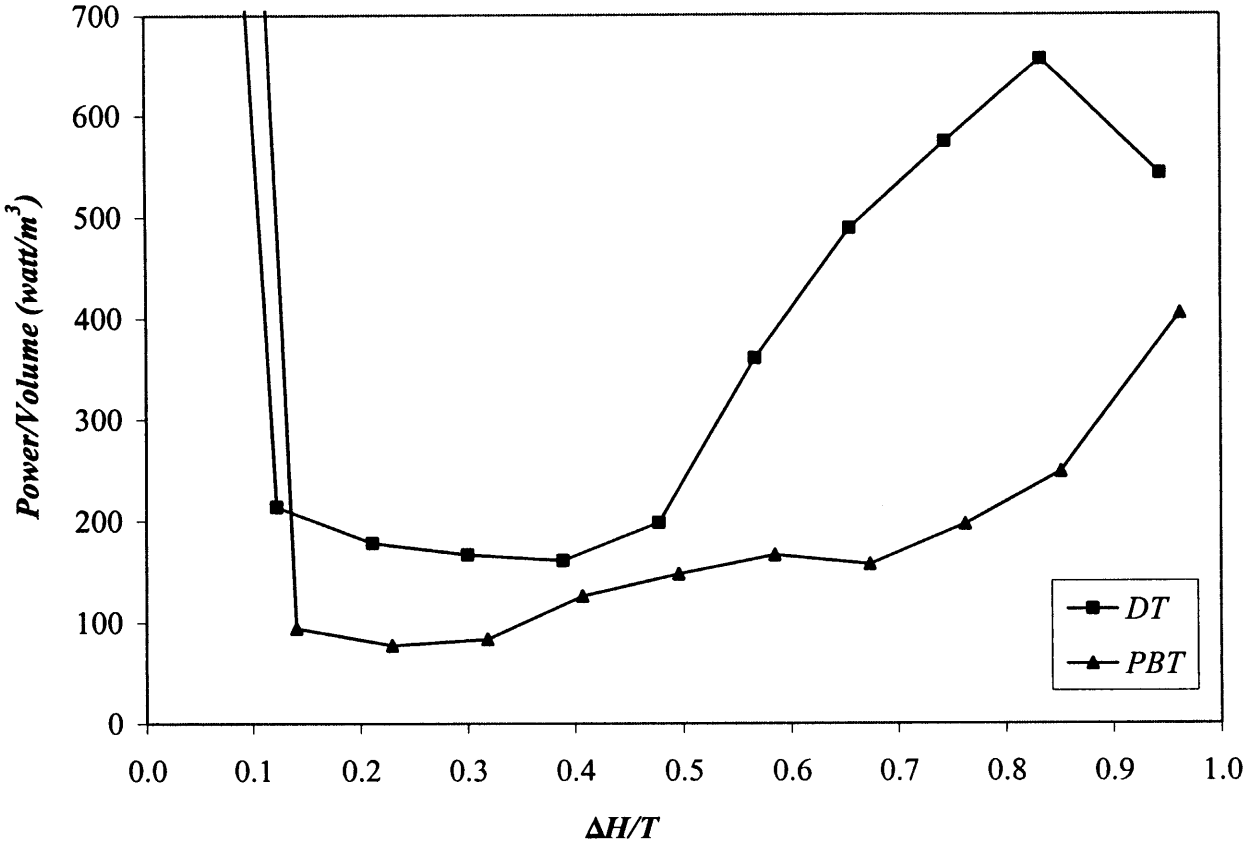

Figure A.34 Comparison of P/V vs. ΔH at C=0.0254m.

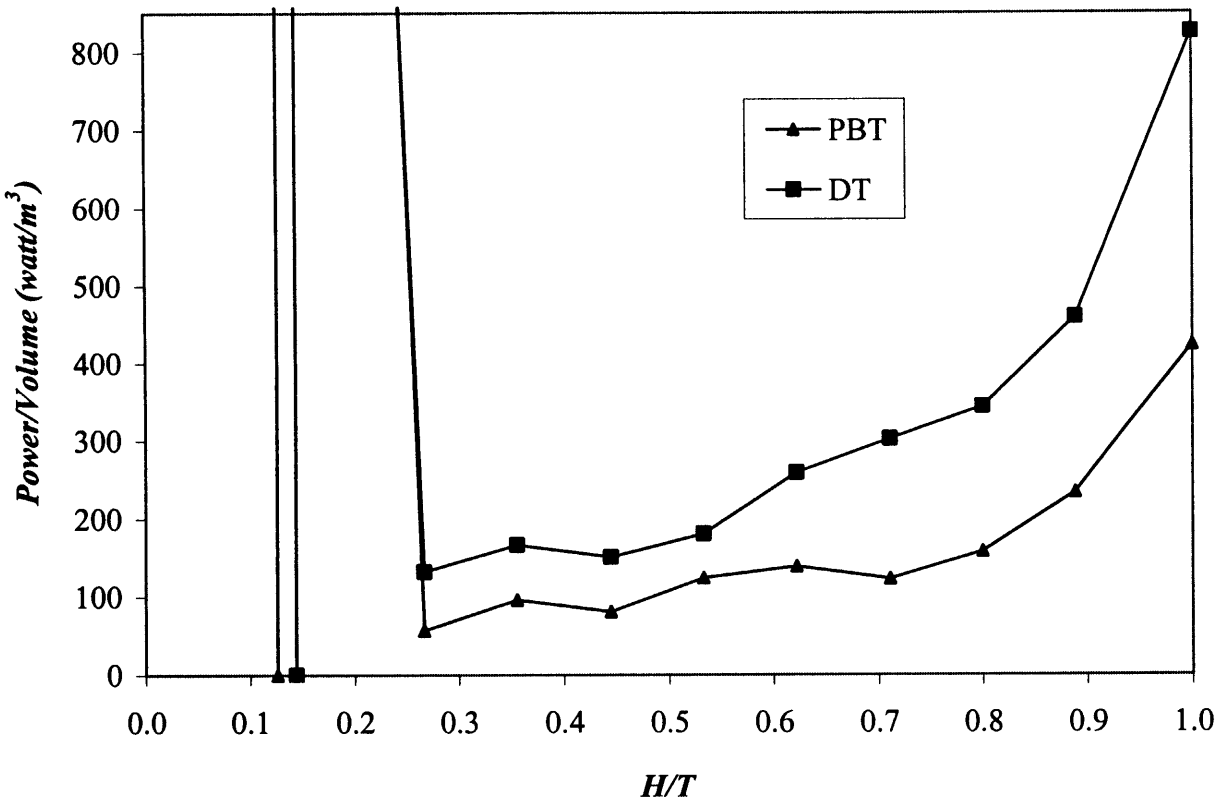

Figure A.35 Comparison of P/V vs. H at C=0.0508m.
The vertical lines were drawn in correspondence of $H=C_b$ for each curve.

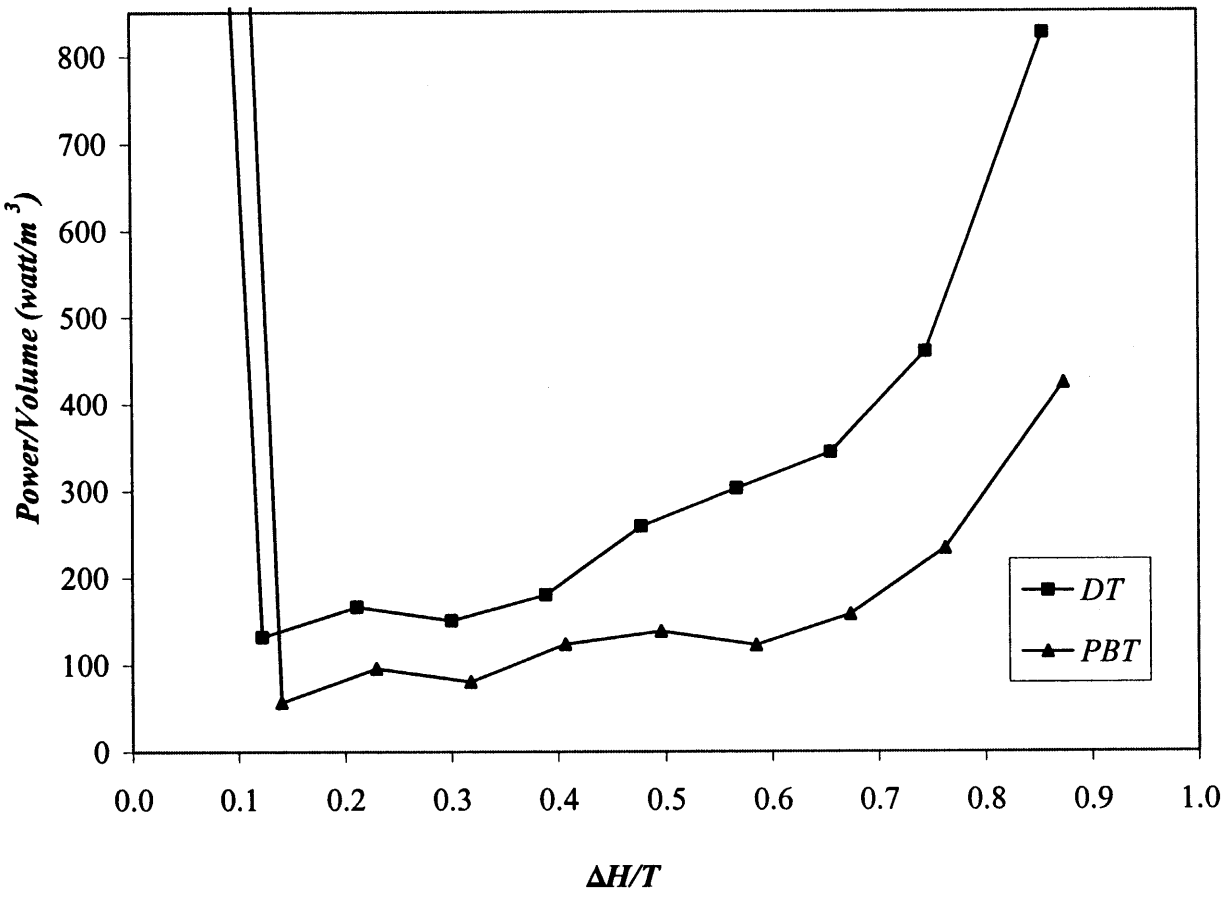

Figure A.36 Comparison of P/V vs. ΔH at C=0.0508m.

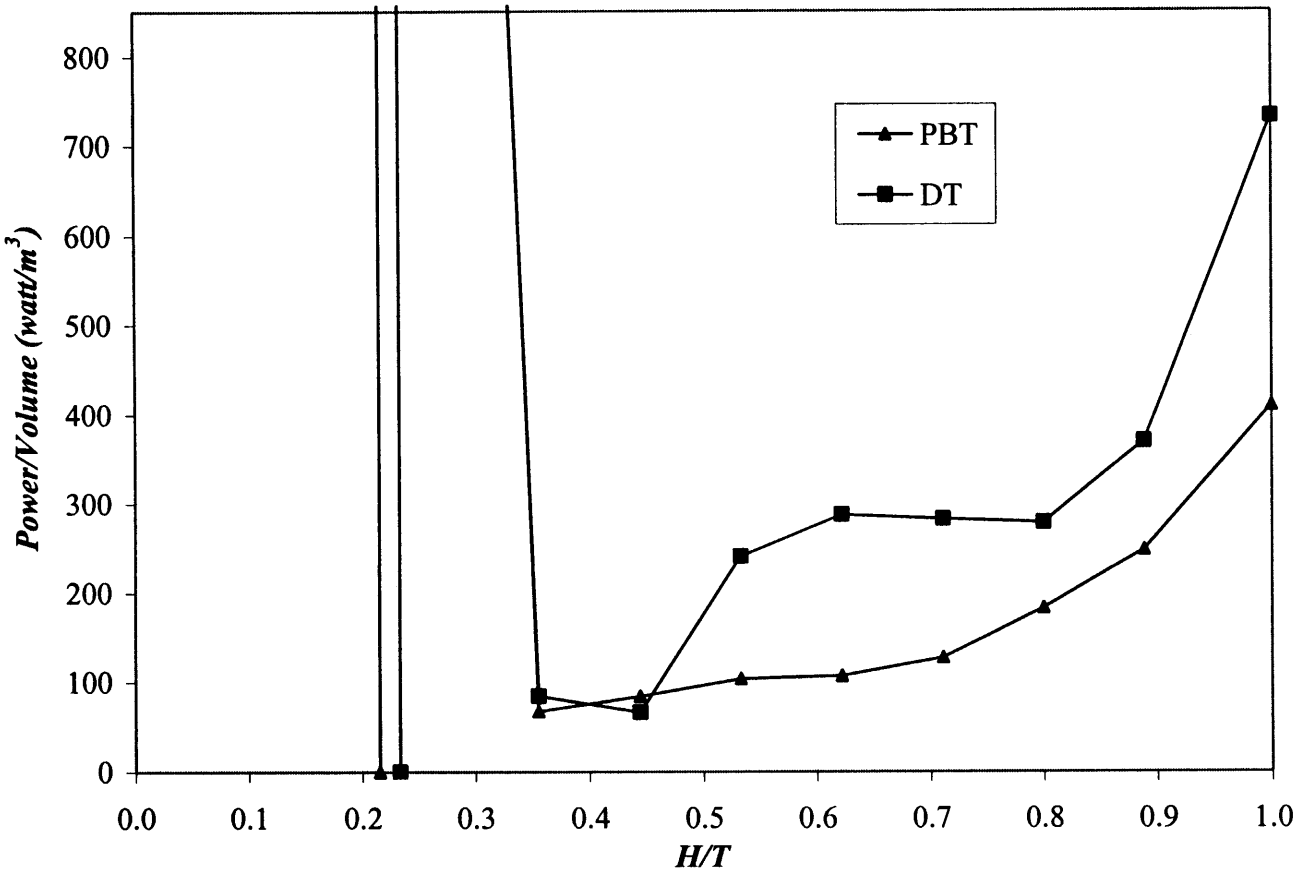

Figure A.37 Comparison of P/V vs. H at C=0.0762m.
The vertical lines were drawn in correspondence of $H=C_b$ for each curve.

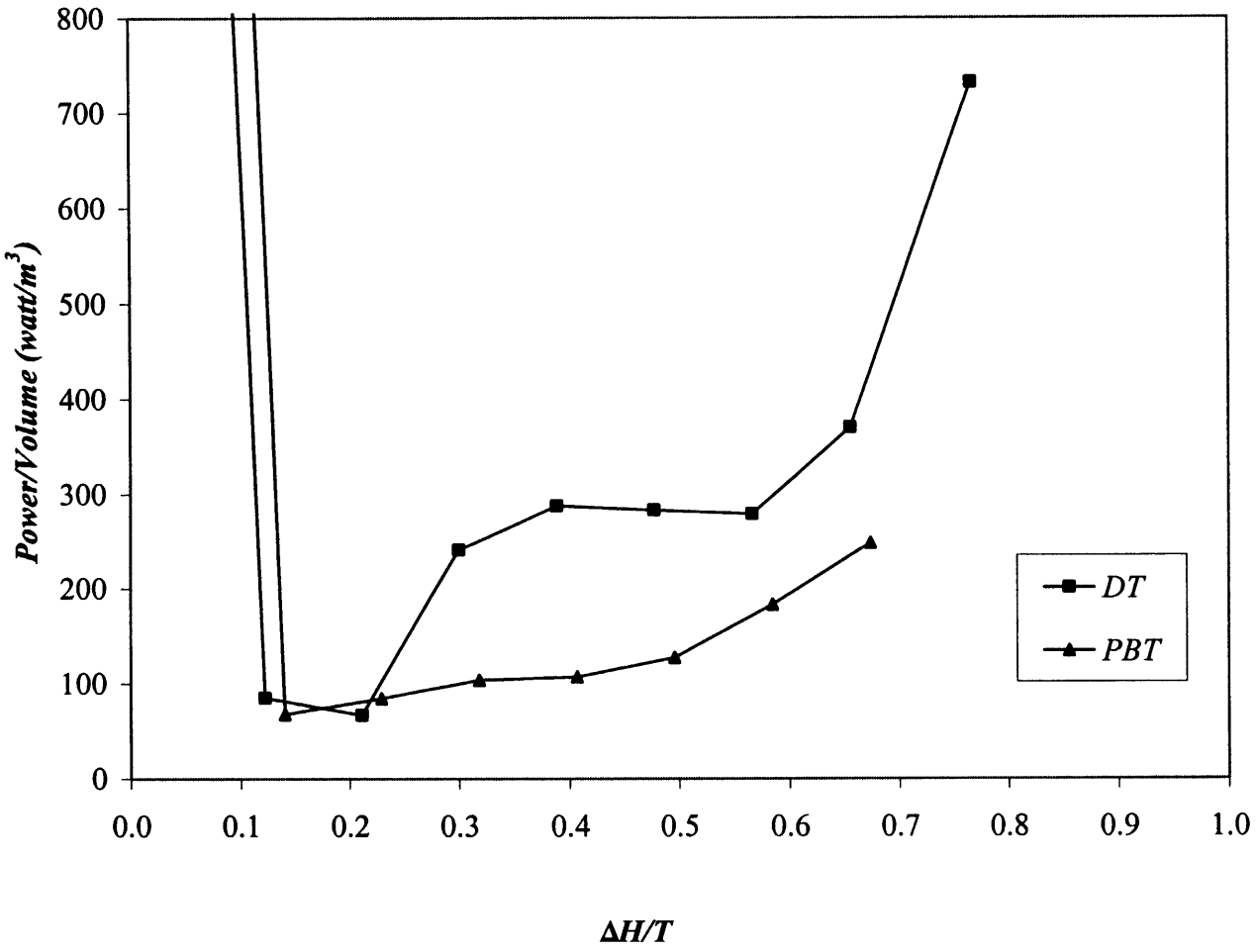

Figure A.38 Comparison of P/V vs. ΔH at C=0.0762m.

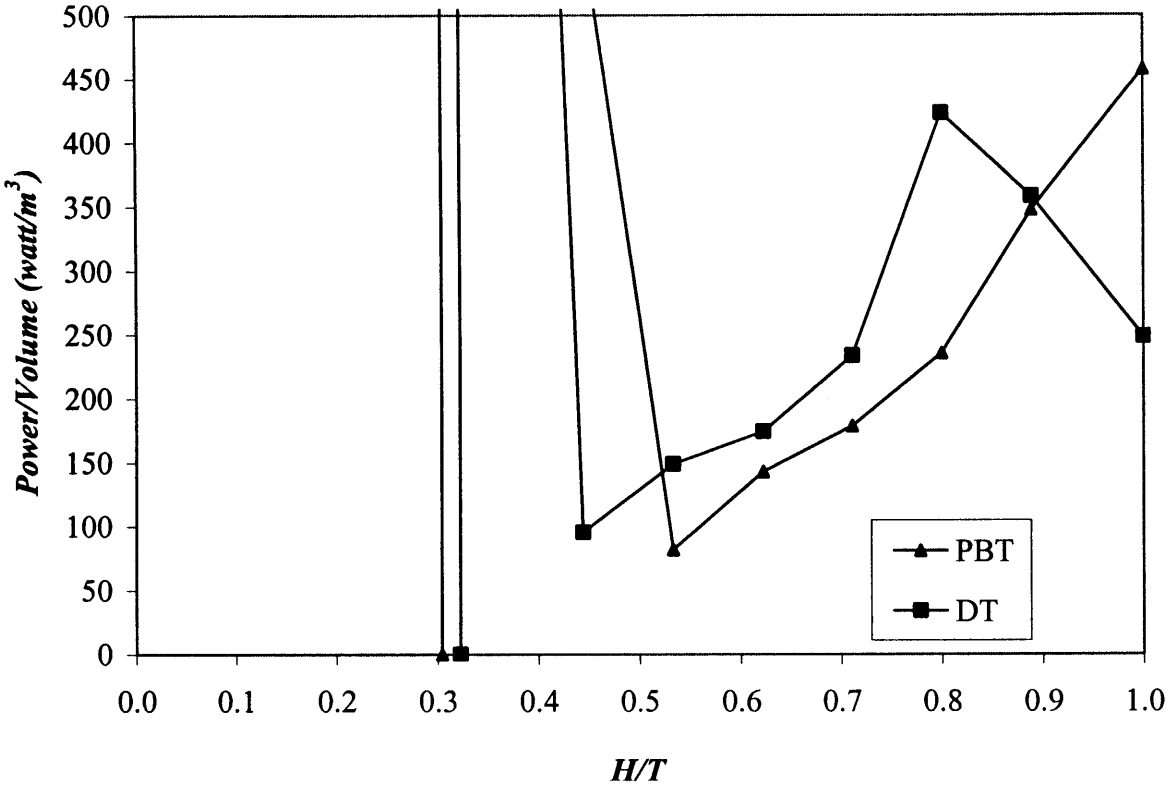

Figure A.39 Comparison of P/V vs. H at C=0.1016m.
The vertical lines were drawn in correspondence of $H=C_b$ for each curve.

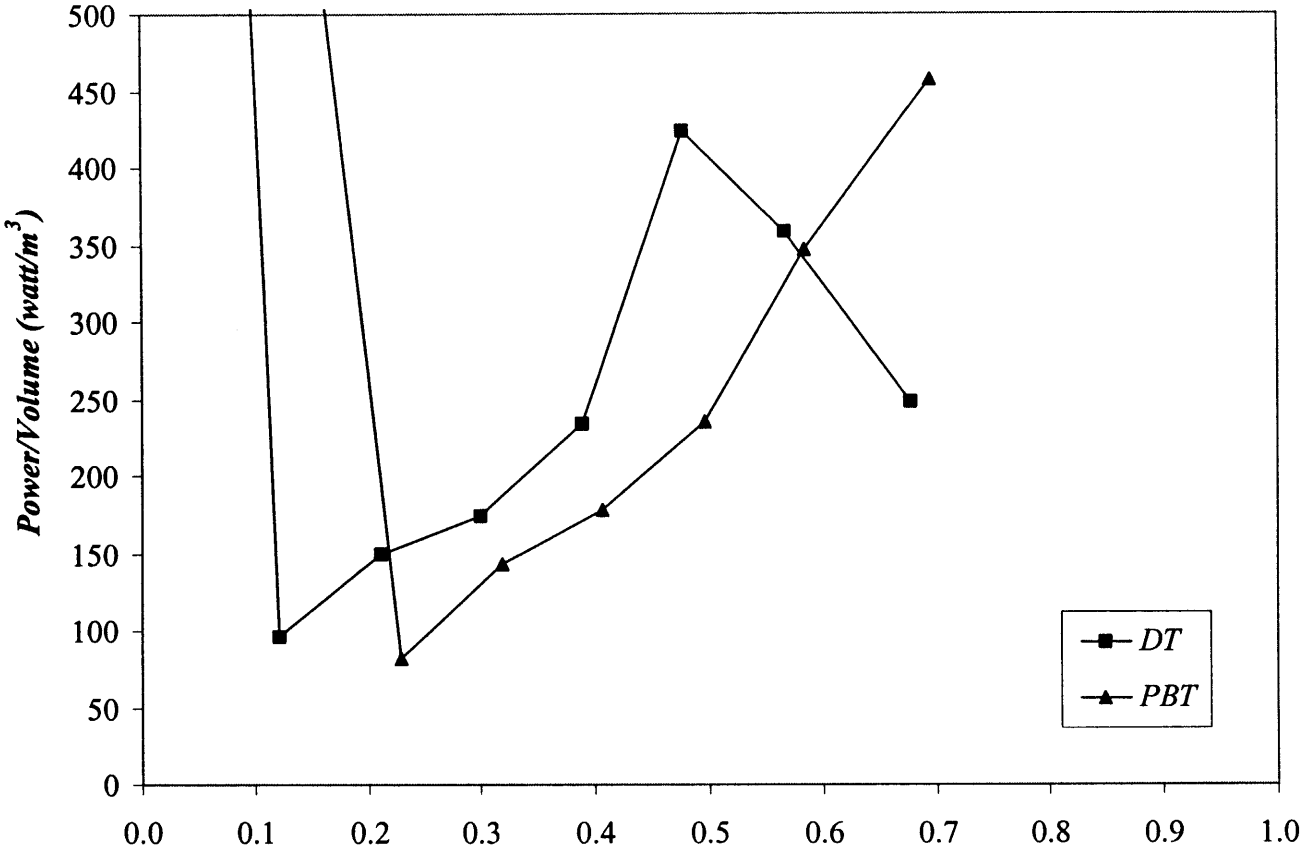

Figure A.40 Comparison of P/V vs. ΔH at C=0.1016m.

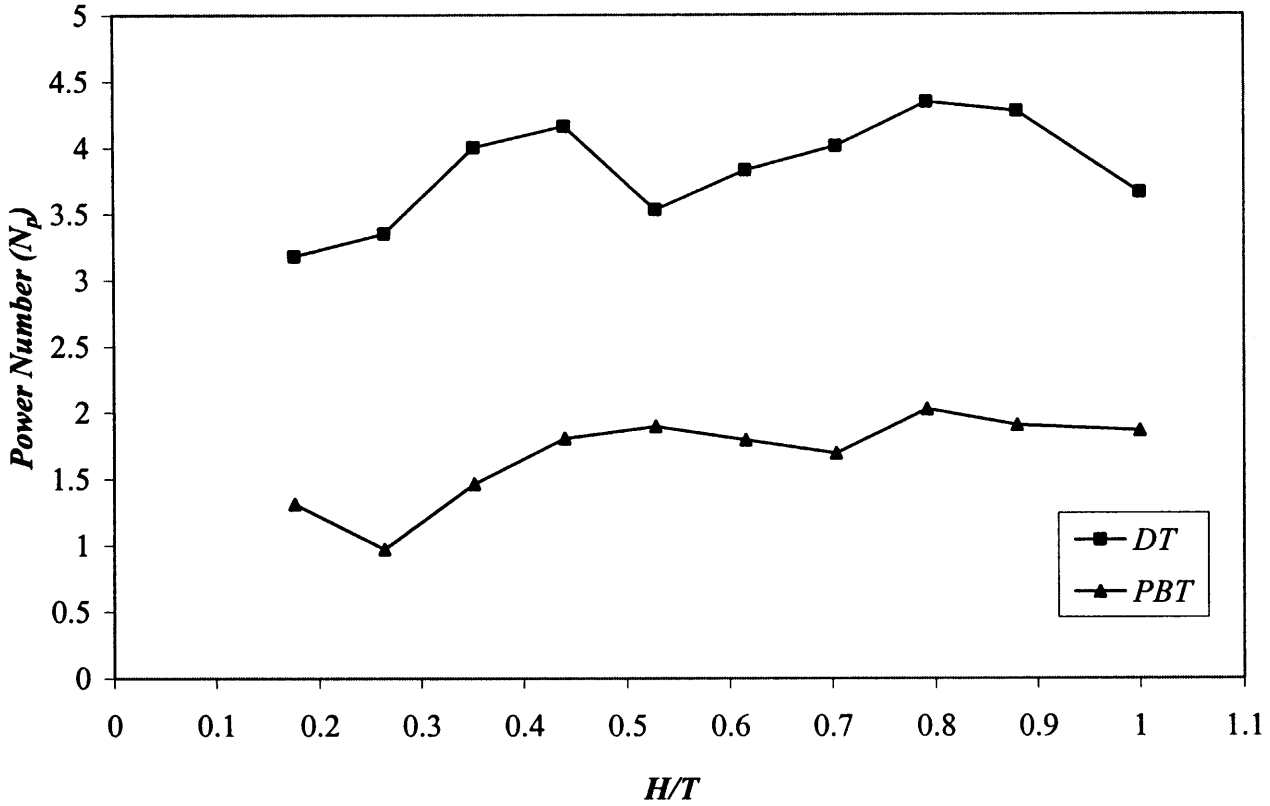

Figure A.41 Comparison of N_p vs. H at C=0.0254m.

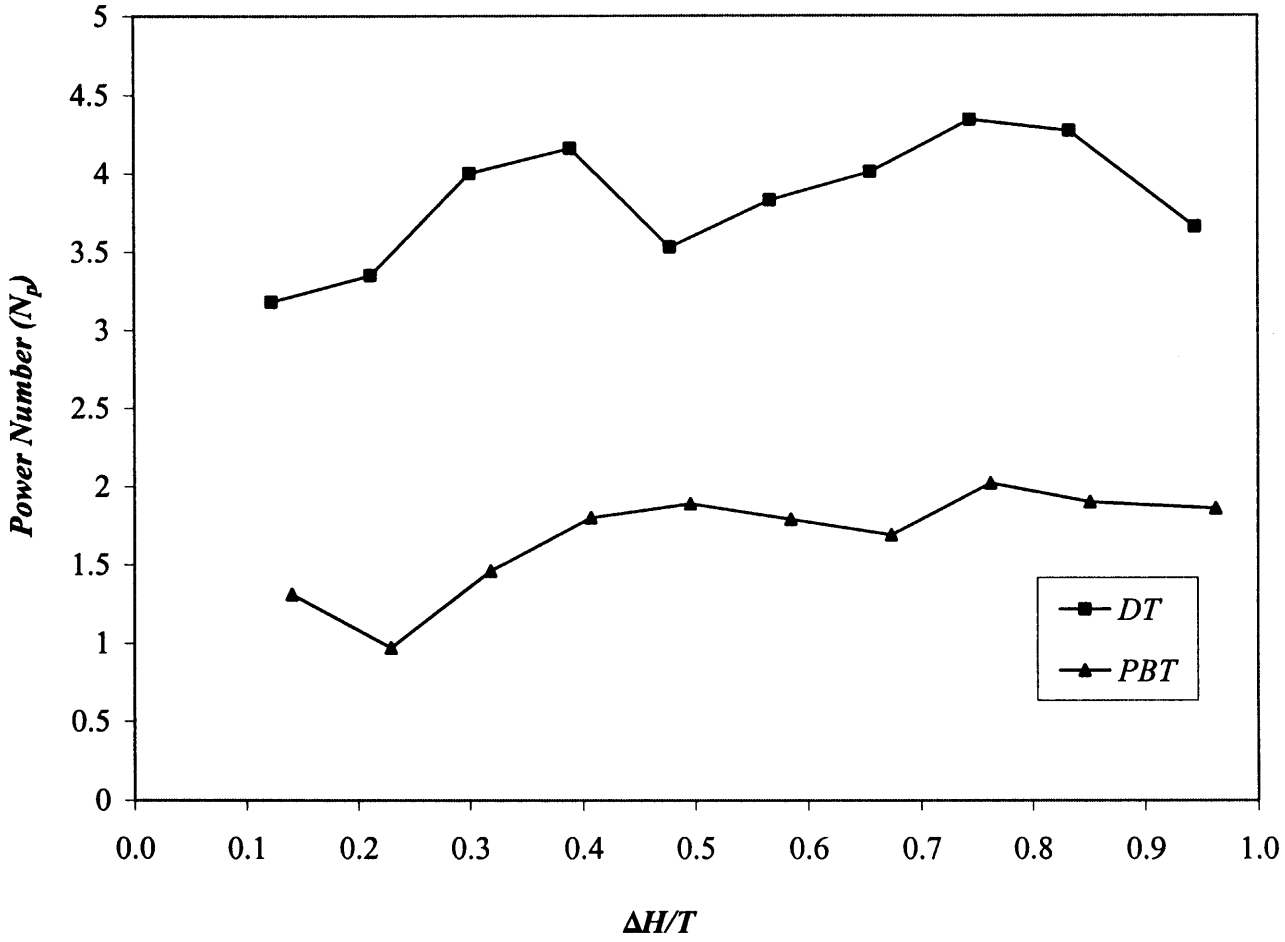

Figure A.42 Comparison of N_p vs. ΔH at C=0.0254m.

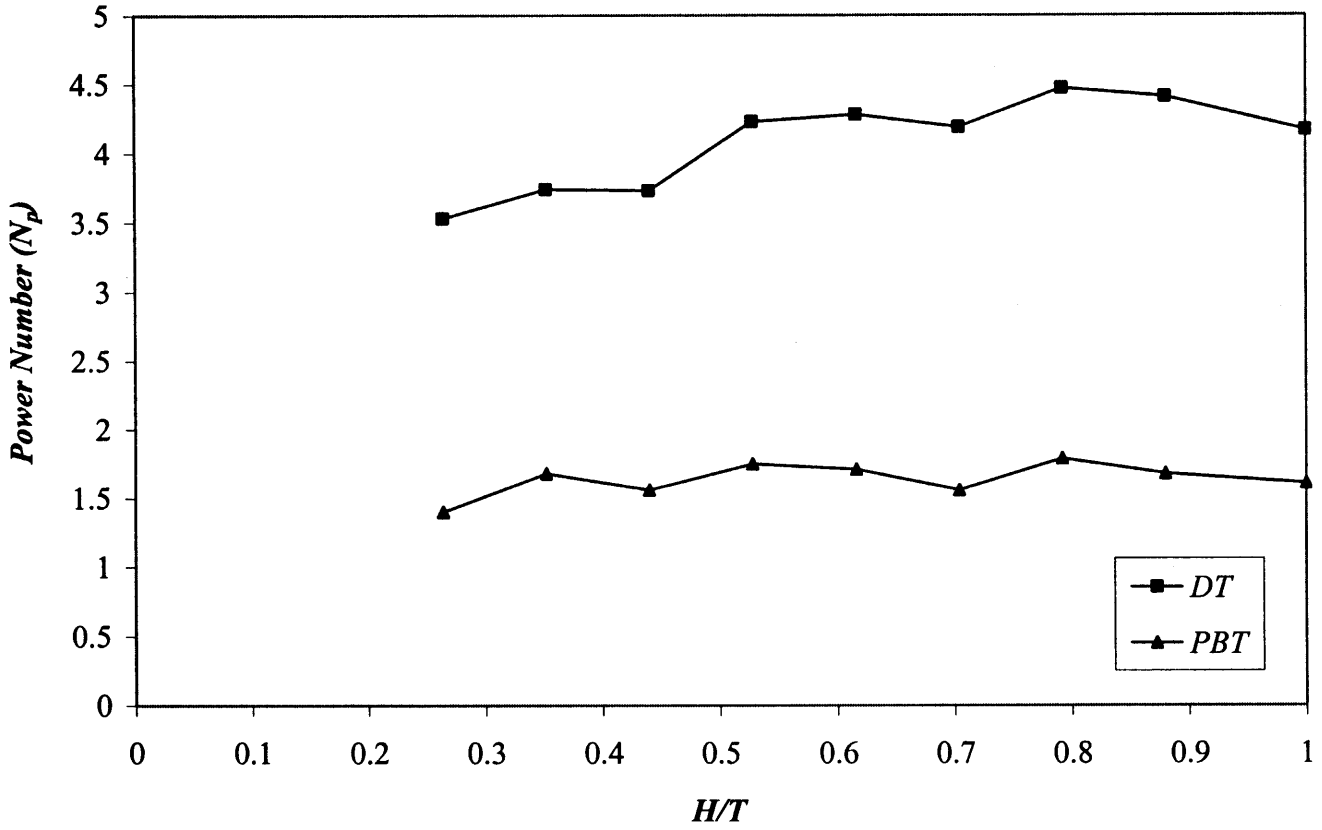

Figure A.43 Comparison of N_p vs. H at C=0.0508m.

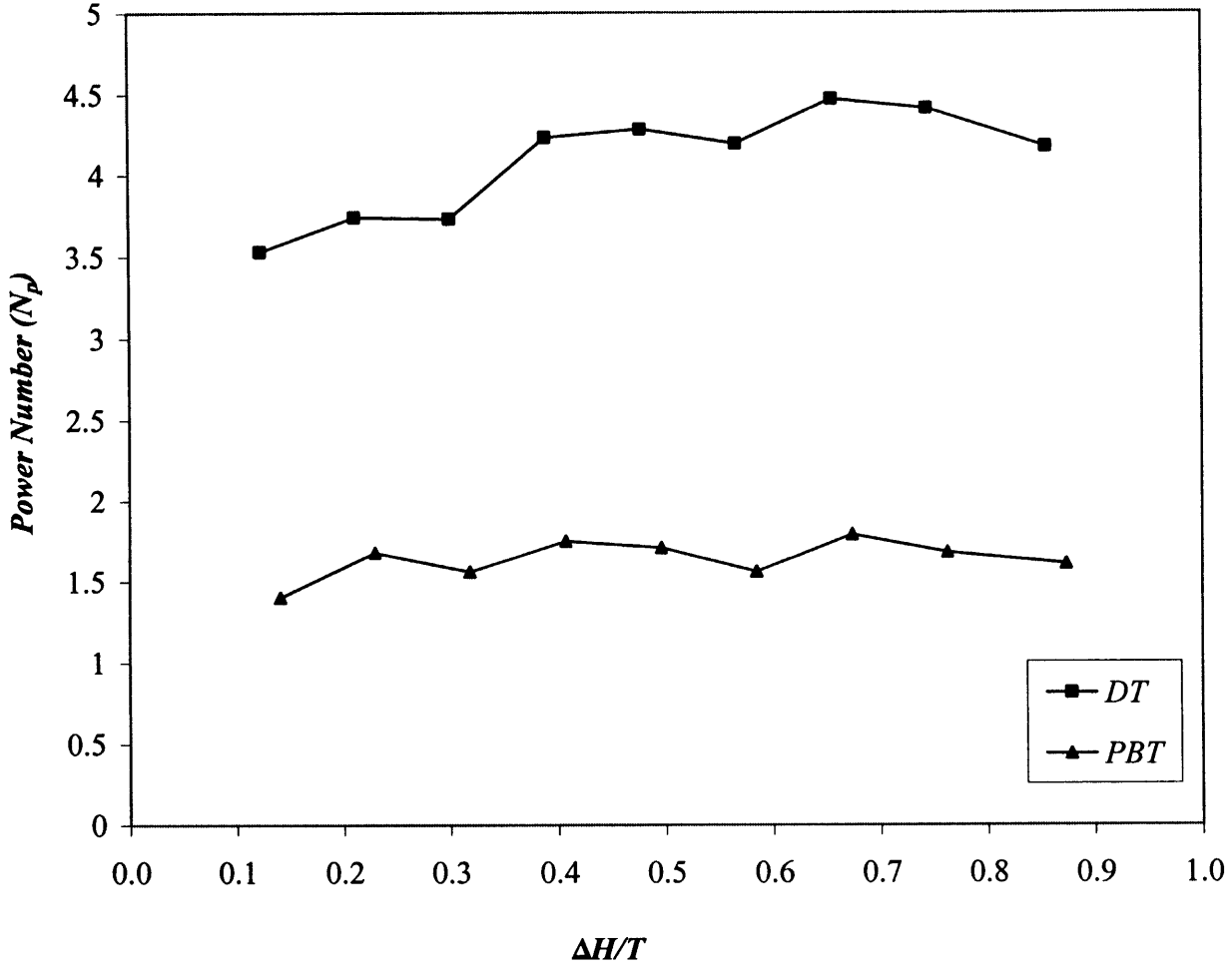

Figure A.44 Comparison of N_p vs. ΔH at C=0.0508m.

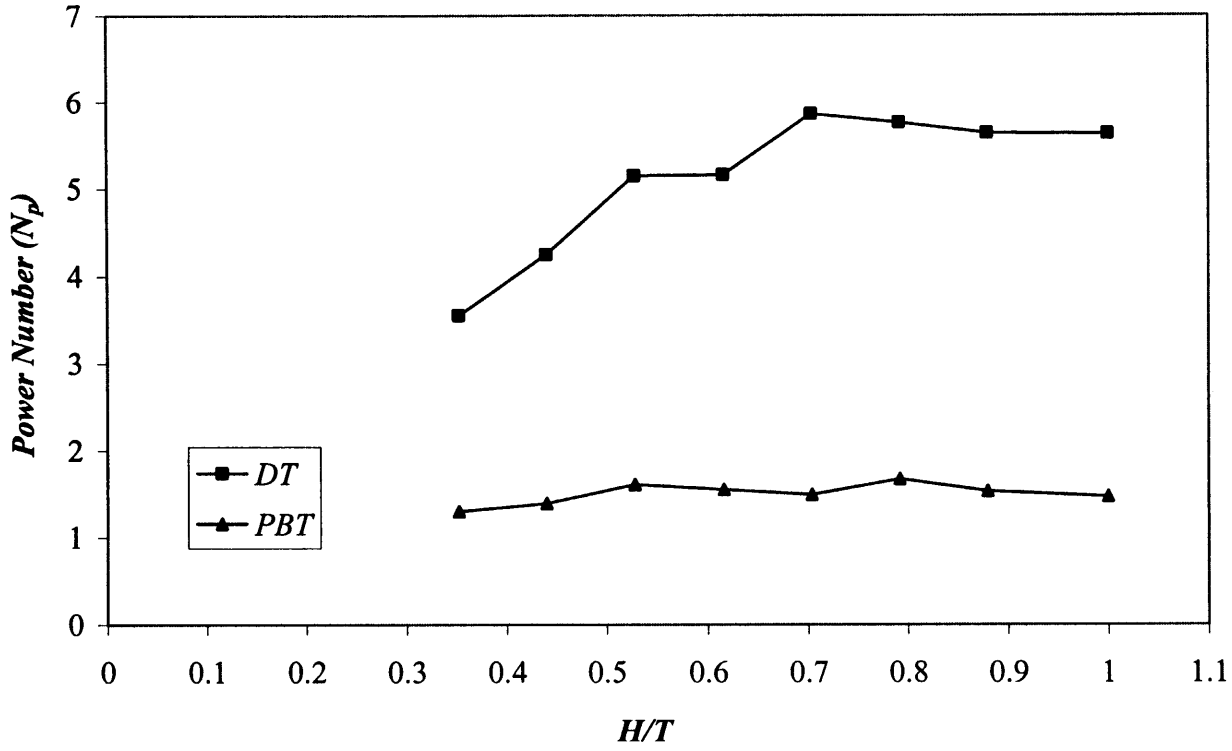

Figure A.45 Comparison of N_p vs. H at C=0.0762m.

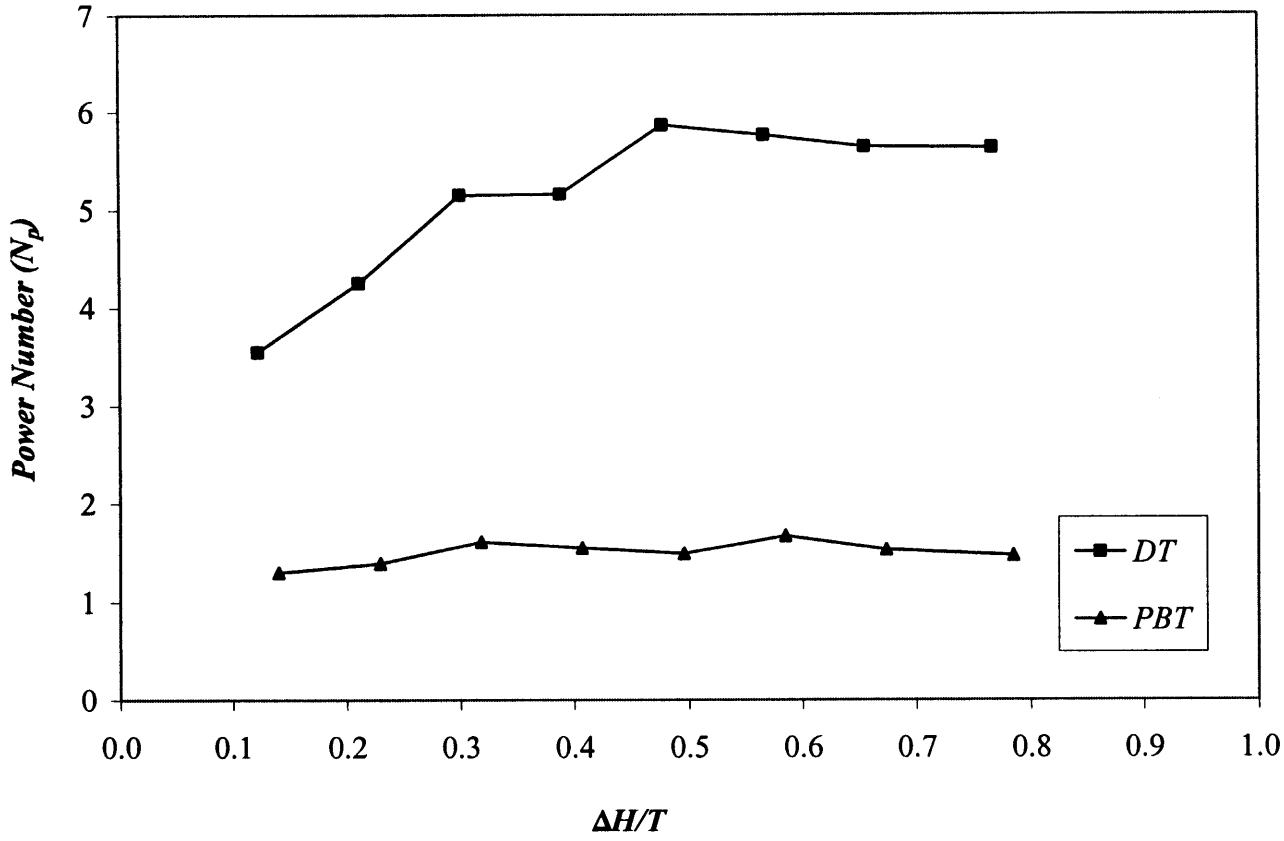

Figure A.46 Comparison of N_p vs. ΔH at C=0.0762m.

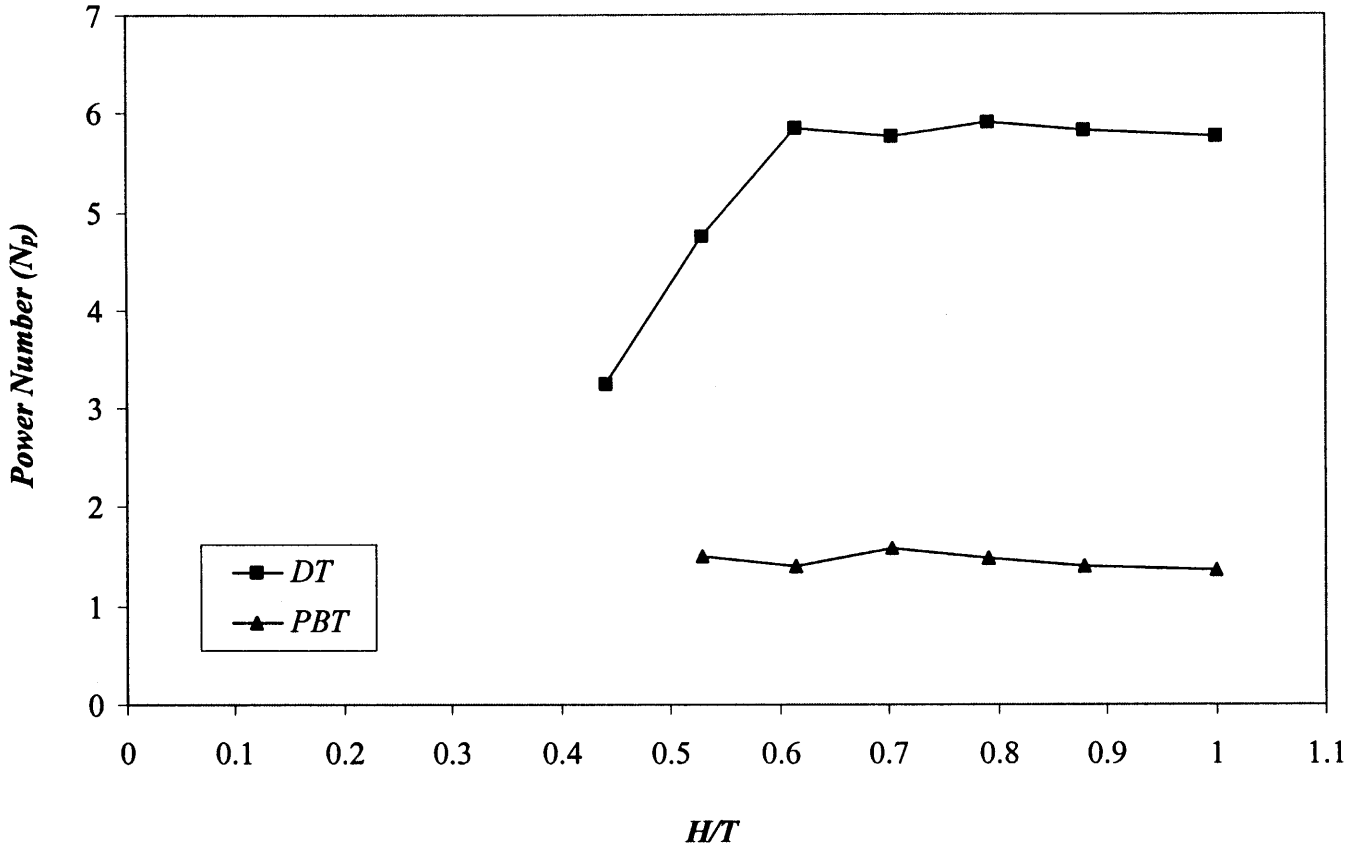

Figure A.47 Comparison of N_p vs. H at C=0.1016m.

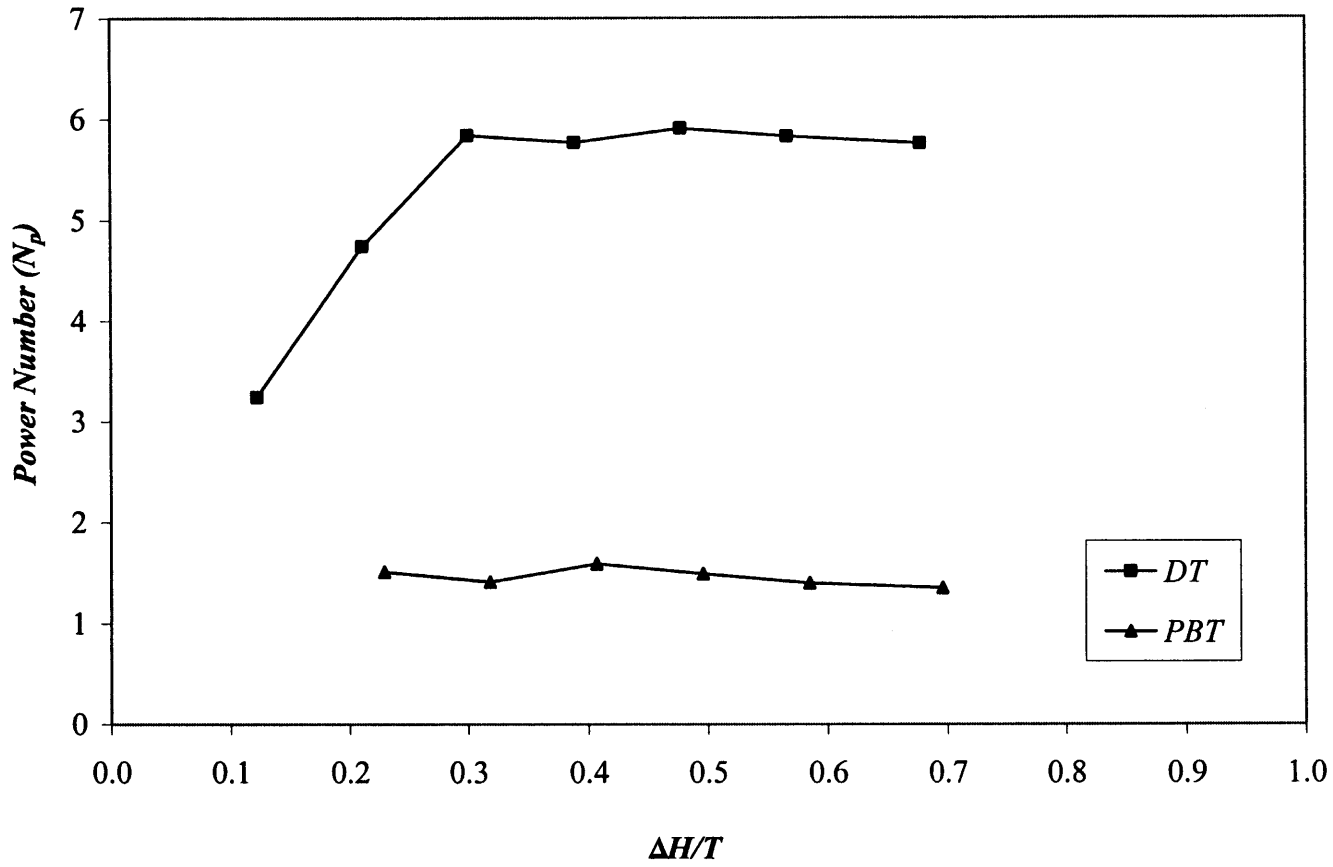

Figure A.48 Comparison of N_p vs. ΔH at C=0.1016m.

APPENDIX B

TABLES FOR CHAPTER 5

This Appendix includes tables showing the effect of liquid height on the minimum agitation speed for complete liquid-liquid dispersion N_{cd} (in rpm), power P (in watts), power/volume P/V, (in watts/m^3) and power number (N_p) for DT (Tables B.1-B.8) and PBT (Tables B.9-B.16).

Table B.1 Effect of H on N_{cd} **(DT)**

H/T	C_b/T= 0.055	H/T	C_b/T= 0.144	H/T	C_b/T= 0.233	H/T	C_b/T= 0.322
0.15	∞	0.21	-	0.27	-	0.33	-
0.18	164	0.24	∞	0.3	-	0.36	-
0.26	169	0.26	150	0.33	∞	0.39	-
0.35	180	0.35	175	0.35	146	0.42	∞
0.44	190	0.44	185	0.44	137	0.44	169
0.53	222	0.53	204	0.53	212	0.53	181
0.62	279	0.62	240	0.62	232	0.62	192
0.7	315	0.7	260	0.7	234	0.7	220
0.79	342	0.79	285	0.79	242	0.79	280
0.88	367	0.88	325	0.88	277	0.88	273
1	376	1	405	1	360	1	250

Table B.2 Effect of H on P **(DT)**

H/T	C_b/T= 0.055	H/T	C_b/T= 0.144	H/T	C_b/T= 0.233	H/T	C_b/T= 0.322
0.15	∞	0.21	-	0.27	-	0.33	-
0.18	0.68	0.24	∞	0.3	-	0.36	-
0.26	0.85	0.26	0.63	0.33	∞	0.39	-
0.35	1.06	0.35	1.06	0.35	0.54	0.42	∞
0.44	1.28	0.44	1.2	0.44	0.53	0.44	0.76
0.53	1.89	0.53	1.72	0.53	2.3	0.53	1.42
0.62	4.01	0.62	2.88	0.62	3.2	0.62	1.94
0.7	6.21	0.7	3.84	0.7	3.6	0.7	2.97
0.79	8.21	0.79	4.91	0.79	3.99	0.79	6.05
0.88	10.42	0.88	7.3	0.88	5.88	0.88	5.69
1	9.48	1	14.43	1	12.8	1	4.34

Table B.3 Effect of H on P/V **(DT)**

H/T	C_b/T= 0.055	H/T	C_b/T= 0.144	H/T	C_b/T= 0.233	H/T	C_b/T= 0.322
0.15	∞	0.21	-	0.27	-	0.33	-
0.18	213.89	0.24	∞	0.3	-	0.36	-
0.26	178.24	0.26	132.11	0.33	∞	0.39	-
0.35	166.71	0.35	166.71	0.35	84.93	0.42	∞
0.44	161.04	0.44	150.98	0.44	66.68	0.44	95.62
0.53	198.16	0.53	180.34	0.53	241.15	0.53	148.88
0.62	360.37	0.62	258.82	0.62	287.58	0.62	174.34
0.7	488.32	0.7	301.96	0.7	283.09	0.7	233.55
0.79	573.86	0.79	343.2	0.79	278.89	0.79	422.88
0.88	655.5	0.88	459.23	0.88	369.9	0.88	357.95
1	542.15	1	825.24	1	732.02	1	248.2

Table B.4 Effect of H on N_p **(DT)**

H/T	C_b/T= 0.055	H/T	C_b/T= 0.144	H/T	C_b/T= 0.233	H/T	C_b/T= 0.322
0.15	-	0.21	-	0.27	-	0.33	-
0.18	3.18	0.24	-	0.3	-	0.36	-
0.26	3.35	0.26	3.53	0.33	-	0.39	-
0.35	4	0.35	3.74	0.35	3.55	0.42	-
0.44	4.16	0.44	3.73	0.44	4.25	0.44	3.24
0.53	3.53	0.53	4.23	0.53	5.15	0.53	4.74
0.62	3.83	0.62	4.28	0.62	5.16	0.62	5.84
0.7	4.01	0.7	4.19	0.7	5.86	0.7	5.77
0.79	4.34	0.79	4.47	0.79	5.76	0.79	5.91
0.88	4.27	0.88	4.41	0.88	5.64	0.88	5.83
1	3.66	1	4.17	1	5.63	1	5.76

Table B.5 Effect of ΔH on N_{cd} **(DT)**

ΔH/T	C_b/T= 0.055	ΔH/T	C_b/T= 0.144	ΔH/T	C_b/T= 0.233	ΔH/T	C_b/T= 0.322
0.09	∞	-	-	-	-	-	-
0.12	164	0.09	∞	-	-	-	-
0.21	169	0.12	150	0.09	∞	-	-
0.30	180	0.21	175	0.12	146	0.09	∞
0.39	190	0.30	185	0.21	137	0.12	169
0.48	222	0.39	204	0.30	212	0.21	181
0.57	279	0.48	240	0.39	232	0.30	192
0.66	315	0.57	260	0.48	234	0.39	220
0.74	342	0.66	285	0.57	242	0.48	280
0.83	367	0.74	325	0.66	277	0.57	273
0.94	376	0.86	405	0.77	360	0.68	250

Table B.6 Effect of ΔH on P **(DT)**

ΔH/T	C_b/T= 0.055	ΔH/T	C_b/T= 0.144	ΔH/T	C_b/T= 0.233	ΔH/T	C_b/T= 0.322
0.09	∞	-	-	-	-	-	-
0.12	0.68	0.09	∞	-	-	-	-
0.21	0.85	0.12	0.63	0.09	∞	-	-
0.30	1.06	0.21	1.06	0.12	0.54	0.09	∞
0.39	1.28	0.30	1.2	0.21	0.53	0.12	0.76
0.48	1.89	0.39	1.72	0.30	2.3	0.21	1.42
0.57	4.01	0.48	2.88	0.39	3.2	0.30	1.94
0.66	6.21	0.57	3.84	0.48	3.6	0.39	2.97
0.74	8.21	0.66	4.91	0.57	3.99	0.48	6.05
0.83	10.42	0.74	7.3	0.66	5.88	0.57	5.69
0.94	9.48	0.86	14.43	0.77	12.8	0.68	4.34

Table B.7 Effect of ΔH on P/V **(DT)**

ΔH/T	C_b/T= 0.055	ΔH/T	C_b/T= 0.144	ΔH/T	C_b/T= 0.233	ΔH/T	C_b/T= 0.322
0.09	∞	-	-	-	-	-	-
0.12	213.89	0.09	∞	-	-	-	-
0.21	178.24	0.12	132.11	0.09	∞	-	-
0.30	166.71	0.21	166.71	0.12	84.93	0.09	∞
0.39	161.04	0.30	150.98	0.21	66.68	0.12	95.62
0.48	198.16	0.39	180.34	0.30	241.15	0.21	148.88
0.57	360.37	0.48	258.82	0.39	287.58	0.30	174.34
0.66	488.32	0.57	301.96	0.48	283.09	0.39	233.55
0.74	573.86	0.66	343.20	0.57	278.89	0.48	422.88
0.83	655.50	0.74	459.23	0.66	369.90	0.57	357.95
0.94	542.15	0.86	825.24	0.77	732.02	0.68	248.20

Table B.8 Effect of ΔH on N_p **(DT)**

ΔH/T	C_b/T= 0.055	ΔH/T	C_b/T= 0.144	ΔH/T	C_b/T= 0.233	ΔH/T	C_b/T= 0.322
0.09	∞	-	-	-	-	-	-
0.12	3.18	0.09	∞	-	-	-	-
0.21	3.35	0.12	3.53	0.09	∞	-	-
0.30	4	0.21	3.74	0.12	3.55	0.09	∞
0.39	4.16	0.30	3.73	0.21	4.25	0.12	3.24
0.48	3.53	0.39	4.23	0.30	5.15	0.21	4.74
0.57	3.83	0.48	4.28	0.39	5.16	0.30	5.84
0.66	4.01	0.57	4.19	0.48	5.86	0.39	5.77
0.74	4.34	0.66	4.47	0.57	5.76	0.48	5.91
0.83	4.27	0.74	4.41	0.66	5.64	0.57	5.83
0.94	3.66	0.86	4.17	0.77	5.63	0.68	5.76

Table B.9 Effect of H on N_{cd} **(PBT)**

H/T	C_b/T= 0.055	H/T	C_b/T= 0.144	H/T	C_b/T= 0.233	H/T	C_b/T = 0.322
0.15	∞	0.21	-	0.27	-	0.09	-
0.18	166	0.24	∞	0.3	-	0.18	-
0.26	200	0.26	150	0.33	∞	0.27	-
0.35	194	0.35	190	0.35	189	0.36	-
0.44	224	0.44	204	0.44	215	0.44	∞
0.53	246	0.53	236	0.53	232	0.53	220
0.62	276	0.62	259	0.62	248	0.62	283
0.7	283	0.7	272	0.7	280	0.7	304
0.79	302	0.79	295	0.79	316	0.79	356
0.88	345	0.88	356	0.88	372	0.88	428
1	428	1	455	1	465	1	495

Table B.10 Effect of H on P **(PBT)**

H/T	C_b/T= 0.055	H/T	C_b/T= 0.144	H/T	C_b/T= 0.233	H/T	C_b/T = 0.322
0.15	∞	0.21	-	0.27	-	0.09	-
0.18	0.3	0.24	∞	0.3	-	0.18	-
0.26	0.37	0.26	0.27	0.33	∞	0.27	-
0.35	0.53	0.35	0.61	0.35	0.43	0.36	-
0.44	1	0.44	0.64	0.44	0.67	0.44	∞
0.53	1.41	0.53	1.18	0.53	0.99	0.53	0.78
0.62	1.85	0.62	1.54	0.62	1.19	0.62	1.59
0.7	2	0.7	1.56	0.7	1.62	0.7	2.27
0.79	2.81	0.79	2.26	0.79	2.62	0.79	3.37
0.88	3.94	0.88	3.71	0.88	3.95	0.88	5.52
1	7.23	1	7.57	1	7.33	1	8.18

Table B.11 Effect of H on P/V **(PBT)**

H/T	C_b/T= 0.055	H/T	C_b/T= 0.144	H/T	C_b/T= 0.233	H/T	C_b/T = 0.322
0.15	∞	0.21	-	0.27	-	0.09	-
0.18	94.36	0.24	∞	0.3	-	0.18	-
0.26	77.59	0.26	56.62	0.33	∞	0.27	-
0.35	83.35	0.35	95.93	0.35	67.63	0.36	-
0.44	125.82	0.44	80.52	0.44	84.3	0.44	∞
0.53	147.83	0.53	123.72	0.53	103.8	0.53	81.78
0.62	166.26	0.62	138.4	0.62	106.94	0.62	142.89
0.7	157.27	0.7	122.67	0.7	127.39	0.7	178.5
0.79	196.41	0.79	157.97	0.79	183.13	0.79	235.56
0.88	247.86	0.88	233.39	0.88	248.49	0.88	347.25
1	404.29	1	423.3	1	409.88	1	457.41

Table B.12 Effect of H on N_p **(PBT)**

H/T	C_b/T= 0.055	H/T	C_b/T= 0.144	H/T	C_b/T= 0.233	H/T	C_b/T = 0.322
0.15	-	0.21	-	0.27	-	0.09	-
0.18	1.31	0.24	-	0.3	-	0.18	-
0.26	0.97	0.26	1.4	0.33	-	0.27	-
0.35	1.46	0.35	1.68	0.35	1.3	0.36	-
0.44	1.8	0.44	1.56	0.44	1.39	0.44	-
0.53	1.89	0.53	1.75	0.53	1.61	0.53	1.51
0.62	1.79	0.62	1.71	0.62	1.55	0.62	1.41
0.7	1.69	0.7	1.56	0.7	1.49	0.7	1.59
0.79	2.02	0.79	1.79	0.79	1.67	0.79	1.49
0.88	1.9	0.88	1.68	0.88	1.53	0.88	1.4
1	1.86	1	1.61	1	1.47	1	1.35

Table B.13 Effect of ΔH on N_{cd} **(PBT)**

ΔH/T	C_b/T= 0.037	ΔH/T	C_b/T= 0.126	ΔH/T	C_b/T= 0.215	ΔH/T	C_b/T= 0.304
0.11	∞	-	-	-	-	-	-
0.14	166	0.11	∞	-	-	-	-
0.23	200	0.14	150	0.11	∞	-	-
0.32	194	0.23	190	0.14	189	-	-
0.41	224	0.32	204	0.23	215	0.14	∞
0.50	246	0.41	236	0.32	232	0.23	220
0.58	276	0.50	259	0.41	248	0.32	283
0.67	283	0.58	272	0.50	280	0.41	304
0.76	302	0.67	295	0.58	316	0.50	356
0.85	345	0.76	356	0.67	372	0.58	428
0.96	428	0.87	455	0.78	465	0.70	495

Table B.14 Effect of ΔH on P **(PBT)**

ΔH/T	C_b/T= 0.037	ΔH/T	C_b/T= 0.126	ΔH/T	C_b/T= 0.215	ΔH/T	C_b/T= 0.304
0.11	∞	-	-	-	-	-	-
0.14	0.3	0.11	∞	-	-	-	-
0.23	0.37	0.14	0.27	0.11	∞	-	-
0.32	0.53	0.23	0.61	0.14	0.43	-	-
0.41	1	0.32	0.64	0.23	0.67	0.14	∞
0.50	1.41	0.41	1.18	0.32	0.99	0.23	0.78
0.58	1.85	0.50	1.54	0.41	1.19	0.32	1.59
0.67	2	0.58	1.56	0.50	1.62	0.41	2.27
0.76	2.81	0.67	2.26	0.58	2.62	0.50	3.37
0.85	3.94	0.76	3.71	0.67	3.95	0.58	5.52
0.96	7.23	0.87	7.57	0.78	7.33	0.70	8.18

Table B.15 Effect of ΔH on P/V **(PBT)**

ΔH/T	C_b/T= 0.037	ΔH/T	C_b/T= 0.126	ΔH/T	C_b/T= 0.215	ΔH/T	C_b/T= 0.304
0.11	∞	-	-	-	-	-	-
0.14	94.36	0.11	∞	-	-	-	-
0.23	77.59	0.14	56.62	0.11	∞	-	-
0.32	83.35	0.23	95.93	0.14	67.63	-	-
0.41	125.82	0.32	80.52	0.23	84.30	0.14	∞
0.50	147.83	0.41	123.72	0.32	103.80	0.23	81.78
0.58	166.26	0.50	138.40	0.41	106.94	0.32	142.89
0.67	157.27	0.58	122.67	0.50	127.39	0.41	178.50
0.76	196.41	0.67	157.97	0.58	183.13	0.50	235.56
0.85	247.86	0.76	233.39	0.67	248.49	0.58	347.25
0.96	404.29	0.87	423.30	0.78	409.88	0.70	457.41

Table B.16 Effect of ΔH on N_p **(PBT)**

ΔH/T	C_b/T= 0.037	ΔH/T	C_b/T= 0.126	ΔH/T	C_b/T= 0.215	ΔH/T	C_b/T= 0.304
0.11	-	-	-	-	-	-	-
0.14	1.31	0.11	-	-	-	-	-
0.23	0.97	0.14	1.4	0.11	-	-	-
0.32	1.46	0.23	1.68	0.14	1.3	-	-
0.41	1.8	0.32	1.56	0.23	1.39	0.14	-
0.50	1.89	0.41	1.75	0.32	1.61	0.23	1.51
0.58	1.79	0.50	1.71	0.41	1.55	0.32	1.41
0.67	1.69	0.58	1.56	0.50	1.49	0.41	1.59
0.76	2.02	0.67	1.79	0.58	1.67	0.50	1.49
0.85	1.9	0.76	1.68	0.67	1.53	0.58	1.4
0.96	1.86	0.87	1.61	0.78	1.47	0.70	1.35

Table B.17 Comparison of $N_{cd\text{-}smp}$ vs. $N_{cd\text{-}vis}$

$N_{cd\text{-}vis}$ (rpm)	$N_{cd\text{-}smp}$ (rpm)
221	230
174	176
165	171
151	153
220	224
342	345
110	104

Table B.18 Reproducibility Data

DT	$N_{cd\text{-}vis}$ (rpm) at H=0.2286m					Reproducibility (%)
	Set I	Set II	Set III	Set IV	Set V	
C=1	342	354	329	336	347	± 2.82
C=2	285	310	281	276	295	± 4.72
C=3	242	245	251	236	239	± 2.38
C=4	280	264	276	283	282	± 2.77
Average Reprocibility						± 3.17
PBT	$N_{cd\text{-}vis}$ (rpm) at H=0.2286m					Reproducibility (%)
	Set I	Set II	Set III	Set IV	Set V	
C=1	302	316	289	296	308	± 3.46
C=2	295	281	300	302	298	± 2.83
C=3	316	304	298	305	325	± 3.41
C=4	356	340	351	364	345	± 2.63
Average Reprocibility						± 3.08

REFERENCES

Armenante, P.M. and Chang, G.M., " Power Consumption in Agitated Vessel provided with Multiple–Disk Turbine," *Ind. Eng. Chem.*, vol. 37, pp. 284 – 291, 1998.

Armenante, P.M. and Huang, Y.T., " Experimental Determination of the Minimum Agitation Speed for Complete Liquid–Liquid Dispersion in Mechanically Agitated Vessels," *Ind. Eng. Chem.*, vol. 31, pp. 1398 – 1406, 1992.

Bates, R.L., Fondy, P.L. and Corpstein, R.R., " An Examination of Some Geometric Parameters of Impeller Power," *Ind. Eng. Chem. Process. Des. and Dev.*, vol. 2, pp. 310 – 314, 1963.

Chudacek, M.W., "Impeller Power Numbers and Impeller Flow Numbers in Profiles Bottom Tanks," *Ind. Eng. Chem. Process. Des. and Dev.*, vol. 24, pp. 858 – 867,1985.

Gray, D.J., Treybal, R.E. and Barnett, S.M., " Mixing of Single and Two Phase Systems: Power Consumption of Impellers," *AIChE J.*, vol. 28, pp.195 – 199, 1982.

Harnby, N., Edwards, M.F. and Nienow, A.W., *Mixing in Process Industries,* Butterworth – Heinemann, second ed., 1992.

Hixxon, A.W. and A. H. Tenney, A.H., *Trans. Am. Inst. Chem. Eng.,* vol. 31, pp. 113-127, 1935.

Hudcova, V., Machon, V. and Nienow, A.W., " Gas–Liquid Dispersion with Dual Rushton Turbine Impellers," *Biotechnol. Bioeng.*, vol. 34, pp. 617 – 628, 1989.

Laity, D.S. and Treybal, R.E., *AIChE J.,* vol. 3, pp. 176 – 180, 1957.

McCabe, W.L. and Smith, C.J., *Unit Operations of Chemical Engineering*, McGraw – Hill Chemical Eng. Series, third ed., 1976.

Nagata, S., "*Mixing: Principles and Applications,*" Kodansha Scientific Books, third ed., 1975.

Nagata, S., "Studies on Agitation of two Immiscible Liquids," *Trans. Soc. Chem. Eng.,* vol. 8, pp. 43 – 48, 1960.

Nienow, A.W. and Lilly, M.D., " Power Drawn by Multiple Impellers in Sparged Agitated Vessels." *Biotechnol. Bioeng.,* vol. 21, pp. 2341 – 2345, 1979.

O' Kane, K., " The effect of Geometric Parameters on the Power Consumption of Turbine Impellers Operating in Nonviscous Fluids," *Proceedings of the 1st European Conference on Mixing and Centrifugal Separation*, Cambridge, England, Sept 9 – 11, 1974; BHRA Fluid Engineering: Cranfield, UK; Paper A3, pp 23 – 31.

O'Connell, F.D. and Mack. D.E., *Chem. Eng. Engr. Progr.*, vol. 46, pp. 358, 1950.

Oldshue, J.Y., " Fluid Mixing Technology," *McGraw–Hill Publications Co.*, second ed., 1983.

Quinn, J.A. and Sigloh, D.B., " Phase Inversion in Mixing of Two Immiscible Liquids," *Can. J. Chem. Eng.*, vol. 41, pp. 15 – 18, 1963.

Raghava Rao, K.S. M. S. and Joshi, J.B., " Liquid Phase Mixing in Mechanically Agitated Vessels," *Chem. Eng. Commun.*, vol. 74, pp. 1 – 25, 1988.

Rewatker, V.B., Raghava Rao., K.S.M.S., and Joshi, J.B., " Power Consumption in Mechanically Agitated Contactors Using Pitched Bladed Turbine Impeller," *Chem. Eng. Commun.*, vol. 88, pp. 69 – 90,1990.

Rushton, J.H., Costich, E.W. and Everett, H.J., " Power Characteristics of Mixing Impellers," *Chem. Eng. Prog.*, vol. 46 (Part I), pp. 395 – 402, vol.46 (Part II), pp. 467 – 476, 1950.

Skelland, A.H.P. and Lee, J.M., " Agitator Speed in Baffled Vessels for Uniform Liquid–Liquid Dispersion," *Ind. Eng. Chem. Proc. Des. Dev.*, vol.17, pp. 473 – 478, 1978.

Skelland, A.H.P. and Ramsey, G.G., " Minimum Agitation Speed for Complete Liquid–Liquid Dispersion," *Ind. Eng. Chem. Res.*, vol. 26, pp. 77 – 81, 1987.

Skelland, A.H.P. and Seksaria, R., " Minimum Impeller Speed for Liquid–Liquid Dispersion in Baffles Vessels," *Ind. Eng. Chem. Proc. Des. Dev.*, vol.17, pp. 56 – 61, 1978.

Tatterson, G.B., " Fluid Mixing and Gas Dispersion in Agitated Tanks," *McGraw – Hill Publications Co.*, 1991.

van Heuven, J.W. and Beek, W.J., " Power Input, Drop Size and Minimum Stirrer Speed for Liquid-Liquid Dispersion in Stirred Tanks," *Solvent Extraction, Proc. Int. Solvent Extraction Conf;* Gregory, J. G., (Ed.); (Soc. Chem. Ind., London) Paper 51, pp. 70-81, 1971.

White, A.M. and Brenner, E., " Studies in Agitation vs. the Correlation of Power Data," *Trans. Ame. Ins. Chem. Eng.*, vol. 30, pp. 585 – 597, 1934.